UNIVERSITÉ DU QUÉBEC

THÈSE PRÉSENTÉE À
L'UNIVERSITÉ DU QUÉBEC À TROIS-RIVIÈRES

COMME EXIGENCE PARTIELLE
DU DOCTORAT EN SCIENCES DE L'ÉNERGIE ET DES MATÉRIAUX
OFFERT EN EXTENSION PAR L'INSTITUT NATIONAL DE LA
RECHERCHE SCIENTIFIQUE

PAR
SADESH KUMAR NATARAJAN

NOVEL CARBON NANOSTRUCTURES AS CATALYST SUPPORT FOR POLYMER ELECTROLYTE MEMBRANE FUEL CELLS

JANVIER 2009

RESUME

La technologie de la pile à combustible à membrane électrolytique polymère (PEMFC – *Polymer Electrolyte Membrane Fuel Cell*) a fait des progrès rapides dans les dernières années. Un secteur actif se penche sur l'amélioration de la performance à long terme de catalyseurs à support de carbone, ce qui a été reconnu comme un des problèmes les plus importants à résoudre pour la mise en marché des PEMFCs. La partie centrale d'une PEMFC est l'assemblage membrane-électrode (MEA), qui est composé de deux électrodes (anode et cathode) et d'une membrane échangeuse de cations. Ces électrodes sont en général fabriquées de noir de charbon (le plus souvent du Vulcan XC-72) sur un support de papier carbone ou de tissu carbone.

Les couches de catalyseur (CL – *Catalyst Layer*) faisant partie des électrodes sont l'endroit où ont lieu les réactions électrochimiques et sont composées d'un catalyseur (Pt ou alliage de Pt) supporté par du noir de charbon, des ionomères pour la conduction protonique, et des ligands en Teflon® pour l'hydrophobicité. Comme mentionnée ci haut, la durabilité de ces CLs est le problème crucial pour le développement et la mise en marché des PEMFCs.

Malgré son utilisation répandue, le noir de charbon est sujet à une oxydation électrochimique par des oxydes de surface et éventuellement se transforme en CO_2 à la cathode d'une pile à combustible où il est sujet à des hauts degrés d'acidité, de tension, de température et d'humidité. Au fur et à mesure que le carbone est oxydé, les nanoparticules métalliques du catalyseur seront perdus de l'électrode ou s'agglomèreront en particules plus grandes. L'oxydation du support de carbone peut aussi mener à des changements d'hydrophobicité superficielle qui peut mener à des difficultés de transport des gaz. De plus, le catalyseur fait de métaux nobles soutenus sur un support en carbone accélère le taux de corrosion du carbone en se servant de l'eau produite à la cathode comme combustible pour l'oxydation.

Plusieurs groupes de recherche ont proposé qu'un carbone avec un plus grand degré de graphitisation puisse être plus résistant à la corrosion dans le voisinage cathodique. Donc, l'objectif primaire de ce mémoire est de préparer et d'explorer des nanostructures de carbone (CNS – *Carbon Nanostructures*, en licence à l'Institut de recherche sur

l'hydrogène, Québec, Canada), un matériau avec un plus grand degré de graphitisation, comme les nanotubes au carbone, comme support du catalyseur dans les PEMFCs.

Le broyage mécanique à haute énergie d'un charbon activé avec des catalyseurs métalliques de transition sous atmosphère d'hydrogène, suivie d'un chauffage à 700 °C sous argon dans un tube de quartz, mène à la formation de structures de carbone nanocristallines que nous appelons CNS. Cependant, les CNS formé dans le tube de quartz après le chauffage sont accompagnées inévitablement par des impuretés telles que particules métalliques, carbone amorphe et autres nanoparticules de carbone. Ces impuretés sont un frein sérieux à la caractérisation des propriétés des nanostructures. De plus, puisque la surface des CNS est elle-même plutôt inerte, il est difficile de contrôler l'homogénéité et la distribution des nanoparticules de Pt subséquemment déposées. Dans ce travail de recherche, nous avons démontré une nouvelle procédure pour purifier et fonctionnaliser simultanément les CNS par un mélange d'acides sous des conditions de reflux. Pour étudier et quantifier ces nanostructures, il faut faire appel aux techniques de diffraction aux rayons-X, de mesures de conductivité électrique, de mesures de surface spécifique, d'analyses thermogravimétriques, de spectroscopies aux photoélectrons de rayons-X et à la microscopie électronique à transmission. Des études de voltamétrie cyclique furent faites sur différents échantillons pour comprendre la relation entre la composition du mélange acide et son influence sur la production de groupes fonctionnels surfaciques. Une telle fonctionnalisation des surfaces des CNS augmente la réactivité, améliore la spécificité et fournit un chemin pour la déposition du Pt. Il est aussi démontré qu'un mélange 1:1 de 7.5M d'acide sulfurique et 15M d'acide nitrique produit une composition accrue de groupes fonctionnels non-acides par rapport à d'autres compositions acides commentées dans ce mémoire.

Nous avons aussi montré une nouvelle méthode pour déposer et disperser le platine sur les CNS via un mécanisme chimique spécifique de nucléation. Pour étudier et quantifier ces CNS platinés nous avons utilisé la diffraction aux rayons-X, l'analyse thermogravimétrique, la spectroscopie d'adsorption atomique et la microscopie électronique à transmission à haute résolution. Des nanoparticules de Pt d'une taille moyenne de 4 nm furent dispersées de façon homogène sur des CNS qui furent préalablement fonctionnalisées par la méthode décrite ci-haut.

La nature corrosive du support en carbone est un aspect crucial pour la commercialisation des PEMFCs. Dans cette optique, les oxydations électrochimiques de combinaisons Pt/CNS vs Pt/C furent étudiées dans le présent travail. L'oxydation superficielle de ces matériaux a été comparée à la suite de traitements potentiostatiques allant jusqu'à 200 h sous des conditions simulant l'environnement cathodique (80 °C, acide sulfurique 0.5 M, et un potentiel constant de 1.2 V). Les performances du catalyseur Pt/CNS et Pt/C sur une période de temps similaire furent aussi évaluée en mesurant la tension d'une cellule avec une charge constante après divers intervalles d'oxydation à 1.2 V. L'agglomération du Pt et les changements en groupes fonctionnels surfaciques de ces matériaux de carbone, suite aux divers intervalles d'oxydation électrochimique, furent évalués via des études de patrons de diffraction à rayons-X et de thermogravimétrie. La caractérisation électrochimique subséquente à des intervalles de traitement différents par ces deux méthodes suggère que le CNS est plus stable électrochimiquement que le Vulcan XC-72, avec moins de formation d'oxyde surfacique et de perte de surface active du Pt

A. OBJECTIFS

L'objectif de ce travail est d'étudier le comportement du charbon activé (CNS201) durant le broyage à haute énergie en présence de métaux de transition et sous hydrogène afin de préparer des CNS bien définies ayant des surfaces spécifiques plus grandes. Si on comprend l'effet de la composition sur la croissance des CNS et comment les conditions de broyage influencent l'adsorption de l'hydrogène sur les charbons, on pourra préparer de meilleurs CNS avec un plus grand degré de graphitisation. Ce mémoire explore aussi leur conductivité électrique, surface spécifique BET et porosité.

Les CNS bruts préparés dans notre laboratoire sont accompagnés d'impuretés indésirables telles que métaux de transition ou oxydes métalliques, carbone amorphe et autres nanoparticules de carbone. L'objectif principal de ce mémoire est de déposer de façon homogène les particules de Pt sur les surfaces des CNS et d'évaluer la durabilité du support sous environnement cathodique simulé. Afin de distribuer les particules de Pt sur la surface du carbone et de pouvoir utiliser ce carbone en tant que support pour le catalyseur, les impuretés indésirables doivent être enlevées, et des groupes fonctionnels doivent être attachés à la surface des atomes de carbone. Ces groupes fonctionnels

facilitent la déposition et la dispersion des nanoparticules de Pt sur les CNS par l'entremise d'un mécanisme de nucléation chimique spécifique. Pour réaliser cet objectif, nous avons développé une méthode pour purifier et fonctionnaliser les CNS en une seule étape en utilisant une solution d'acide nitrique et d'acide sulfurique. Un aspect important de cette méthode est l'optimisation de la composition du mélange d'acides et des conditions du reflux. Ceci demanda l'application de la spectroscopie photo électronique à rayons-X (XPS) pour analyser et comparer les résultats des différentes solutions, l'état chimique et électronique des éléments, composition en carbone et oxygène des CNS non-oxydés et CNS oxydés. Les spectres XPS furent obtenus en irradiant ces échantillons par un faisceau de rayons-X et simultanément en mesurant l'énergie cinétique et le nombre d'électrons s'échappant des premiers 1-10 nm du matériau analysé.

Il est bien connu que la dimension des nanoparticules de Pt ainsi que leur distribution sont des facteurs clé qui déterminent leur activité pour la réaction de réduction de l'oxygène (ORR - *Oxygen Reduction Reaction*) et la performance des PEMFCs. Il a aussi été rapporté que la taille des nanoparticules de Pt augmente et que la surface électrochimique diminue pendant la durée de vie des PEMFCs. La quantité de Pt sur le support de carbone fut estimée par spectroscopie atomique d'absorption (AAS) avec un appareil Varian Spectra AA 55 et par analyseur thermogravimétrique (TGA). Le TGA est aussi utilisé avec les CNS non-platinés pour étudier le type de structures carboniques nanocristallines présentes dans nos échantillons. Là aussi des études des patrons de diffraction à rayons-X et de microscopie électronique de transmission à haute résolution (HRTEM) furent faites pour estimer les dimensions et la distribution des nanoparticules de Pt.

Un objectif additionnel de ce mémoire était d'étudier les performances électrochimiques du Pt supporté sur des CNS par des mesures de voltamétrie cyclique (CV). Cette méthode permet, par exemple, la comparaison de propriétés électrochimiques des échantillons de Pt/CNS fabriqués ou prétraités de différentes manières. Cette partie de nos recherches implique aussi l'estimation de l'étendue de la surface active des catalyseurs de Pt supportés sur du noir de charbon et CNS.

La durabilité du matériau de l'électrode est un facteur important qui limite la commercialisation des PEMFCs. Par conséquent, l'objectif final de ce travail de recherche était de clarifier les facteurs essentiels reliés à la dégradation des électrodes des PEMFCs et aussi d'étudier la durabilité de la CL cathodique de MEAs préparées avec Pt/C et Pt/CNS. Cet objectif demande l'étude de la dégradation du matériau de carbone suite à une oxydation électrochimique accélérée de la cathode. La fabrication et vérification des MEAs, la caractérisation des catalyseurs, l'analyse de la taille des particules de Pt et leur surface active, et les changements dans les groupes fonctionnels surfaciques des carbones sont quelques-uns des facteurs essentiels impliqués dans ce travail.

B. PREPARATION DES CNS

Le carbone de départ est du charbon activé commercial (CNS201) qui a été préalablement chauffé à 1 000 °C sous vide pendant 90 min pour se débarrasser de toute humidité et autres impuretés. En première étape, dans un creuset d'acier durci du CNS201 prétraité fut mélangé à une certaine quantité de Fe et de Co (99.9 % purs). Des proportions typiques sont 50 pd.%, 44 pd.%, et 6 pd.% pour le C, le Fe, et le Co respectivement. Trois à cinq billes en acier durci furent utilisées pour le broyage, de masse relative échantillon/poudre de 35 à 1. L'hydrogène fut alors introduit dans le creuset à une pression de 1.4 MPa, et l'échantillon fut broyé pendant 12 h. Le broyeur est un SPEX®, qui a un rendement d'énergie mécanique plus grand qu'un broyeur planétaire, mais qui a le désavantage de contaminer l'échantillon en Fe par attrition. Cependant, ceci peut être négligé vu que le Fe était un des catalyseurs métalliques ajoutés au creuset. En deuxième étape, l'échantillon broyé est transféré sous gaz inerte (argon) dans un tube en quartz, qui est alors chauffé à 700 °C pendant 90 min.

C. IDENTIFICATION DES STRUCTURES

Des mesures de patrons de diffraction à rayons-X sur poudre furent faites pour caractériser les changements structurels des CNS. Ces mesures furent prises avec un diffractomètre Rigaku utilisant le rayonnement Cu Kα (λ = 1.54054 Å) et une géométrie Thêta/2Thêta. Le patron de diffraction de rayons-X de la Figure 4.2 montre le pic

principal à 27° associé à l'empilement des plans (002) graphitiques du CNS et l'absence des plans de graphitisation supérieur du Vulcan XC-72.

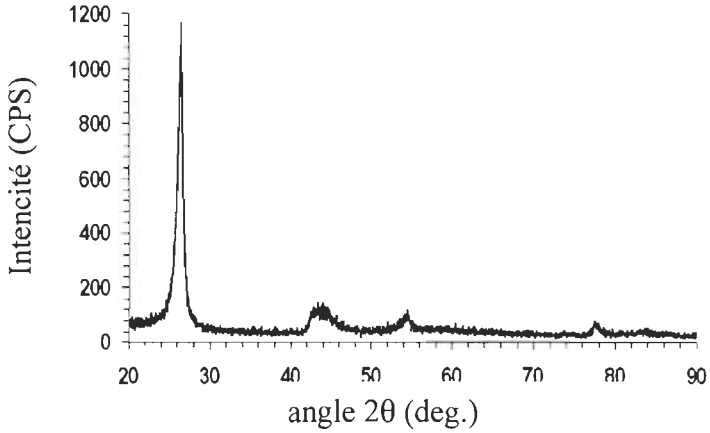

Figure 4.2 Patron de diffraction XRD des CNS brut.

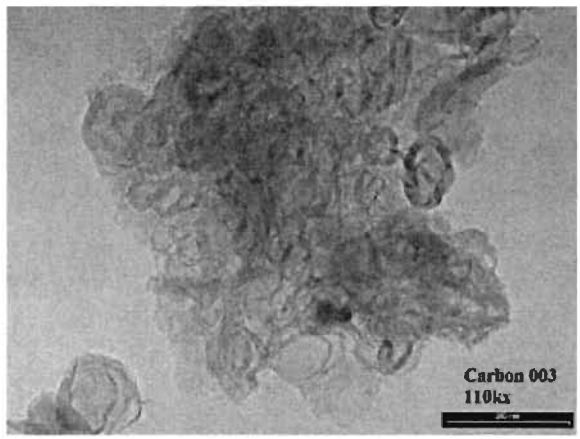

Figure 5.2 Image TEM des CNS purifiés et fonctionnalisés.

L'image TEM à la Figure 5.2 confirme et complète le résultat des mesures de patrons de diffraction à rayons-X. Comme cette figure le montre, des nanostructures sphériques concentriques fermées peuvent être décelées. De plus on peut voir des plans de graphite, qui sont courbés jusqu'à 180°.

D. PURIFICATION ET FUNCTIONALISATION

La génération de groupes fonctionnels sur la surface des CNS peut être accomplie par des techniques de modification chimique avec des proportions variables d'agents oxydants forts, l'acide sulfurique (H_2SO_4) et l'acide nitrique (HNO_3), qui oxydent de façon efficace les impuretés du catalyseur métallique, les nanoparticules de carbone, et les liens C-C

faibles dans les CNS hautement structurés. De plus, ce traitement crée des sites actifs sur les CNS pour faciliter l'homogénéité de la déposition du métal sur la surface par toute méthode de platinization conventionnelle.

Tableau 5.1 Différentes proportions et concentrations de H_2SO_4 et HNO_3 utilisées comme oxydants de surface.

Échantillon	D	E	F	G	H	I
H_2SO_4 : HNO_3	1 : 1	1 : 1	1 : 1	3 : 1	3 : 1	3 : 1
Molarité du H_2SO_4	3 M	5 M	7.5 M	5 M	10 M	15 M
Molarité du HNO_3	5 M	9 M	15 M	6 M	15 M	20 M
Pourcentage obtenue	41.88	41.43	41.55	43.69	40.02	31.45

Dans le présent travail, la surface des CNS fut modifiée chimiquement par reflux d'échantillon de 500 mg sous différentes concentrations et proportions d'un mélange H_2SO_4/HNO_3 à une température optimisée de 120 °C pendant 3 h (échantillons D, E, F, G, H & I - Tableau 4.1). Le mélange brun foncé résultant fur dilué avec de l'eau déminéralisée et filtrée avec un microfiltre en céramique dont les pores vont de 5 à 10 µm de diamètre. Le précipité fut lavé pour neutraliser le pH et sécher durant la nuit à 120 °C sous atmosphère d'azote. Le Tableau 4.1 montre les proportions et concentrations d'acides utilisées pour les différents échantillons. Pour comparer l'effet du traitement d'oxydation par acides, un échantillon de CNS traité fut purifié avec du HCl (*trace metal solution*) plutôt qu'avec du H_2SO_4/HNO_3 afin d'explorer les sites actifs disponibles sans fonctionnalisation de la surface.

E. DENSITE DES CNS APRES PURIFICATION

La Figure 5.3 est un graphique de l'analyse thermogravimétrique d'un échantillon de CNS qui montre une température de décomposition centrée sur 738 °C pour à peu près 90 pd.% de l'échantillon. La perte de 10 pd.% entre 20 °C et 600 °C est attribuée à de l'eau et du carbone amorphe. Aux fins de comparaison, cette figure montre aussi une courbe TGA de nanotubes de carbones, qui mesure une température de décomposition entre 510 °C et 645 °C. Cependant, il n'y a pas de température de combustion unique pour les

nanotubes puisque celle-ci est fonction de non seulement le degré de graphitisation, mais aussi de leur prétraitement. Puisque la température d'oxydation des CNS est relativement élevée, nous concluons que nos échantillons possèdent un degré élevé de graphitisation. De plus, les résultats des TGA font aussi preuve de la pureté des CNS.

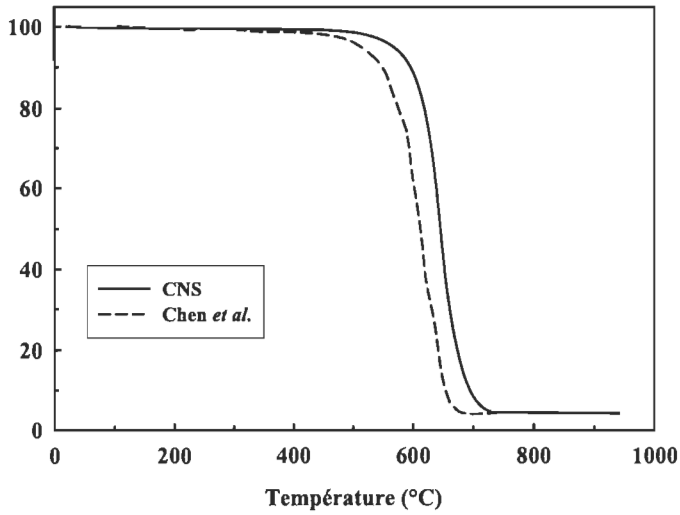

Figure 5.3 Résultats d'analyse TGA typique sous atmosphère d'O2.

F. MESURES DE CONDUCTIVITE ELECTRIQUE ET DE POROSITE

La conductivité électrique des CNS fut mesurée avec un analyseur d'impédance HP4284A. L'échantillon était comprimé entre deux électrodes d'aluminium à l'intérieur d'une cavité cylindrique en acrylique (type *plunger*). Un ressort calibré comprime la poudre à une pression maximale de 40 atm. La conductivité électrique de l'échantillon dépend fortement de la pression de compression, et augmente rapidement avec celle-ci. Pour des raisons de comparaison, les conductivités électriques des échantillons mesurés dans ce mémoire l'étaient à une pression de 40 atm. Avec la conductance (G) mesurée par l'analyseur d'impédance, la superficie des électrodes (S =19.6 mm^2) et la longueur typique de l'échantillon (L = 0.3 cm), la conductivité électrique σ est donnée par $\sigma = GL/S$. La conductivité électrique calculée moyenne des CNS était de 0.9 S cm^{-1} par rapport à 1.0 S cm^{-1} pour le Vulcan XC-72, ce qui est en accord avec la valeur rapportée par Pantea *et al.* [77].

La surface spécifique des CNS fut déterminée à partir de mesures d'isothermes d'adsorption d'azote et par analyse BET. Avant de commencer ces mesures, l'échantillon

fut dégazé sous vide pendant 5 h, et la masse mesurée avant et après le dégazage. Les mesures d'isotherme d'adsorption à l'azote à 77 K ont été faites avec un instrument Quantachrome AS-1-MP. Les résultats montrent une surface totale de 352.6 $m^2 g^{-1}$; une superficie externe de 196.5 $m^2 g^{-1}$; un volume microporeux de 0.14 $cm^3 g^{-1}$, et un diamètre moyen microporeux de 1.6 nm.

La surface des macropores, leurs volume et rayon furent obtenus à partir de mesures d'isothermes d'intrusion au Hg mesurés avec un porosimètre Quantachrome Autoscan (pression maximale jusqu'à 60 000 psi). Les résultats montrent une surface cumulative des macropores de 42.8 $m^2 g^{-1}$ jusqu'à une pression de 58 000 psi; un volume total de 635 $mm^3 g^{-1}$, avec un pic distinctif à 120 $mm^3 g^{-1}$ qui correspond à un rayon de pore de 1 μm, comme le montre la Figure 5.4.

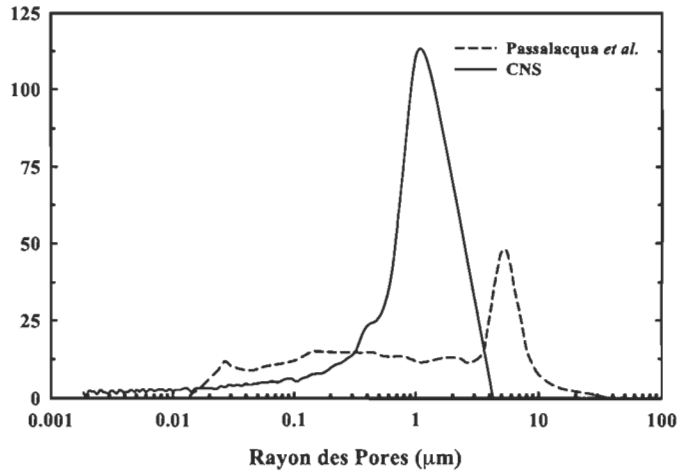

Figure 5.4 Volume poreux en fonction du rayon poreux à partir de données d'intrusion au Hg.

Cette figure contient aussi, pour fin de comparaison, les données de Passalacqua *et al.* [78] pour le Vulcan XC-72. On peut voir que le CNS a un volume de macropores plus grand que le noir de charbon (le noir de charbon ne possède pratiquement pas de volume microporeux). Si on compare le pic à 1 μm pour les CNS au pic principal de Passalacqua *et al.* à 5.5 μm, ce déplacement du rayon des pores explique en partie le plus grand volume des pores des CNS.

G. GROUPES FONCTIONNELS SURFACIQUES

La technique XPS fut utilisée pour analyser et comparer la composition élémentaire, l'état chimique, et l'état électronique des liaisons carbone et oxygène des échantillons B (CNS non oxydés chimiquement) et F. Des spectres XPS furent obtenus en irradiant tour à tour les deux échantillons avec un faisceau de rayons-X et simultanément mesurant le nombre d'électrons et leurs énergies cinétiques qui s'échappent des premiers 1 à 10 nm du matériau analysé. Comme le montre la Figure 5.5b les résultats expérimentaux confirment l'existence de groupes fonctionnels surfaciques tels que hydroxyles, carbonyles et carboxyles générés par oxydation chimique. Les études XPS démontrent clairement que le CNS traité avec un mélange d'acide sulfurique et acide nitrique produit des pics O_{1s} augmentés par rapport à l'échantillon de CNS purifié au HCl (Figure 5.5a). Dans l'échantillon B, un petit montant seulement d'oxygène est décelé, ce qui peut être interprété comme une espèce d'oxygène adsorbé. De plus, le rapport des superficies des pics O_{1s} dans les échantillons F et B est d'environ 2.21:1, ce qui indique une efficacité supérieure du traitement d'oxydation chimique pour fonctionnaliser les CNS.

En référence aux études XPS de fibres de carbones oxydées en surface [79, 80], l'analyse des pics O_{1s} des courbes obtenus suggère la présence de groupes fonctionnels surfaciques nouveaux et additionnels avec une énergie de liaison à 533.00 eV pour l'échantillon F. D'autres pics attribués à des groupes de phénol (532.05 eV), carbonyle (530.95 eV) et carboxyle (533.76 eV) peuvent aussi être repérés dans les deux échantillons.

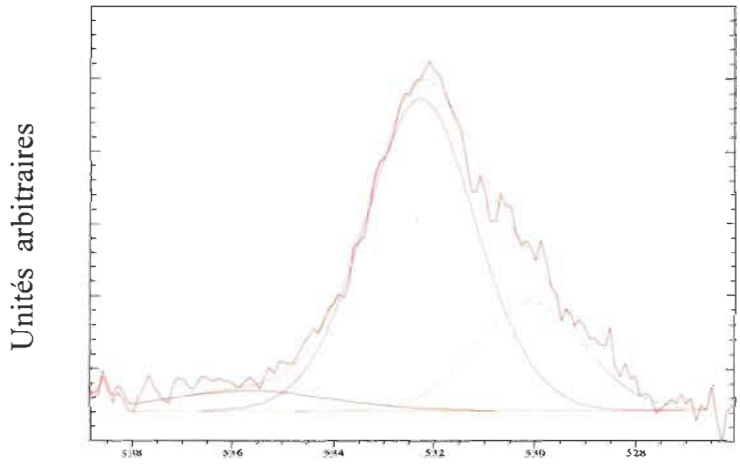

(a)

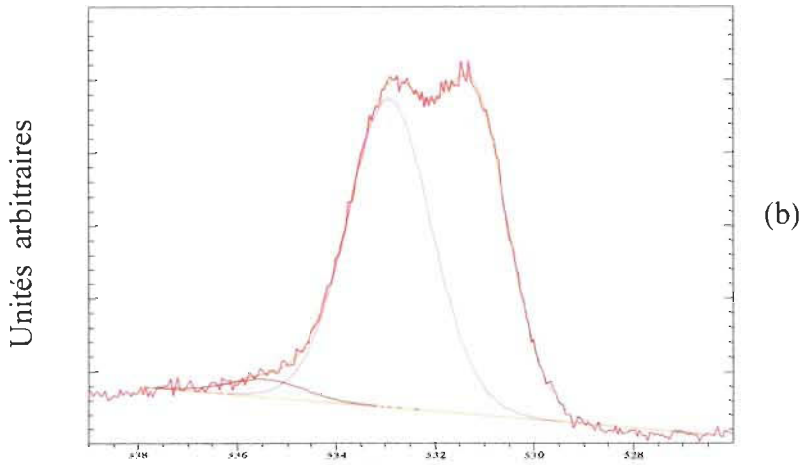

Figure 5.5 (a) CNS (échantillon F) après fonctionnalisation (b) CNS (échantillon B) avant fonctionnalisation.

H. PLATINISATION DU CNS

Une des étapes les plus importantes dans la préparation des catalyseurs des PEMFCs consiste à attacher des nano particules de Pt aux sites fonctionnalisés du CNS. Dans cette étape un montant déterminé de CNS (400 mg) était en suspension dans 40 ml de solution d'éthylène glycol, et agité pendant 30 min pour bien disperser 10 mg de CNS par ml de solution d'éthylène glycol. Afin d'obtenir des nanoparticules de Pt de quelques nanomètres de diamètre, 6.5 ml d'acide hexachloro-platinic fut ajouté goutte par goutte, suivie par de l'eau déminéralisée par intervalles de 10 min pour former des concentrations d'eau de 5 %, 10 % et finalement 20 % de la solution complète. Le but était d'obtenir une quantité de Pt déposée en particules de taille nanométrique, et non-pas de déterminer la relation entre l'addition d'eau et la dimension des nanoparticules. Cependant, cette méthode fut investigué dans notre laboratoire pour permettre un contrôle adéquat sur la taille des nanoparticules de Pt.

L'hypothèse qui expliquerait l'influence de l'addition d'eau sur la dimension des nanoparticules de Pt résultants serait comme suit : l'absence d'eau favoriserait la formation métallique alors que sa présence favoriserait la formation d'oxyde ou d'hydroxyacétates. Par conséquent, la présence d'une faible quantité d'eau dans la solution à un effet tampon sur le taux de formation des particules métalliques et donc de

produire des nanoparticules de taille contrôlable à des valeurs spécifiques. La valeur du pH de la solution fut ajustée au-delà de 13 par l'addition de NaOH dans la solution d'éthylène glycol. Le pH de la solution colloïdale initiale de Pt hydroxyde est très important pour obtenir des nanoparticules stables de Pt dans le glycol. Si la valeur de pH est inférieure à ~12, alors au lieu d'une solution colloïdale métallique, on obtiendrait un précipité durant l'étape de chauffage suivante. La solution fut chauffée dans un bain d'huile à 140 °C pour réduire le Pt complètement. Des conditions de reflux furent utilisées pour maintenir une quantité d'eau constante dans le système glycol-eau. Un débit d'argon fut passé à travers le système de réaction pour éliminer l'oxygène et enlever les produits organiques secondaires. Après filtration, lavage et séchage (120 °C sous azote sec, 12 à 15 h) les échantillons de Pt/CNS furent obtenus et désignés échantillons B_{Pt}, D_{Pt}, E_{Pt}, F_{Pt}, G_{Pt}, H_{Pt} et I_{Pt}. Un échantillon commercial de 20 pd.% Pt sur Vulcan XC-72 (désigné comme C_{Pt}) fur utilisé comme comparaison.

I. CARACTERISATION DU PT/CNS

Les échantillons de Pt/CNS furent caractérisés en enregistrant leurs spectres de diffraction XRD dont l'un de ceux-ci est montré à la Figure 5.6. Le spectre de diffraction XRD identifie le réseau cubique faces centrées des pics caractéristiques cristallins Pt (111), Pt (200), Pt (220), Pt (311) et Pt (222). Les dimensions moyennes des nanoparticules furent calculées selon la formule de Scherrer (Équation 5.1) basé sur le pic Pt (111) et lister au Tableau 5.2.

Tableau 5.2 Surface active et utilisation du platine avec CNS et l'échantillon C_{Pt} avec Vulcan.

Échantillon	B_{Pt}	C_{Pt}	D_{Pt}	E_{Pt}	F_{Pt}	G_{Pt}	H_{Pt}	I_{Pt}
Quantité Pt sur CNS (pd.%)	5.3	20	11.3	14.0	11.9	11.10	8.60	9.70
Électro adsorption ($mC\ cm^{-2}$)	2.95	25.04	15.79	17.23	24.19	10.33	15.76	28.35
Électro désorption ($mC\ cm^{-2}$)	1.85	28.60	15.19	15.38	24.94	7.47	12.05	23.23
Charge coulombique pour la désorption ($mC\ cm^{-2}$)	2.40	26.82	15.49	16.31	24.57	8.90	13.91	25.79
Charge spécifique ($mC\ g^{-1}$)	12.00	134.1	77.45	81.53	122.83	44.49	69.53	128.95
EAS ($m^2\ g^{-1}$)	5.71	63.86	36.88	38.82	58.49	21.19	33.11	61.41
Diamètre des cristallites de Pt (nm)	6.70	4.00	5.33	8.69	6.83	9.50	5.69	5.97
Surface géométrique des particules Pt sur GC (cm^2)	5.90	9.89	7.419	4.55	6.59	4.16	6.95	6.62
Utilisation du Pt (%)	13.69	91.32	70.28	120.62	142.85	71.96	67.35	131.06

Quelques images HRTEM du Pt/CNS (échantillon F_{Pt}) sont montrées à la Figure 5.7. Les images indiquent une distribution uniforme des nanoparticules du Pt métallique sur la surface des CNS fonctionnalisée.

La Figure 5.8a montre la distribution des dimensions des nanoparticules de Pt supporté par les CNS à partir de nanoparticules choisis aléatoirement dans l'image HRTEM. Il est évident de l'histogramme de la Figure 5.8b que ces particules de Pt sont petites (2.8 à 5.8 nm), et distribuées uniformément sur les CNS, ce qui est en bon accord avec la valeur typique de 4 nm pour les nanoparticules de Pt supporté par le Vulcan XC-72 commercial.

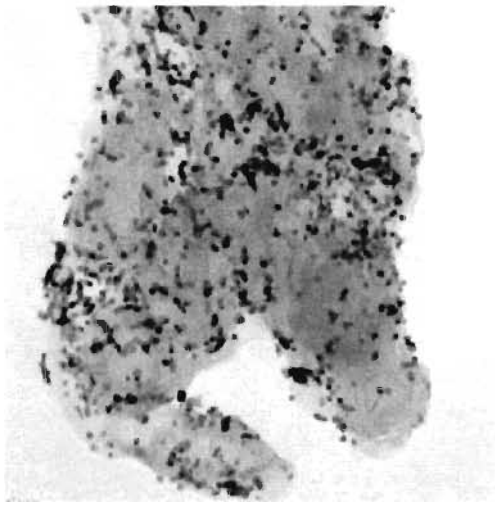

Figure 5.7 Images HRTEM de nanoparticules de Pt supportées sur CNS fonctionnalisé.

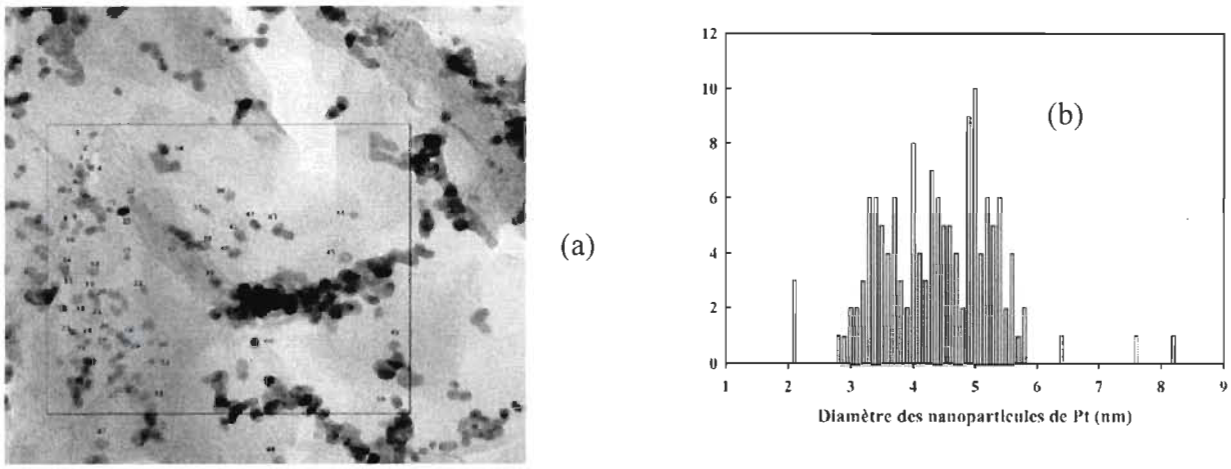

Figure 5.8 (a) Décompte de particules de Pt d'une image HRTEM (b) Distribution des diamètres des particules de Pt obtenue de l'image HRTEM en (a).

Une analyse par spectroscopie atomique d'adsorption (AAS) fut faite sur tous les échantillons platinisés (voir Tableau 5.2) pour évaluer la quantité de nanoparticules de Pt déposé sur les sites fonctionnalisés des CNS. Il est évident que l'échantillon B purifié au HCl avait moins d'oxydes sur sa surface comparée aux échantillons de CNS fonctionnalisés chimiquement. Cependant, il y a peu de sites actifs à sa surface (échantillon B_{Pt}) qui peuvent supporter une quantité de Pt allant jusqu'à 5.3 pd.%.

La voltamétrie cyclique (CV) fut employée pour obtenir la surface électrochimique active des différents échantillons préparés pour ce travail. Ici la CV fut utilisée dans une cellule

conventionnelle à trois électrodes étanches à l'air contenant une solution 1M H_2SO_4 à température ambiante. L'arrangement comprend une électrode de carbone vitrifié (GC) de 2 mm de diamètre, une électrode auxiliaire à fil de platine, et une électrode de référence Ag/AgCl (sat. KCl). Les mesures furent prises à température ambiante avec un poste de travail électrochimique Zahner IMe6. Les charges coulombiques échangées durant l'adsorption et la désorption de l'hydrogène sur les sites actifs de Pt furent calculées par la procédure employée par Pozio *et al.* [81].

En conclusions, nous avons purifier et fonctionnaliser les échantillons de CNS avec un mélange 1:1 de 7.5M d'acide sulfurique et 15M d'acide nitrique, qui avait démontré une performance électrochimique semblable à celle du Pt/C (ETEK) grâce à sa structure poreuse. En plus, la méthode proposée dans ce mémoire avait généré presque 50 % des groupes carbonyles avec moins de 5 % de groupes fonctionnels acides. Ailleurs dans la littérature, il est proposé que ces groupes C=O, agissant comme points d'ancrage pour les nanoparticules de Pt, entravent l'agglomération et la diffusion surfacique des particules de Pt à travers les couches de graphène sous conditions d'oxydation de la cathode.

J. MESURES DE DURABILITE

Le manque de durabilité des PEMFCs est une barrière majeure à la commercialisation de ces systèmes pour des applications stationnaires ou de transport. La dégradation du catalyseur est due à la dissolution et à l'agglomération des nanoparticules de Pt et la corrosion du support de carbone résulte de l'oxydation électrochimique, et cette dernière étant plus prononcée à la cathode où l'oxygène est réduit. Récemment, Kangasniemi *et al.* [33] ont publié les résultats de leur étude sur l'oxydation du Vulcan XC-72 sous différentes échelles de tensions et de températures dans des conditions simulant une PEMFC. Malgré son utilisation répandue, le noir de charbon subit une oxydation électrochimique en oxydes surfaciques et éventuellement se transforme en CO_2 à la cathode d'une PEMFC où il est sujet à des conditions élevées d'acidité, de tension, d'humidité et de température. Donc, quand le support de carbone est totalement corrodé, les nanoparticules de Pt sont perdues de l'électrode ou s'agglomèrent en des particules plus grandes. Le même groupe a étudié aussi l'influence du Pt sur la corrosion du support de carbone et a trouvé que le Pt accélère le taux de corrosion du noir de charbon. Un

procédé générique proposé pour expliquer la formation par étapes de l'oxyde surfacique est montré de façon schématique à l'Équation (4), dans laquelle l'indice inférieur « s » désigne des espèces surfaciques. Il est entendu que l'eau est la source de l'oxygène dans cette réaction [82-86].

$$C_s \rightarrow C_s^+ + e^- \quad (1)$$

$$C_s^+ + \tfrac{1}{2} H_2O \rightarrow C_sO + H^+ \quad (2)$$

$$2C_sO + H_2O \rightarrow C_sO + CO_2 + 2H^+ + 2e^- \quad (3)$$

$$R\text{-}C_s\text{-}H \rightarrow R\text{-}C_s\text{-}OH \rightarrow R\text{-}C_s{=}O \rightarrow R\text{-}C_sOOH \rightarrow R\text{-}H + CO_2 \quad (4)$$

Des études préliminaires [50, 87] ont conclu que les matériaux de carbone avec un haut degré de graphitisation tels que des nanotubes de carbones sont plus stables que le noir de charbon. La raison est que le noir de charbon non graphitisé a une structure turbostratique dans laquelle des cristallites de graphite se mêlent à du carbone amorphe qui n'a pas d'ordre longue-portée. Ce carbone amorphe et les cassures dans les composantes graphitiques furent facilement attaqués par les oxyacides [88, 89]. Par contre, les nanotubes de carbone ont des surfaces graphitiques bien définies sans plans de base possédant des cassures sauf à leurs deux bouts, excluant les défauts dans leur structure tubulaire. Les nanostructures de carbone préparées dans notre laboratoire ont des propriétés semblables aux nanotubes de carbone, cependant sans forme fixe. Par conséquent, le CNS devrait démontrer des propriétés de durabilité semblables aux nanotubes de carbone pour leur utilisation comme support catalytique dans les PEMFCs. L'objectif de cette section est de faire une étude comparative des catalyseurs Pt/C et Pt/CNS suivant des traitements potentiostatiques pour des périodes allant jusqu'à 200 h sous les conditions simulant l'environnement cathodique d'une PEMFC.

Les performances d'une PEMFC d'une cellule unique furent caractérisées en fournissant de l'hydrogène humidifié à 80°C et 100 % d'humidité relative (RH) à l'anode et de l'air humidifié à 70°C et 80 % RH à la cathode avec un rapport stœchiométrique de 1.5 et 2, respectivement. La pression des gaz aux électrodes fut maintenue à 30 psig à l'aide d'un régulateur à pression inverse. Préalablement, la cellule fut conditionnée avec une charge constante de 0.5 A cm^{-2} à 80 °C pendant 50 h. La valeur continue du potentiel de la

cellule à une charge de 1 A cm^{-2} fut calculée à partir des valeurs moyennes des données enregistrées sur une période de 1 h. Afin d'aider l'identification du taux de dégradation de la performance entre le Pt/C et le Pt/CNS, de l'azote de haute pureté (UHP) hydraté (100 % RH) fut passé à travers l'électrode de travail (compartiment cathodique) est de l'hydrogène UHP hydraté (100 % RH) fur passé à travers l'électrode auxiliaire (compartiment anodique).

L'anode sert aussi bien d'électrode auxiliaire que d'électrode de référence (RHE). La température de la cellule fut maintenue constante à 80 °C pendant tout le processus et la pression fut atmosphérique. Ensuite le poste de travail Zahner fur branché en mode voltamétrie cyclique et un potentiel constant de 1.2 V fur appliqué entre l'électrode de travail et la RHE pour accélérer l'oxydation du support de carbone de la couche catalytique (CL) de la cathode. Le potentiel fut maintenu pendant une période de 15 h au cours de cycles répétés de cette expérience.

Avant de mesurer le potentiel à circuit ouvert (OCV – *Open Circuit Voltage*) et le potentiel avec charge, l'alimentation en gaz, les conditions d'humidité et de pression furent rétroajustées aux valeurs mentionnées ci-haut. Après ces mesures, la MEA fut conditionnée pour un bref laps de temps avec une charge de 0.5 A cm^{-2} à 80 °C pendant 30 min. Ce cycle de manipulations fut répété au cours de l'expérience. La Figure 6.1 résume la procédure de corrosion accélérée développée dans notre laboratoire pour évaluer la dégradation de la couche catalytique dans les PEMFCs.

La Figure 6.2 montre les changements relatifs dans le potentiel d'opération de la MEA à des intervalles de temps différents d'oxydation accélérée de la cathode pour le Pt/C (MEA1) et le Pt/CNS (MEA2). Les potentiels sous une charge de 1 A cm^{-2} pour chacune des cellules montrent une décroissance linéaire lente au cours des premières 60 h d'opération dans les deux cas, dont les cathodes avaient été oxydées électro chimiquement avec un potentiel de 1.2 V et à 80 °C.

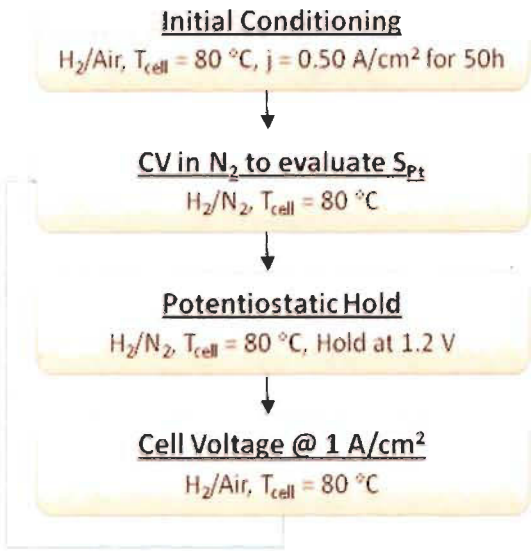

Figure 6.1 Épreuve de corrosion accélérée pour évaluer la dégradation de la couche catalytique.

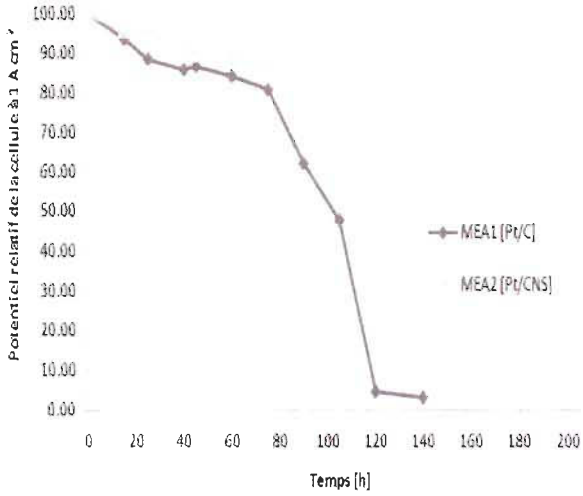

Figure 6.2 Changements de potentiel relatif de la cellule à 1 A cm^{-2} de la MEA1 et de la MEA2 au cours de l'oxydation électrochimique jusqu'à 200 h.

Les fluctuations dans les courbes avant les 60 h de fonctionnement sont attribuées aux niveaux d'humidification de la membrane électrolytique et de l'ionomère dans la couche catalytique. Après 60 h de fonctionnement, on observe une décroissance marquée dans le potentiel de la cellule pour la MEA2, alors qu'une baisse beaucoup plus rapide est observée pour la MEA1. On constate que presque 95 % du potentiel de la cellule fut perdu pour la MEA1 après 140 h du processus d'oxydation accélérée, alors que la baisse du potentiel de la cellule pour la MEA2 ne fut que de 25 %. De plus, la plus grande perte de potentiel pour les deux MEAs a lieu entre 60 h et 140 h, comme le montre la Figure 6.4. Cependant, le taux de chute de potentiel pour la MEA2 est très faible après 140 h. La chute additionnelle fut de seulement 2.36 % après une oxydation continue additionnelle de 60 h. Ceci indique que les CNS avec un contenu graphitique et ordre longue-portée élevé est moins sujet à corrosion sous conditions d'oxydation comparée au Vulcan. Une tendance semblable fut observée aussi pour la mesure d'OCV (Figure 6.4), indiquant que la dégradation de la membrane avait causé la chute de performance de la cellule. Au cours d'une opération prolongée, les MEAs préparées avec du Pt/CNS peuvent possiblement donner une plus grande durabilité que les MEAs préparées avec du Pt/C.

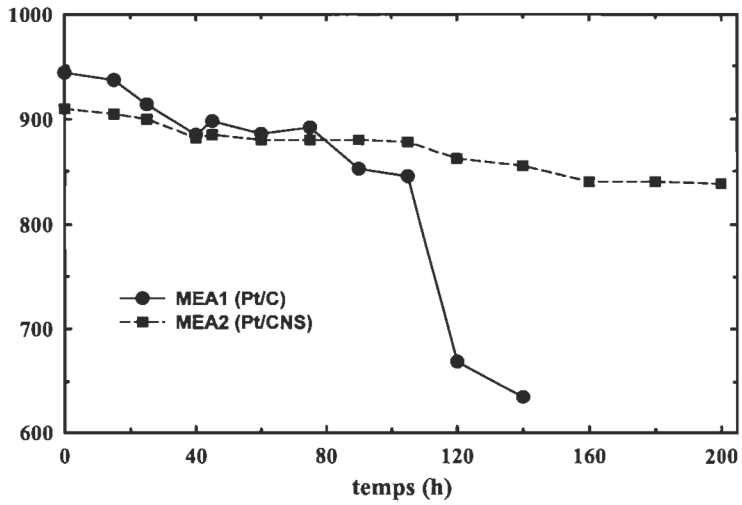

Figure 6.4 Pertes de OCV de la cellule de la MEA1 et de la MEA2 au cours d'une oxydation électrochimique jusqu'à 200 h.

K. PERTE EN SUPERFICIE

Précédant les mesures électrochimiques (CV), le catalyseur de Pt supporté sur du C et CNS fur conditionné dans un four cylindrique et sous une atmosphère de 10 % hydrogène et 90 % argon pendant 1 h à 300 °C afin d'enlever les contaminants de surface et recuire les cristaux de Pt. Des disques de carbone vitrifié (GC) (BASI, 3 mm, 0.07069 cm^2), furent polis à un fini miroir de 0.05 μm (alumina, BASI) avant chaque manipulation et servirent de support pour le Pt/C et Pt/CNS. Une encre contenant le catalyseur supporté en suspension aqueuse fut préparée en dispersant par ultrasons 25 mg de catalyseur dans de l'eau déminéralisée (Millipore) dans un rapport de 2 $mg_{catalyst}$/ml. Un aliquote de 20 μl de la suspension re-dispersée fut alors pipeté sur le disque. Afin d'obtenir une distribution uniforme de cette suspension, l'électrode GC fut séchée à température ambiante pendant une heure avant de la mettre dans un four préchauffé à 80 °C pendant une heure additionnelle. Après évaporation complète de la gouttelette d'eau, 20 μl d'une solution diluée de Nafion (5 pd.% Nafion, Aldrich) fut pipetées sur la surface poudreuse séchée pour renforcer l'adhérence entre la poudre catalytique et l'électrode. Les voltamétries cycliques furent exécutées dans une cellule étanche thermostatée (80 °C) à trois électrodes conventionnelles contenant un électrolyte de 0.5M H_2SO_4. Les potentiels furent mesurés à l'aide d'une électrode à Ag/AgCl (Sat. KCl), mais tous les potentiels mentionnés partout dans cette étude sont référencés à la RHE. Un potentiel continu de

1.2 V fut appliqué à l'électrode de travail et fut tenu pendant 0, 15, 30, 45... et 175 h afin d'oxyder électrochimiquement les carbones. Des voltamogrammes furent enregistrés pour chaque période de temps pour pouvoir calculer le taux et la perte de la surface active du catalyseur causer par l'oxydation électrochimique.

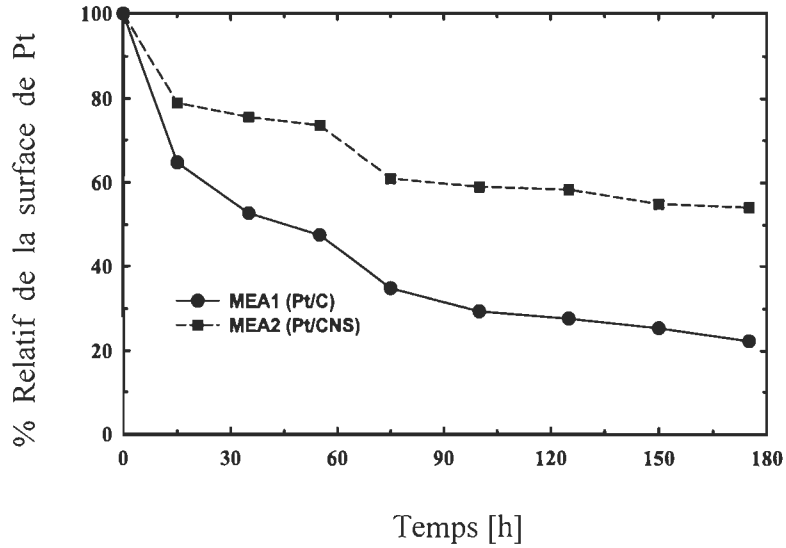

Figure 6.5 Pourcentage de pertes relatives de surface active du Pt pour le Pt/C et le Pt/CNS au cours d'une oxydation électrochimique jusqu'à 175 h.

Pour quantifier l'étendue de la perte en superficie de platine, des mesures de voltamétrie cyclique furent conduites sur du Pt/C et Pt/CNS dans un électrolyte de 0.5 M H_2SO_4 purgé au N_2 à différents intervalles de temps au cours de leur traitement à 1.2 V et 80 °C. La quantité de charges coulombiques impliquée durant la désorption de l'hydrogène fut utilisée pour calculer la surface active de platine des électrodes comme décrit à la Section 5.3.3.4, après avoir corrigé pour la capacité à doubles couches. La Figure 6.5 montre le changement relatif de la surface pour le Pt/C et le Pt/CNS à différents intervalles de temps durant le traitement d'oxydation électrochimique. Durant les premières 15 h d'oxydation, une perte de presque 35 % en surface du Pt fut observée pour le Pt/C, alors que pour le Pt/CNS 20 % a été perdu, comme le montre la Figure 6.5. Pour les 40 h suivantes, la dissolution des nanoparticules de Pt supporté par des CNS fut presque trois fois moindre quand le Pt supporté par du. Après 75 h d'oxydation, une tendance continue décroissante de perte de surface fut observée pour le Pt/C, alors que la perte de surface du

Pt est très petite pour le Pt/CNS. La perte de surface active de Pt explique la chute du potentiel d'opération de la cellule comme mentionné précédemment.

Deux processus d'agglomération des nanoparticules de Pt ont été proposés pour expliquer la perte de surface active électrochimique du Pt dans un électrolyte aqueux [90, 91] responsables de la chute rapide du potentiel de la cellule ainsi que du OCV : (1) dissolution/reprécipitation [92, 94] et (2) migration [95, 96] (diffusion en surface de nanoparticules de Pt). La corrosion rapide du support fait de noir de charbon à la cathode sous des conditions simulées d'oxydation accélérée semble indiquer que ces deux processus d'agglomération sont observés pour le MEA1. La perte de surface spécifique explique le fait que certaines des espèces ioniques du Pt furent redéposées sur d'autres nanoparticules de Pt, produisant une croissance de particules de Pt (*electrochemical Ostwald ripening*). Certaines des espèces ioniques de Pt sont diffusées à l'extérieur de l'électrode et entrent dans la membrane polymère de l'électrode. En général, dans une PEMFC, il existe un gradient de concentration d'oxygène aussi bien que d'hydrogène à travers la membrane polymère électrolytique (*crossover*). Dans la membrane et à proximité de la cathode, il y a une concentration plus élevée d'oxygène et une concentration plus faible d'hydrogène. Sous ces conditions plus riches en oxygène, les ions de Pt forme une bande mais ont de la difficulté à se transformer en Pt métallique parce qu'un noyau très petit de Pt est instable sous un potentiel élevé (potentiel mixte composé d'hydrogène et d'oxygène dissolus). Par conséquent, la génération de la bande de Pt métallique a lieu plus facilement près de l'anode mais, la génération de la bande de Pt ionique à lieux près de la cathode, comme le montre la Figure 6.7. La formation de noyaux de Pt dans la membrane près de l'anode, accélérée par la présence accrue d'hydrogène, stimule la dégradation de l'ionomère. La dégradation typique de la membrane à proximité de la bande de Pt, près de l'anode, à des potentiels proches de l'OCV, vient de la formation de peroxyde d'hydrogène au cours du processus de réduction à deux électrons de l'oxygène. La dégradation de la membrane est reflétée comme une chute soudaine de performance de la MEA1.

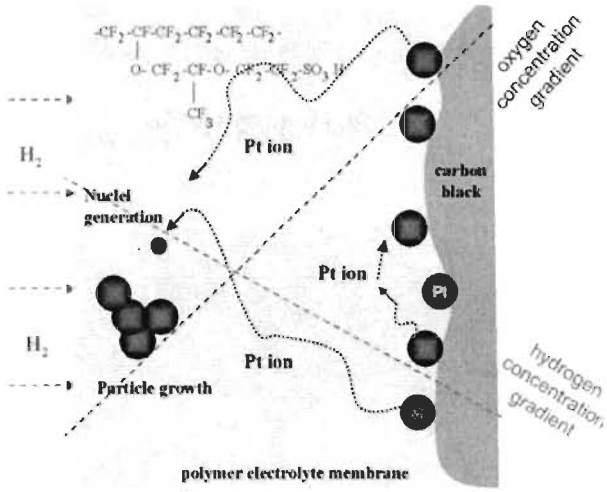

Figure 6.7 Dessin schématique du Pt dans une membrane électrolytique à polymère près de la cathode.

Bien que le CNS préparé dans notre laboratoire contient presque 50 % de groupes C=O comme points d'ancrage du Pt, nous ne pouvons pas exclure la possibilité de la croissance de particules de Pt par migration comme pour MEA1. Par conséquent, la décroissance dans la surface électrochimique active du Pt supporté par des CNS est causée principalement par la dissolution de Pt ancré sur d'autres groupes fonctionnels. Une partie des espèces de Pt ioniques s'agglomère sur d'autres particules de Pt, menant à une croissance de ces particules, et une petite fraction des espèces ioniques diffuse dans la membrane pour former une bande ionique près de la cathode. Bien que nous n'ayons pas fait d'image HRTEM d'une coupe transversale de MEAs qui validerait cette théorie, la performance continue de la MEA2 après décroissance initiale semble confirmer notre hypothèse.

L. CHANGEMENTS DANS LA TAILLE DES PARTICULES

La Figure 6.10 montre une croissance de 20 % dans la taille des particules de platine à partir de sa valeur initiale sur une période d'oxydation électrochimique allant jusqu'à 150 h. L'hypothèse de pourquoi la surface de platine supportée par des CNS subit une perte de 40 % soit causée principalement par la dissolution et l'agglomération d'ions de Pt est considéré comme suit : Premièrement, la chute en pourcentage du potentiel d'opération de la cellule est cinq fois moindre pour la MEA2 comparé à la MEA1. Ceci s'explique par le fait que la densité apparente de la bande de Pt ionique formée proche de la couche

cathodique dans la MEA2 est plus faible que dans la MEA1. Deuxièmement, la bande de Pt est près de la couche catalytique cathodique et a accès à une plus grande concentration d'oxygène grâce au plus grand volume poreux et une meilleure propriété d'hydrophobicité des CNS. La présence de cet oxygène entrave la réduction du Pt ionique and donc, empêche une détérioration additionnelle de la membrane. Troisièmement, si la bande de platine avait été réduite proche de la couche catalytique de l'anode, alors la performance de MEA2 aurait chuté de façon significative à cause de la dégradation de la membrane. Cependant ceci n'est pas le cas pour le MEA2, pour lequel le taux de perte du potentiel d'opération de la cellule est beaucoup moindre comparé à la MEA1.

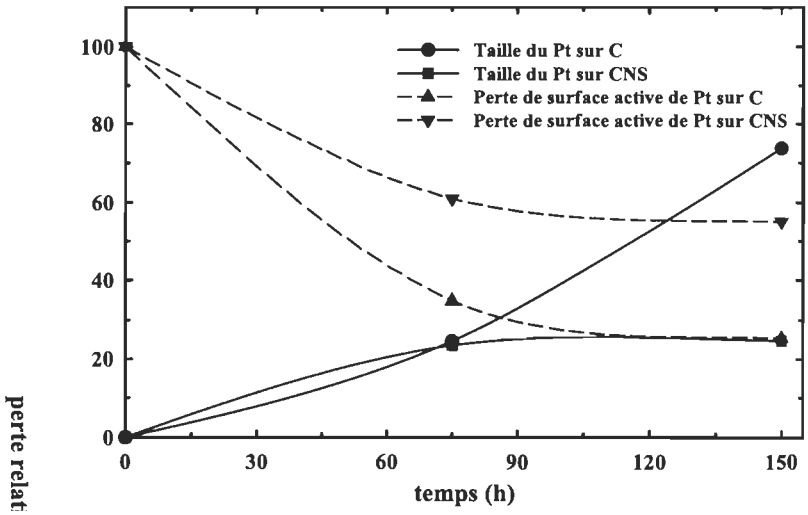

Figure 6.10 Croissance de la taille des particules de Pt comme observée par XRD reliée à la perte de surface active du catalyseur au cours d'oxydation électrochimique du Pt/C et du Pt/CNS.

M. CONCLUSION

À l'intérieur de l'étendue de ce mémoire, un nombre de techniques ont été développées afin d'explorer l'aptitude des CNS à servir de support catalytique dans les PEMFCs. De plus, la durabilité du support est un facteur important dans la commercialisation des PEMFCs. Donc, nous avons examiné la perte de surface spécifique de ce matériau et l'avons comparée à celle du noir de charbon. Le résumé du travail de ce mémoire est comme suit :

- Le broyage mécanique du graphite ou du charbon activé avec des catalyseurs métalliques de transition suivi d'un traitement thermique sous argon est une technique efficace pour préparer des poudres nanostructurées de carbone.
- L'analyse BET de nos échantillons de CNS donna une surface spécifique de 352.6 $m^2 g^{-1}$, un volume microporeux de 0.14 $cm^3 g^{-1}$, et un diamètre microporeux moyen de 1.6 nm. L'analyse des données d'intrusion au Hg donna un rayon macroporeux de 45.8 $m^2 g^{-1}$ et un volume total macroporeux de 635 $mm^3 g^{-1}$.
- La température d'oxydation des CNS était aussi élevée que celle des nanotubes de carbone, indiquant un contenu accru de composantes graphitiques.
- L'oxydation chimique avec une solution 1:1 de 7.5M d'acide sulfurique et 15M d'acide nitrique montra une amélioration notable pour enlever les impuretés et produire des groupes fonctionnels de surface par rapport à d'autres traitements d'oxydation.
- Avec la moitié de Pt supporté sur des CNS par rapport au Pt/C, le Pt/CNS montra des performances électrochimiques semblables au Pt/C, indiquant l'influence d'une structure à porosité accrue favorisant les transports de masse et de concentration.
- Au cours des études de durabilité sur l'électrocatalyseur, la perte de surface spécifique du Pt était due à la croissance de la taille des particules. Cependant, la diffusion des espèces ioniques de Pt dans la membrane causant une dégradation sur un temps d'opération fut observée sur une MEA préparée avec du Pt/C.
- La perte de surface du Pt fut observée en tant que résultat de corrosion du support de carbone sous conditions cathodiques simulées.
- Les caractérisations électrochimiques montrent que les CNS préparés dans nos laboratoires possèdent une meilleure résistance à la corrosion et une performance supérieure par rapport au Vulcan XC-72.

À partir des résultats obtenus dans cette étude, nous pouvons conclure que les CNS peuvent être un bon candidat comme matériau de support pour les catalyseurs dans les PEMFCs, montrant moins de perte de surface sans sacrifice d'activité catalytique.

Ce travail de recherche donna lieux à 3 articles (en annexe):

[1] Sadesh Kumar Natarajan et Jean Hamelin, "Electrochemical Durability of Carbon Nanostructures as Catalyst Support for PEMFCs", *Journal of the Electrochemical Society* 156(2), pp. B210-B215 (2009).

[2] Sadesh Kumar Natarajan, D. Cossement et J. Hamelin, "Synthesis and Characterization of Carbon Nanostructures as Catalyst Support for PEMFCs", *Journal of the Electrochemical Society* 154(3), pp. B310-B315 (2007).

[3] Sadesh Kumar Natarajan et Jean Hamelin, "Homogeneous Pt Deposition on Chemically Modified Carbon Nanostructures as Catalysts for PEMFCs", *Electrochimica Acta* 52(11), pp. 3741-3757 (2007).

ABSTRACT

Polymer electrolyte membrane fuel cell (PEMFC) technology has advanced rapidly in recent years, with one of active area focused on improving the long-term performance of carbon supported catalysts, which has been recognized as one of the most important issues to be addressed for the commercialization of PEMFCs. The central part of a PEMFC is the membrane electrode assembly (MEA) which consists of two electrodes (anode and cathode) and a cation exchange membrane. These electrodes are commonly made of carbon black (most often, Vulcan XC-72) supported on carbon paper or carbon cloth backings. The catalyst layers in the electrodes are where the electrochemical reactions take place and are made of a catalyst (Pt or Pt alloy) supported on carbon black, ionomers for proton conducting, and Teflon binders for hydrophobicity. As mentioned earlier, the durability of these catalyst layers is a crucial issue in PEMFC development and commercialization. Despite its widespread use, carbon black undergoes electrochemical oxidation to surface oxides and eventually to CO_2 at the cathode of a PEMFC, where it is subjected to high acidity, high potential, high temperature and high humidity. As carbon is corroded away, the catalyst metal nanoparticules will be lost from the electrode or aggregated to larger particles. Oxidation of carbon support can also lead to changes in surface hydrophobicity that can cause gas transport difficulties. Moreover, the noble metal catalyst supported on carbon support accelerates the corrosion rate of carbon black using the water produced at the cathode as a fuel for oxidation. Several research groups have proposed that carbon material with more graphite component can be more resistant to corrosion under cathode environment. Therefore, it is the primary objective of this thesis to prepare and investigate carbon nanostructures (CNS, licensed to Hydrogen Research Institute – IRH, Québec, Canada), the carbon material with more graphite component like carbon nanotubes (CNTs) for use as catalyst support in PEMFCs.

High energy ball-milling of activated carbon along with transition metal catalysts under hydrogen atmosphere, followed by heat-treatment leads to nanocrystalline structures of carbon called CNS. However, CNS formed in the quartz tube after heat-treatment is inevitably accompanied by many impurities such as metal particles, amorphous carbon

and other carbon nanoparticules. Such impurities are a serious impediment to detailed characterization of the properties of nanostructures. In addition, since the surface of CNS is itself rather inert, it is difficult to control the homogeneity and size distribution of Pt nanoparticules. In this thesis work, we demonstrated a novel mean to purify and functionalize CNS via acid-oxidation under reflux conditions. To investigate and quantify these nanostructures X-ray diffraction, electrical conductivity measurements, specific surface area measurements, thermogravimetric analysis, X-ray photoelectron spectroscopy and transmission electron microscopy studies were used. Cyclic voltammetry studies were performed on different samples to derive estimates for the relationship between the composition of the acid mixture and their influence in producing high density of surface functional groups. Such surface functionalization on CNS enhances the reactivity, improves the specificity and provides an avenue for Pt deposition. It was also shown that a 1:1 mixture of 7.5 M sulphuric acid and 15 M nitric acid have generated higher composition of non-acidic functional groups over other acid compositions discussed in this thesis. In this thesis, we also demonstrated a novel method to deposit and disperse platinum clusters on carbon nanotubes via a chemically specific nucleation mechanism. To investigate and quantify these platinized CNS X-ray diffraction, thermogravimetric analysis, atomic adsorption spectroscopy and high resolution transmission electron microscopy were used. An average Pt cluster size of 4 nm was dispersed homogeneously on CNS that was functionalized with the method described above.

The corrosive nature of carbon support material is a crucial issue for the commercialization of PEMFC systems. Therefore, electrochemical oxidations of Pt/CNS compared with Pt/C were studied in this thesis with the aim to understand their durability as catalyst support in PEMFCs. The surface oxidation of the catalyst materials has been compared following potentiostatic treatments up to 200 h under condition simulating the PEMFC cathode environment (80 °C, nitrogen purged 0.5 M sulphuric acid, and a constant potential of 1.2 V). The degradation of Pt catalysts and the carbon support was also evaluated by measuring the cell voltage at constant load after different oxidation intervals at 1.2 V. The agglomeration of Pt catalyst particles and the changes in surface functional groups of the carbon material at different intervals of electrochemical

oxidation was evaluated using X-ray diffraction and thermogravimetric studies. The subsequent electrochemical characterization at different treatment time intervals by both the above methods suggests that CNS is electrochemically more stable than Vulcan XC-72 with less surface oxide formation and Pt surface area loss without sacrificing catalytic activity.

This work has resulted in 3 articles (in appendix):

[1] Sadesh Kumar Natarajan and Jean Hamelin, "Electrochemical Durability of Carbon Nanostructures as Catalyst Support for PEMFCs", *Journal of the Electrochemical Society* 156(2), pp. B210-B215 (2009).

[2] Sadesh Kumar Natarajan, D. Cossement and J. Hamelin, "Synthesis and Characterization of Carbon Nanostructures as Catalyst Support for PEMFCs", *Journal of the Electrochemical Society* 154(3), pp. B310-B315 (2007).

[3] Sadesh Kumar Natarajan and Jean Hamelin, "Homogeneous Pt Deposition on Chemically Modified Carbon Nanostructures as Catalysts for PEMFCs", *Electrochimica Acta* 52(11), pp. 3741-3757 (2007).

Student

Director of Research

ACKNOWLEDGMENTS

At the outset, I would like to thank Prof. Jean Hamelin for supervising me and for creating a wonderful opportunity to work on this fascinating subject. His dynamic, innovative and friendly nature certainly made me think without boundaries in different areas of research along with this research work full of confidence to a grand success. This dissertation thesis is a result of his constant encouragement and support. I am thankful for him for the continuing help and gentility.

I would also like to extend my sincere thanks to the directors of hydrogen research institute *late* Tapan K. Bose and Richard Chahine for their constant support throughout the course of my work.

Further it cannot be stressed enough that none of this work would have been possible without the contribution of my colleagues at Hydrogen Research Institute (IRH) and department of physics - Lyubov Lafi, Marie-Andrée Leduc, Lucie Bellemare, France Lemay, Hélène Boisclair and Valérie Sandra Ramanantsoa, for all their helpful comments and advice throughout the course of this work. Thank you! A special thanks to Daniel Cossement, Marie-Hélène Bégin and Agnes Lejeune for helping me with preparation and characterization of carbon materials. Also, I would like to thank Robert Drolet for all his services and guidance in the mechanical lab.

In continuation, I would like to thank all my other colleagues at IRH during the years for providing a nice social atmosphere and a good working environment. Also, I extend my sincere thanks to my parents and friends for their immense love, faith in my abilities and constant encouragement, which gave me strength to complete this work successfully.

Financial support from Natural Sciences and Engineering Research Council of Canada (NSERC), Department of Physics, University of Québec at Trois-Rivières and Hydro-Québec are gratefully acknowledged.

The value of this thesis remains to be judged by those who read it. At least for me personally, this work has been a rewarding experience for the past three years. Thank you all.

TABLE OF CONTENT

LIST OF FIGURES

LIST OF TABLES

1. INTRODUCTION

As the demand for environmentally friendly and cost effective alternatives to traditional power sources continues to grow, it is becoming evident that future energy generation may be somewhat different from that of the present. Many of today's industries, including automotive manufacturers, are investing considerable resources in finding and implementing new technologies to replace conventional power production methods in order to stay competitive in future markets. One of these newly emerging technologies is the fuel cell, which harnesses the chemical energy of hydrogen to produce electrical energy with clean by-products. Although it has been around for more than a century, it is only recently that technological advances have made them competitive with traditional power production methods. This chapter discusses different types of fuel cells in general and of solid polymer electrolyte membrane fuel cells (PEMFC) in particular and addresses my thesis objectives.

There are several fuel cell technologies available, the choice of electrolyte being the governing design factor. High temperature fuel cells, *e.g.* molten carbonate and solid oxide fuel cells (MCFCs and SOFCs), which operate at temperatures between 600 °C and 1 000 °C are generally considered for stationary power generation, for instance replacing gas turbines for producing electricity from natural gas. The high operating temperature, however, results in long start-up times and therefore lower temperatures are desired for mobile (notebooks and mobile phones) and traction (cars and trucks) applications.

The most viable low temperature fuel cell technology today is perhaps the polymer electrolyte membrane fuel cell (PEMFC) [1-3]. The technology is already partly on its road to commercialisation, with a vast spectrum of operating systems and demonstration projects going on globally: submarines, space shuttles, backup power for mobile phone stations, cars and city buses, as well as smaller portable systems providing power for laptops and mobile phones, just to mention a few. These show that the polymer fuel cell may be successfully implemented for electric power generation in various applications. In fact, submarines and backup power for mobile phone stations, the PEMFC technology is already a commercial product, albeit the systems produced are in small series. However, for most other applications there are still a few obstacles yet to be overcome before a

broad commercialisation will be possible. This is mainly due to the fact that the cost of a fuel cell system, compared to other alternatives such as batteries or small diesel-electric generators, is too high today by around roughly one order of magnitude. The system cost will indeed be lowered by mass production, but for at least two of the components, the polymer electrolyte membrane and the catalyst used for oxygen reduction, also scientific breakthroughs may have to be necessary.

The relatively low temperatures of the PEMFC today, generally below 100 °C, result in expensive catalysts having to be used in order to increase the rate of the chemical reactions, especially the oxygen reduction reaction (ORR) at the cathode, where large amounts of platinum need to be used. Even with other electrolyte materials, that allows operation up to 200 °C, platinum or alloys containing platinum, is still the only really viable oxygen reduction catalyst known today in acid media [4-6]. At the current level of the state-of-the-art technology (cathode Pt loading: 0.4 mg cm^{-2}; anode: as low as 0.05 mg cm^{-2}), the Pt storage in the earth would be short to power the growing automobile market with a 100 kW fuel cell stack which needs 100 g Pt. According to the United States Department of Energy [7] cost reduction targets, the total platinum loading in a membrane electrode assembly (MEA) must be reduced to < 0.03 mg cm^{-2}. At present, two approaches [8-9] toward the reduction of Pt usage in the PEMFC catalysts are continuing to be very active:

(a) exploration of non-noble metal or low platinum content alloy catalysts, and
(b) reduction of Pt loading through the usage of non-precious, high surface area, electrically conductive supports.

With respect to non-noble metal catalysts, there have been no significant breakthroughs in the areas of materials and technology. However, several research groups are currently working on this most difficult task of replacing Pt by non-noble metal catalysts. As for this approach of using non-noble metal catalysts, several candidates, such as transition metal chalcogenides [10-11], transition metal oxides [12], macrocycles (porphyrin or phthalocyanine) whether heat treated or not [13-14] and so on, have been proposed over the years for cathode electrocatalysts. The calculated volumetric activity, which is the product of the volumetric site density and the average turn-over frequency of Fe catalyst

is 159 times below the target of $1/10^{th}$ performance of Pt state-of-the-art technology set by Gasteiger *et al.* [16]. To split the target drops for volumetric site density and average turn-over frequency by factors of approximately 25 and 7, respectively. With the average turn-over frequency being a characteristic for Fe site, the performance improvement has to come from volumetric site density. The enhancement of volumetric site density can be achieved by increasing the catalyst loading. However, the additional catalyst loading compromises 100 μm cathode thickness limit set by Gasteiger *et al.* [16] and consecutive performance drop can be expected due to mass- and charge-transport limitations.

Recent studies on Pt alloy catalysts have attracted wide attention as a candidate to reduce Pt loading, to achieve high performance, to increase in power density and to reduce the electrode cost of PEMFC stacks. Many approaches have been reported for Pt catalytic activity enhancement towards ORRs in fuel cell applications [17-21]. In particular, Pt alloyed with Ni, Co, Cr, Fe and Mn have attracted much interest due to their enhanced catalytic activities towards ORR in PEM fuel cell developments. Mukerjee and Srinivasan [22] reported carbon-supported Pt/Cr, Pt/Co and Pt/Ni alloy catalysts showed a performance gain of 20 to 30 mV over Pt at low current density range. Later, Johnson Matthey [16, 18-22] investigated carbon-supported Pt/Fe, Pt/Mn, Pt/Ni, Pt/Ti, Pt/Cr and Pt/Cu alloy catalysts for PEMFCs, demonstrating that Pt/Ti, Pt/Mn and Pt/Fe catalysts could enhance fuel cell performance by 20 to 40 mV at a practical current density range. Tafel plot with slope 60 mV dec^{-1} were found for Pt alloys, which are similar to that of pure Pt catalysts, suggesting that the ORR mechanisms and activity may not be changed significantly. Recently, ternary Pt alloys together with binary Pt alloys have been developed. Tamizhmani and Capuano [23] reported that a carbon-supported Pt/Cr/Cu ternary alloy showed two times greater activity towards ORR than pure Pt. The mixture of Pt/Cr/Cu alloy with base metal oxides such as copper oxide and chromium oxide could enhance the activity by a factor of six compared to a pure Pt catalyst [23].

However, with many positive reports factored in Pt alloy catalysts, one concern with Pt alloys in the fuel cell environment is dissolution of transition metal. A recent study [24] with Pourbaix diagrams indicate that most alloy metals mentioned above are soluble at a potential between 0.3 and 1 V versus standard hydrogen electrode (SHE) and at a pH of around 0. The value of 0 is a typical pH of the medium to which Pt alloys are subjected to

with perfluorosulfonic acid as an electrolyte in PEMFCs. Metal cations from the dissolution could easily exchange with a proton of the membrane because of a stronger affinity of metal cations than proton with the sulfonic group [25]. Exchange of metal cations with the sulfonic group might affect the performance of the fuel cell as categorized to three aspects [25]: (a) decreasing the ionic conductivity as low as 50% down from its original value; (b) reducing water content and dehydrating membranes and (c) suppressing ORR kinetics by a decrease of oxygen concentration or oxygen diffusion coefficient in ionomer film.

The attractive features of high electrical conductivity, chemical stability and low cost lead the extensive application of carbon materials for the precious metal catalyst support [4-6]. In PEMFCs, the most common low Pt loading catalysts are Pt or Pt alloys supported by high surface carbon black used at both anode and cathode. Despite its widespread use, carbon black is known to undergo electrochemical oxidation to surface oxides, and eventually to CO_2 at the cathode of a fuel cell, where it is subject to high acidity, high potential, high humidity, and high temperature (~80 °C) [26-32]. Furthermore, during the start-up and shutdown of a fuel cell, local cathode potential can reach as high as 1.5 V, which significantly speeds up the carbon corrosion [33]. As carbon is corroded away, noble metal nanoparticules will be lost from the electrode or aggregated to larger particles. Oxidation of carbon support can also lead to changes in surface hydrophobicity that can cause gas transport difficulties [26-31]. Several research groups [34-41] have significantly reduced the corrosion on the carbon support by using carbon materials with more graphitic content such as carbon nanotubes, carbon nanofibers, *etc.* In 2004, Daniel Cossement *et al.* filed a U.S. patent [42] for the preparation of carbon nanostructures (CNS) in a two stage process: high-energy ball milling of activated carbon with transition metal catalysts, followed by heat treatment under controlled atmosphere. The CNS originally prepared as a hydrogen storage material was found to have highly-ordered graphitic planes, comparable electrical conductivity of that of carbon black, higher specific area and finally, a structure of carbon filled with meso- and macro-pores. The unique properties of CNS attracted the use of this material as a catalyst support for PEMFCs.

Most of this research work was performed at Hydrogen Research Institute (Institut de recherche sur l'hydrogène) facility, Université du Québec à Trois-Rivières, Quebec, Canada during the period of May 2005 to August 2008.

2. THEORETICAL BACKGROUND OF PEMFCs

2.1 INTRODUCTION

The PEMFC is a relative newcomer in the field of fuel cell technology. The development of this fuel cell type started in the 1950's. The first applications were in space and military systems, submarines and other special applications where cost is not an issue but exceptional performance is required.

Rapid development during the past decade has brought the PEMFC significantly closer to commercial reality. This fuel cell type has received increasing attention especially due to the need of the automotive industry to find a replacement for the internal combustion engine. Prototypes of fuel cell electric vehicles have already been introduced by several companies.

Other promising applications are also emerging. The PEMFC is well suited for applications where quick start-up and quick response to load changes is required and where a low operating temperature and high power density are benefits. Low operation temperature enables, for example, intermittent operation without significant energy losses. PEMFCs are being considered for stationary power generation in peak load and demand-side management applications and other distributed power production purposes. Residential applications have also received a lot of attention in the recent years. Prototype power plants operating on reformed natural gas are being field-tested.

PEMFCs could also be used as power sources in portable electronic devices, which currently are powered by primary or rechargeable batteries. The major disadvantages of batteries are their limited energy capacities and slow recharging. Storing energy for example in the form of hydrogen in metal hydrides, and converting the stored hydrogen to electricity in a fuel cell could allow higher energy capacities with respect to size and weight.

The fundamental difference between fuel cells and batteries is that a fuel cell is only an energy conversion device, whereas batteries are both energy storage and conversion devices. The electrodes of a battery are at the same time reactants, which are consumed in the electrode reactions. Either the depletion of the reactants or the accumulation of by-

products will eventually stop the delivery of power. The battery must then be either recharged by reversing the reaction, or replaced.

In a fuel cell energy system, on the other hand, the conversion and storage functions are separated from each other. It can operate as long as reactants are supplied to the electrodes. The composition of the fuel cell itself remains unchanged. Several benefits result from the separation of the storage and conversion functions. For example, power and energy capacity can be sized independently of each other, and many different fuels can be used as the primary energy source of the system.

2.2 ELECTRODE REACTIONS AND CELL STRUCTURE

The total reaction that takes place in the PEMFC is the reaction of hydrogen with oxygen to produce electricity, heat and water. At the anode, hydrogen atoms are oxidized and at the cathode, oxygen is reduced. The electrons liberated in the anode reaction are consumed in the cathode reaction when a load is connected to the electrodes. The protons migrate to the cathode through the electrolyte membrane. The principle is illustrated in Figure 2.1 [43].

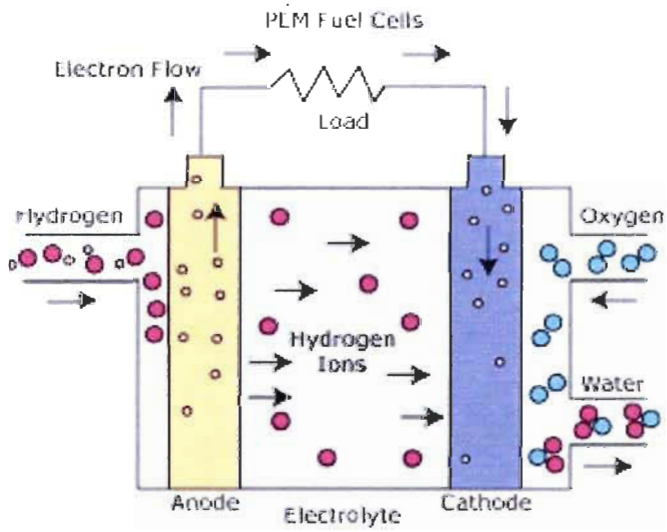

Figure 2.1 Schematic drawing of an operating PEMFC.

The reaction equations of the half-cells and the total reaction are:

Anode	$H_2(g) \rightarrow 2H^+ + 2e^-$	(2.1)
Cathode	$½\ O_2 + 2H^+ + 2e^- \rightarrow 2H_2O\ (l)$	(2.2)
Overall reaction	$½\ O_2 + H_2 \rightarrow 2H_2O\ (l)$	(2.3)

The main functional parts of one unit cell are illustrated in Figure 2.2. For practical applications, several unit cells are combined in series to produce the desired voltage.

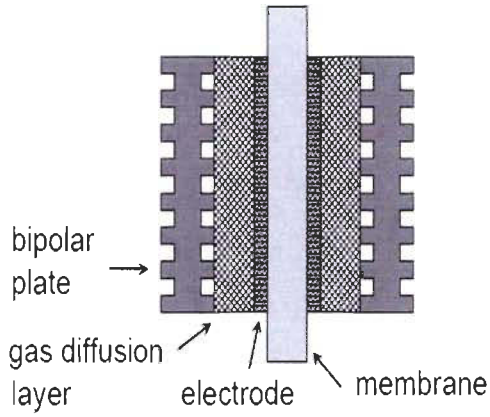

Figure 2.2 Components of a single PEMFC system.

The basic structure of a PEMFC stack is illustrated in Figure 2.3. A high-power stack may also contain cooling plates and other features not appearing in the illustration. The development of stacks was outside the scope of the present work.

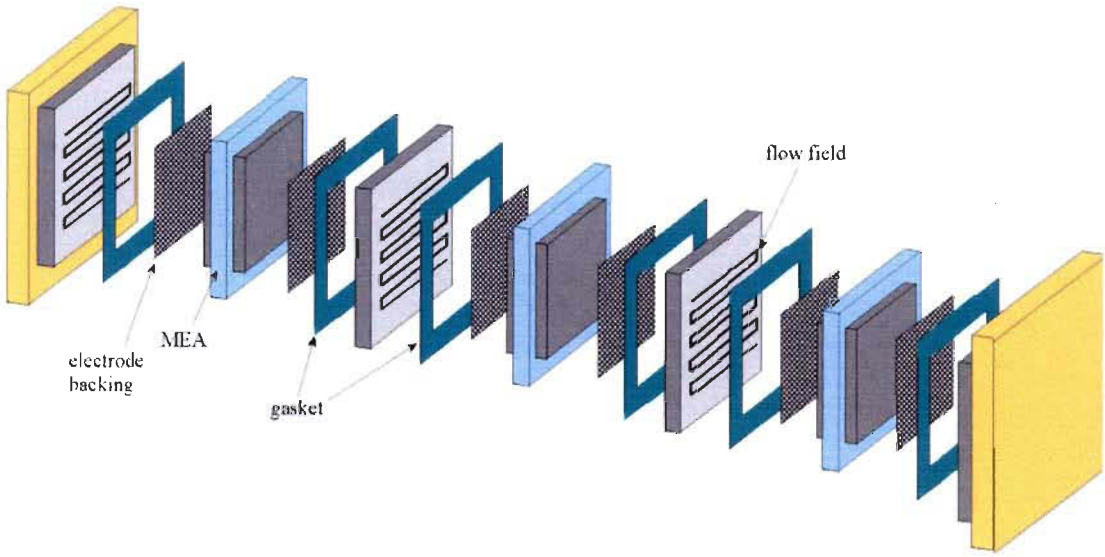

Figure 2.3 Exploded view of a PEMFC stack.

2.3 SOLID POLYMER ELECTROLYTE MEMBRANE

As the abbreviation PEMFC implies, a proton conducting polymer membrane is used as the electrolyte in this fuel cell type. Membrane thickness ranges from 12 to 210 μm for commercial products. The membrane is an acid electrolyte in which the negative ions are immobilized in a polymer matrix. It must remain hydrated in order to be proton conductive, which makes water management a central issue in PEMFC development. The requirement to keep the membrane hydrated also restricts the operation of the cell to temperatures under the boiling point of water.

The benefits of a thin solid electrolyte include high power density and the lack of corrosion and stability problems of liquid electrolytes. Because of the acidic electrolyte, reactant gases that contain carbon dioxide can be used. This is a significant advantage compared to alkaline fuel cells. The membranes used in the experimental part of this work are commercial PTFE-based Nafion membranes by DuPont de Nemours & Company. The development of new membrane materials was not a part of the present work. Nevertheless, understanding of the membrane is necessary for the successful design and operation of the PEMFC.

2.4 MEMBRANE ELECTRODE ASSEMBLY (MEA)

The MEA consists of a membrane and two electrodes, one on each side. The electrodes contain catalyst particles, which are normally either platinum or an alloy of platinum and other noble metals. Due to the low operating temperature, catalysts are essential for achieving good performance.

In order to be able to catalyze the cell reactions, the catalyst particles are to be located in such a way that they form a three-phase boundary. Catalyst particles must be in contact with both electron (in most cases, catalyst support) and proton conductors (Nafion). Passages must be left for reactants to reach the catalyst sites as well as passages for reaction products to exit. An essential goal in electrode development is thus to maximize the utilization of catalyst, *i.e.* the fraction of all catalyst area that is a part of the three-phase boundary.

For acceptable performance, the required amount of real catalyst surface area (*i.e.* the three-phase boundary area) must be considerably higher than the geometric area of the electrode. The electrode must therefore be a three-dimensional porous network of catalyst particles, electronic and protonic conductors and passages open for gas transport.

Traditionally MEAs have been manufactured by impregnating the porous gas diffusion layer with catalyst ink, which is usually placed close to the side facing the membrane. The ink consists of carbon supported catalyst and Nafion emulsion. Electrodes prepared this way are then placed in contact with the membrane. The sandwich structure comprising the catalyst-loaded gas diffusion layers and the membrane is then called the MEA.

The basic problem of gas diffusion electrodes is low utilization of catalyst and thus high catalyst loading required for acceptable performance. The resulting platinum cost is too high for most practical applications. Gas diffusion electrodes and MEAs by E-Tek Inc., ElectroChem Inc. and others are used, however, in this work as anode.

This strive to reduce catalyst loading of the electrodes has led to the development of thin-film electrodes. This means depositing the carbon-supported catalyst as a thin layer on the surface of the membrane. The most widely used is the ink method, in which the carbon supported catalyst is mixed with Nafion emulsion with solvents and then distributed on the membrane by spraying or other suitable method. This may be followed by hot pressing. A catalyst loading of 0.1 to 0.3 mg cm^{-2} per electrode is typically obtained by the ink method while retaining good performance. The thickness of a thin-film electrode is typically 5-15 μm.

When the electrodes are of the thin-film type, the gas diffusion layer does not contain any catalyst. An additional benefit of this concept is that the layers can be separately diagnosed and optimized. The conceptual difference between gas diffusion electrodes and thin-film electrodes is illustrated in Figure 2.4. However, in this thesis all the MEAs prepared either by hand-painting or spraying the catalyst ink over the surface of gas diffusion media.

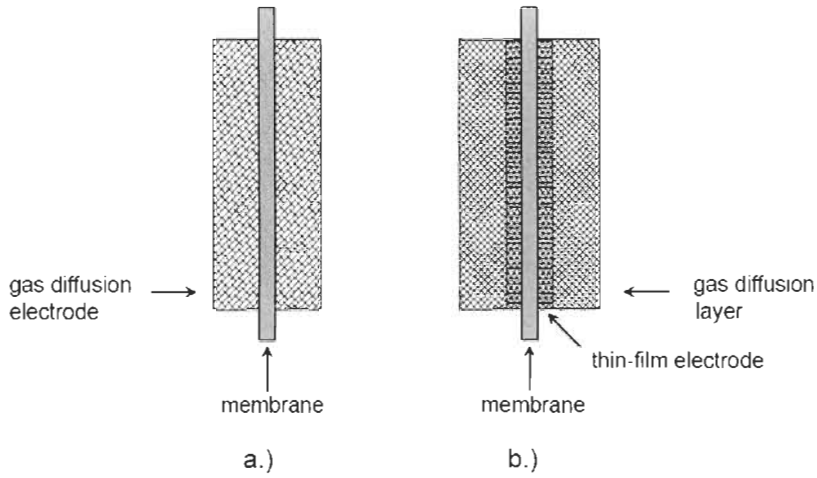

Figure 2.4 Different MEA structures (a) gas diffusion electrodes and (b) thin-film electrodes.

2.5 GAS DIFFUSION LAYER (GDL)

The gas diffusion layer is made of a sufficiently porous, electrically conductive material. The most common materials are carbon cloths and carbon papers, which are commercially available from several manufacturers. The gas diffusion layer provides electric contact between the electrode and the flow field plate. It also enables the reactants to be diffused to the parts of the electrode, which are under the ribs of the flow field plate. At the same time, it must allow the water formed at the cathode via gas channels and permit the passage of water between the gas streams and the membrane surface.

The gas diffusion layers are characterized by their thickness, the presence of hydrophobic and hydrophilic regions, dry resistance to flow and electric properties. Resistance to flow in a dry state should be minimized and electric conductivity maximized. For these reasons, thinner gas diffusion layers are generally better, although this may not be universally true for all fuel cell systems. The typical thickness of commercial products is 300-400 μm.

2.6 ELECTROCATALYSTS IN PEMFCs

2.6.1 FUNDAMENTALS

Platinum, atomic number 78, is a precious metal, roughly three times more expensive than gold. Not only the high price, normally fluctuating around 2 000 USD per ounce is an issue, but also the supply of the precious metal, since the total amount of platinum available on earth may end up being a limiting factor for broad commercialization of fuel cell vehicles. Platinum bulk metal forms a face-centred-cubic (FCC) crystal structure, resulting in surfaces generally based on the 110, 100 or 111 crystal planes, all with somewhat different electrochemical behaviour. The electrocatalytic reactions take place on the available surface of platinum, and one generally aims for the largest surface-to-mass ratio possible. This is done by synthesising small particles in the single nm-range and then dispersing them onto larger carbon support particles. In this way large surface areas are achieved. For instance, given the density for bulk platinum (21.3 g cm^{-3}), 3 nm spherical particles have a theoretical mass specific area of about 47 $m^2 g^{-1}$. To maximize the area one would like to have as small Pt particles as possible, but stability constraints and synthesis methods usually limit the size to a few nanometers. In addition, a smaller particle size is not always beneficial for the catalytic mass activity since other effects such as different lattice constants at smaller sizes, edge effects or different governing crystal planes for smaller particles may lower the activity when decreasing the size of the catalyst particles. A TEM (transmission electron microscopy) picture together with schematic drawing of nm-platinum grains dispersed on a carbon-support particle is shown in Figure 2.5.

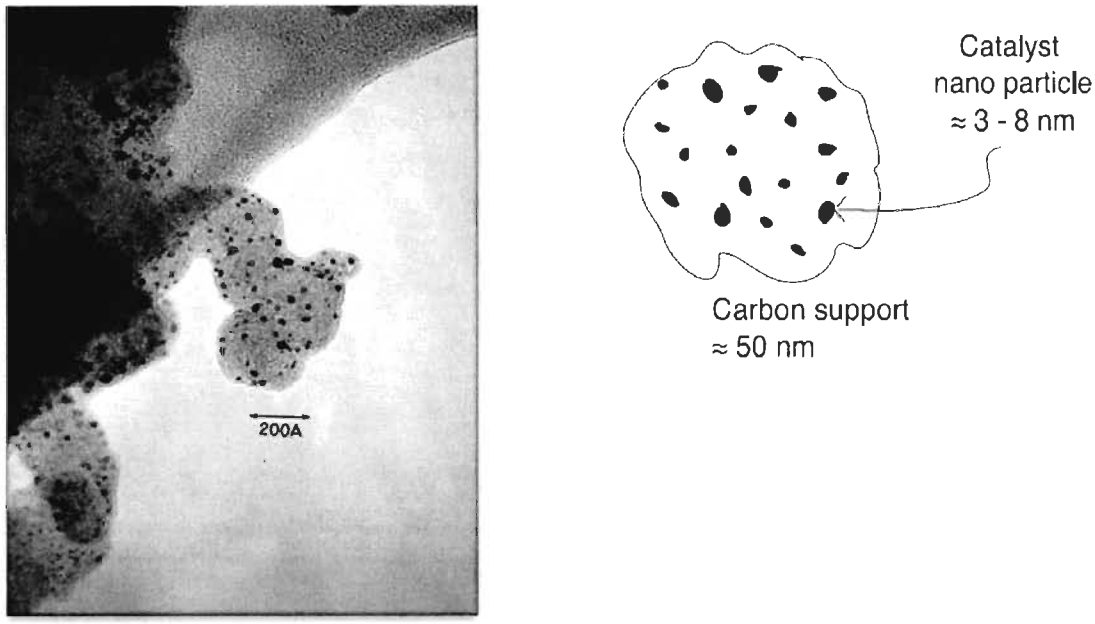

Figure 2.5 Left: TEM image [44] of commercial ETEK 20% Pt dispersed on Vulcan XC-72. Right: Schematic picture of a catalyst supported particle.

Generally, a supported catalyst has a much larger surface area compared with an unsupported catalyst, and a mixed polymer ionomer containing catalyst within the catalyst layer has tremendously increased the number of electrochemical reaction sites, so-called three-phase boundary. Carbon has been used for many years as a support for industrial precious metal catalysts, and activated carbon, carbon black, graphite and graphitized materials have all been applied in various catalytic processes. However, in fuel cell area by far, the application and studies on comparing different forms of carbon support for fuel cell electrocatalysts is quite sparse. Two main types of carbon black have successfully been used as support for Pt catalysts: oil furnace blacks and acetylene blacks. Oil furnace blacks are manufactured from aromatic residue oils from petroleum refineries, while acetylene blacks are made by thermal decomposition of acetylene. In general, furnace blacks have surface areas ranging from 20 to 1 500 $m^2 g^{-1}$, while acetylene blacks typically have areas below 100 $m^2 g^{-1}$, but development products are now available with areas up to 1 000 $m^2 g^{-1}$. However, a common choice of catalyst support material is the furnace black carbon, Vulcan XC-72 prepared by Cabot Corporation with BET surface area of 235 $m^2 g^{-1}$. Important features of a catalyst support include high specific surface area, resistance to corrosion, the adhesion of the catalyst

particles to the support and the interaction with the polymer, *i.e.* the resulting structure and the distribution of the different phases (electron, gas molecule and ion transport) in the electrode.

2.6.2 PLATINUM ELECTROCHEMISTRY

Even though platinum is considered a noble metal it is not at all inert in the voltage window of an operating fuel cell. This is due to the interaction with water, something that is readily seen by performing cyclic voltammetry in an inert atmosphere (Figure 2.6) [45]. Below 0.4 V vs. RHE (the reversible hydrogen electrode) various hydrogen adsorption-desorption peaks appear, the peak positions somewhat depending on the governing crystal plane. The integrated peak charges may be used to assess the electrochemically active platinum surface, since a fully covering monolayer corresponds to a charge of 210 $\mu C\ cm^{-2}$ for a poly-crystalline Pt surface [46].

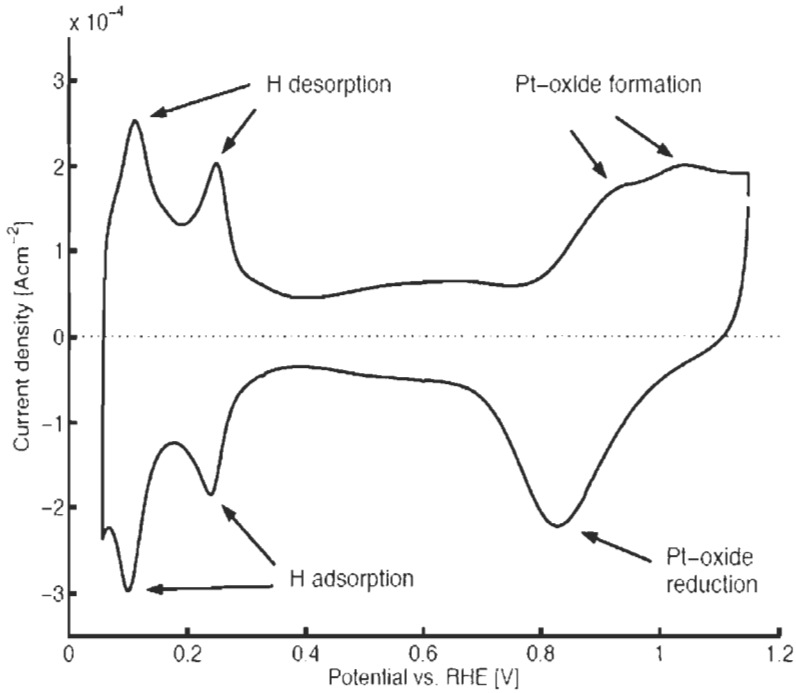

Figure 2.6 A sample CV [45] in nitrogen for a polycrystalline Pt coated on the working electrode.

At potentials above 0.8 V platinum is oxidised. Several different types of oxides and multi-layered oxide films may be produced depending on sweep conditions [47]. Generally one may write:

$$Pt + xH_2O \rightarrow Pt\text{-}O_xH_y + (2x\text{-}y)H^+ + (2x\text{-}y)e^- \quad (2.4)$$

It has also been shown by non-electrochemical methods that the creation and removal of these oxide films may cause structural changes of the platinum crystal close to the surface, and that there are hystereses effects present regarding the structural changes when performing cyclic voltammetry [48]. The oxidation of platinum will normally create a mixed potential at oxygen/platinum electrodes in the presence of water, making it troublesome to experimentally observe the reversible potential for oxygen reduction in practical systems [49].

2.6.3 DURABILITY OF ELECTROCATALYST

Carbon is not thermodynamically stable at higher potentials in the fuel cell environment, something that may be problematic for long-time durability of the electrodes. Carbon support corrosion of cathode catalysts in PEMFCs is a major contributor to the catalyst degradation. In state-of-the-art PEMFCs, carbon black (amorphous carbon + turbostratic structure of carbon) is normally used as catalyst support material. Despite its widespread use, high surface area support is susceptible to corrosive conditions at the cathode, which include high water content (hydrolysis of surface carbon), low pH (<1), high temperature (60 to 90 °C), high oxidative potential (0.6 to 1.2 V), and high concentration of oxygen. It has also been reported that platinum catalyses the oxidation of the carbon support. Oxygen atoms generated by catalyst particles, and at elevated temperature, the surface carbon atoms are able to react with oxygen atoms and/or water to generate gaseous products such as CO and CO_2 that leave the cell along with the cathode gas.

During start-up and shut-down of a fuel cell, local cathode potential can reach as high as 1.5 V, which significantly speeds up carbon corrosion. This loss mechanism removes carbon support from the cell that leads to reduction of the carbon content in the catalyst layer over a period of time. As the carbon support is corroded away, noble metal nanoparticles will be lost from the electrode or aggregated to larger particles, which result in loss of overall fuel cell performance. The remaining dissolved ionic species diffuse out of the electrode into the polymer electrolyte membrane and, in the extreme, a structural collapse of the ionomer. Oxidation of the carbon support can also lead to changes in surface hydrophobicity that can cause gas transport difficulties.

One strategy to reduce Pt/C catalyst performance degradation due to carbon corrosion is to use alternative more stable carbon support. For example, it has been proposed that carbon material with more graphite component can be more stable under oxidative conditions of the cathode environment. Recently, carbon nanotubes have been proposed as promising support material for fuel cell catalyst due to its unique characteristics, including high aspect ratio, high electron conductivity and enhanced mass transport capability.

2.7 INVENTION OF CARBON NANOSTRUCTURES (CNS)

The ideal catalyst support material should have the following characteristics: provide a high electrical conductivity, allow the reactant gas to get to the electrocatalyst easily, have adequate water-handling capability at the cathode where water is generated, and also show good corrosion resistance, as described earlier, cathodes in PEMFCs are under strong oxidizing conditions. Generally, the electrocatalysts are supported on high surface area carbon black with a high mesoporous distribution and graphite component. For PEMFCs, Vulcan XC-72 carbon black is the most widely used carbon support for the preparation of PEMFC catalysts because of its good compromise between electronic conductivity and BET surface area.

Daniel Cossement *et al.* [42] prepared a carbon material with more graphite component, later referred as carbon nanostructures (CNS) in a two stage process: high-energy ball milling of activated carbon with transition metal catalysts under hydrogen atmosphere, followed by heat treatment at 700 °C for 90 min during which CNS grow on the catalyst template. Characterization of this carbon material has shown highly-ordered graphitic planes, comparable electrical conductivity to that of carbon black, higher specific surface and presence of meso/macro pores. The unique properties of CNS were very similar to that of carbon nanotubes have attracted the use of this material as a catalyst support for PEMFCs.

3. THESIS OBJECTIVES

One of the objectives of this work is to study the behaviour of activated carbon (CNS 201) during high energy ball-milling with transition metal catalysts under hydrogen atmosphere and subsequent heat treatment to prepare well defined carbon nanostructures with higher specific surfaces. Having an understanding of the composition that affect the growth of CNS and how the ball milling conditions influence the hydrogen adsorption on pulverized composition are important to prepare better CNS with more graphite component. This thesis also investigates the intensity of CNS, their electrical conductivity, BET surface area and porosity.

The raw CNS prepared in our laboratory is accompanied with unwanted impurities such as transition metal or metal oxides, amorphous carbon and other carbon nanoparticles. The foremost objective of this thesis was to distribute homogeneously the platinum particles on CNS surface and to evaluate the durability of the support under the PEMFC cathode environment. In order to disperse Pt particles on the surface of carbon and for its use as a catalyst support, the unwanted impurities had to be removed and surface functional groups had to be attached to carbon atoms surfaces. These functional groups facilitate the deposition and dispersion of platinum clusters on CNS via a chemically specific nucleation mechanism. Another objective of this thesis was to remove these unwanted impurities and attach surface functional groups to surface carbon atoms in a single step acid-oxidation method. This thesis also concerns to optimize the composition of the acid mixture and also the reflux conditions to effectively remove these impurities and at the same time adds different types of functional groups to CNS. X-ray Photoelectron Spectroscopy (XPS) was used to analyze and compare elemental composition, chemical state and electronic state of the elements, carbon and oxygen composed in non-oxidized CNS and acid oxidized CNS. XPS spectra was obtained by irradiating the above samples with a beam of X-rays, while simultaneously measuring the kinetic energy and number of electrons that escape from the top 1-10 nm of the material being analyzed.

It is well known that the particle size and the distribution of Pt-based catalysts are key factors that determine their oxygen reduction reaction (ORR) activity and cell

performance for PEMFCs. It has also been reported [33, 50] that the catalyst particle size increases and the electrochemical surface area decreases with increased loadings of the supported catalyst. The supported Pt loading was estimated using Atomic Adsorption Spectroscopy (AAS) with Varian Spectra AA 55 and by Thermo Gravimetric Analyzer (TGA). TGA is also performed on non-platinized CNS to study about the type of nanostructures present in the carbon material. There again, XRD pattern and High-Resolution Transmission Electron Microscopy (HRTEM) studies were performed to estimate the dimension and dispersion of Pt clusters. Another objective of this thesis is to study the electrocatalytic surface process of Pt supported on CNS by using the cyclic voltammetry (CV) technique. CV technique enables, for example, comparison of electrocatalytic properties of Pt/CNS catalysts manufactured or pre-treated in different ways. This part of the objective also involved the estimation of the active surface area of Pt catalysts supported on carbon black and CNS.

Electrode material durability is an important factor in limiting the commercialization of PEMFCs. Therefore, the final objective of this research work is to clarify the essential factors related to degradation of PEMFC electrodes and also to study the durability of cathode catalyst layers of MEA prepared with Pt/C and Pt/CNS. This objective involved the study of the degradation in the carbon material upon accelerated electrochemical oxidation under similar conditions of cathode. MEA fabrication and testing, characterization of catalysts, Pt particle size analysis, loss in active surface area and changes in surface functional groups during different time intervals of electrochemical oxidation are some of the essential factors involved in this work.

4. CARBON NANOSTRUCTURES

4.1 INTRODUCTION

Generally, three different techniques are used to produce nanostructured carbons - arc discharge, laser ablation, and chemical vapour deposition (CVD). However, CVD technique is the most widely used, as it has the advantage of producing a large quantity of nanostructures, like multi-walled carbon nanotubes at a relatively low cost. In this study, we present a new technique associated with CVD to produce CNS, where nanostructures are formed on Fe/Co metallic nanocrystals, which is composed of two distinct steps. The first step is high energy ball milling of activated carbon (CNS 201) with transition metal catalysts (Fe and Co) under a hydrogen atmosphere. High energy ball milling pulverizes the contents more rapidly and improves reversible dissociative adsorption of hydrogen on broken carbon sites. The second step involves heating of milled contents under argon atmosphere. It is during this step that the production of methane due to a catalytic reaction between the carbon and the bonded hydrogen is observed, followed by the formation of metallic nanocrystals (Fe, FeCo and Fe_7Co_3), and from a temperature of approximately 700 °C, the formation of CNS on the nanocrystals and H_2 gas.

4.2 PREPARATION OF CNS

The precursor carbon material was initially heated at 1 000 °C under vacuum for 90 min to get rid of moisture content and other impurities. In a hardened steel crucible, pre-treated CNS 201 was mixed with a certain quantity of Fe and Co (99.9% pure). Typical proportions are respectively 50 wt.%, 44 wt.%, and 6 wt.% for C, Fe, and Co, respectively. Three to five hardened steel balls were used during milling, with a relative mass of balls to sample of 35 to 1. Hydrogen was then introduced to the crucible to a pressure of 1.4 MPa and the sample was milled for 12 h. The mill is a SPEX®, which produces more mechanical energy than a planetary mill, but has the disadvantage of contaminating the sample with Fe by attrition. However, this can be ignored considering the fact that Fe was one of the catalysts to the crucible. During the second stage, the milled sample was transferred under an inert atmosphere into a quartz tube, which was then heated to 700 °C for 90 min. The quartz tube is connected to a sampling cylinder for gas analysis.

4.3 THEORY

After ball milling, X-ray analysis showed the formation of Fe, Fe_3C and Fe_7C_3 and also, the analysis of the residual gases in the crucible after milling showed the presence of methane (CH_4) and traces of heavier hydrocarbons. The process could be explained as followed: First, during the mechanical synthesis, a metallic carbon is formed:

$$3Fe + C \rightarrow Fe_3C.$$

The ball milling of the carbon material in a hydrogen atmosphere produces a completely amorphous carbon sample and induces the formation of metallic carbons by mechanical synthesis, such as Fe_3C and Fe_7C_3, and carbon hydrogenation while eventually releasing methane. The chemistry of methanation can be described with the following reaction [51],

$$FeC + 4FeH \rightarrow CH_4 + 5Fe,$$

involving the following sequence of elementary steps:

1. The following reaction involves the reversible dissociative adsorption of hydrogen on the iron surface,

$$H_2 + 2Fe \leftrightarrow 2Fe\text{-}H_{ads}.$$

2. During the mechanical synthesis, the carbon gets adsorbed on the metallic iron surface,

$$Fe + C \rightarrow Fe\text{-}C_{ads},$$

which is hydrogenated by the adsorbed atomic hydrogen in the following steps,

$$FeC + Fe\text{-}H_{ads} \rightarrow Fe\text{-}CH_{ads} + Fe,$$

$$Fe\text{-}CH_{ads} + Fe\text{-}H_{ads} \rightarrow Fe\text{-}CH_{2ads} + Fe,$$

$$Fe\text{-}CH_{2\,ads} + Fe\text{-}H_{ads} \rightarrow Fe\text{-}CH_{3ads} + Fe,$$

$$Fe\text{-}CH_{3\,ads} + Fe\text{-}H_{ads} \rightarrow CH_4 + 2Fe.$$

After milling, the sample is transfer under an inert atmosphere to a quartz tube for heating. Analysis of gas sample collected during the heating stage showed production of methane inside the quartz tube. The process of methane formation is similar as for

milling except that here, the required energy comes from heating. The hydrocarbon catalytic decomposition over metallic precursors (or CVD) and the subsequent graphitic nanostructure formation of has been extensively studied and modeled by Endo *et al.* [52] and Sinnott *et al.* [53] During the heating process, the following reactions are assumed: First, desorption of hydrogen and hydrocarbon formation over the transition metals, then catalytic decomposition of these hydrocarbons over the transition metals and ordered carbon nanostructure formation along with hydrogen production.

4.4 PRODUCTION PROCESS

Figure 4.1 show the variation of gas pressure inside the sampling cylinder during the heat treatment of samples containing carbon material and one of the transition metals selected from the group consisting of Fe, Co and Ni. In all three cases, the variation of gas pressure at different temperatures is identical.

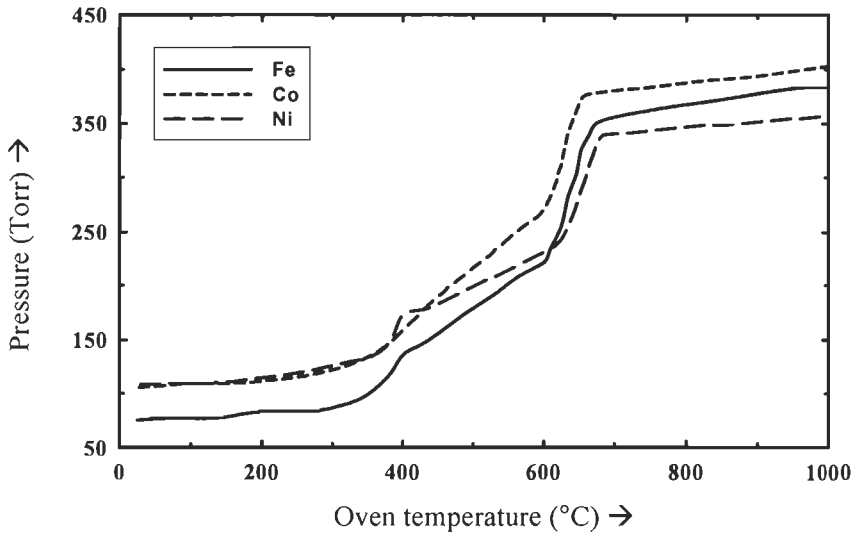

Figure 4.1 Pressure evolutions during heating process with samples containing Fe, Co or Ni.

Initially, a rise in pressure at 300 °C corresponds to continuous desorption of hydrogen attached to metal sites and consecutive production of methane on the catalyst sites. Just over 600 °C, a sharp increase in pressure is explained by one of the following hypothesis: a sudden release of hydrogen covalently bonded to the carbon material or the decomposition of methane on the metallic sites. In this last case, one mole of methane produces two moles of molecular hydrogen, which is consistent with the sharp rise in pressure.

4.5 X-RAY DIFFRACTION (XRD) MEASUREMENTS

X-ray powder diffraction measurements were used to characterize the structural changes of CNS. The measurements were performed with a Rigaku diffractometer using Cu Kα radiation (λ = 1.54054 Å) and Theta/2Theta geometry.

The X-ray pattern of Figure 4.2 show the primary peak at 27° associated with the piling of (002) graphite sheets for as prepared CNS. X-ray analysis also explains the addition of a Co to the crucible before milling, which favours the formation of Fe-Co alloys during heating as opposed to Fe-C compounds. XRD analysis of samples at different temperatures of heat treatment has shown the formation of Fe-Co crystals at temperature as low as 500 °C.

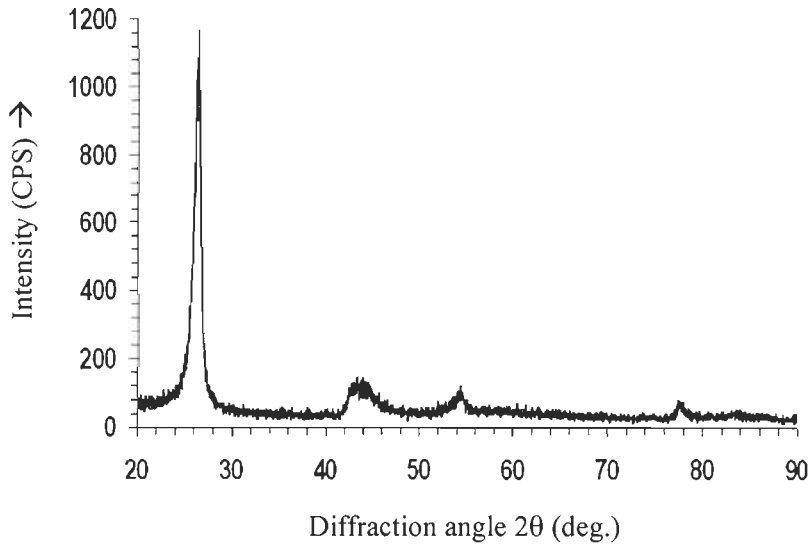

Figure 4.2 XRD pattern of as-prepared CNS.

The hypothesis governing the formation of nanostructures could therefore be the following: during heating, metallic crystals begin forming at approximately 500 °C and at just over 600 °C methane starts decomposing on the crystals with carbon diffusion leading to the formation of nanostructures if the metallic crystal size is sufficiently small. If the crystal formations are too large, graphite layers are formed around them instead. It has to be noted that the metastable alloy phase of Fe and Co formed during the heating process may influence the porosity of CNS. An extensive study on the catalyst metal composition and their transformation in nuclei structure needs to be explored to have control on the type of porosity.

5. HOMOGENEOUS PLATINUM DEPOSITION ON CNS

5.1 INTRODUCTION

CNS prepared in our laboratory was inevitably accompanied by many impurities such as metal or metal oxides, amorphous carbon and other carbon nanoparticles. In addition, since the surface of CNS itself is rather inert, it is difficult to control the homogeneity of Pt metal deposition on the surface by conventional methods. It is therefore important to explore a feasible technique whereby purification and surface modification can take place in a single stage avoiding the loss of structure with multiple steps and also to investigate the details of the modification process. In this work, purification and generation of functional groups on CNS is realized through chemical oxidation treatments. Such surface functionalization enhances the reactivity, improves the specificity and provides an avenue for further chemical modification of the CNS, such as ion adsorption, metal deposition, and grafting reaction. These functional groups facilitate the deposition and dispersion of platinum clusters on CNS via chemically specific nucleation mechanism. More specifically, we have explored the use of sulphuric acid - nitric acid mixture and exploited its oxidizing and acidic effects in the metal deposition on these modified carbon materials.

5.2 LITERATURE REVIEW

Although, there is no literature available as of now to purify and functionalize as-prepared CNS, we sorted out a few methods that were used to treat CNTs accompanied by similar kind of impurities. So far, a number of purification methods have been developed to treat CNTs. Several methods proposed to remove the impurities from as-prepared CNTs that can be categorized by the following four techniques: acid oxidation [54, 55], gas oxidation [56], filtration [57-60] and chromatography [61-63]. It is not only the aim of this section to purify raw CNS, but also to functionalize its inert surface making it available for Pt deposition. Therefore, purification and generation of functional groups on the surface of CNS was realized through chemical oxidation treatments. R. M. Lago *et al.* [64] were first to describe the acid reflux procedure to purify CNTs on a large scale. In this method raw nanotube materials were refluxed in nitric acid to oxidize the metals and carbon impurities. Later, Liu *et al.* [62] reported the use of 3:1

mixture of concentrated H_2SO_4 and HNO_3 to cut the highly tangled long ropes of CNTs into short, open ended pipes, and thus attaching many types of surface functional groups. Other oxidants such as nitric acid, potassium permanganate, ruthenium oxide and sulphuric acid have been also employed to oxidize CNT materials [64-67]. It was evident that the raw CNTs treated with 3:1 acid mixture of sulphuric acid and nitric acid, not only removed the metal impurities, but also enhanced the density of functional groups on carbon surface. Therefore, we explored the use of the same acid mixture with different proportions and concentrations to exploit its oxidizing and acidic effects in the metal deposition on these modified materials.

The size of Pt nanoparticles and their distribution on the carbon support are the key factors that influence the performance of the supported electrocatalyst. Two chemical methods are generally used for the deposition of Pt on carbon surface: impregnation method [68, 69] and colloidal method [70, 71]. There are also alternative methods such as ion exchange method [72], vapour phase method [73] and recently, micro emulsion method [74]. We have selected the standard colloidal method over other techniques due to the availability of literature data to control Pt particle size and the size of Pt particles obtained using this process were narrower compared to other techniques. Of this method, polyol synthesis method was more widely used to distribute Pt nanoparticles in colloidal form. Li *et al.* [75] devised a modified form of polyol synthesis to control the size of Pt particles by adjusting the ratio of water to the ethylene glycol content during the preparation process. We have used this standard technique to platinize CNS with modifications in the mode of adding water into the colloidal solution.

5.3 PURIFICATION AND FUNCTIONALIZATION

5.3.1 EXPERIMENTATION

The generation of functional groups on the surface of CNS can be accomplished by a chemical modification technique with variable proportions of strong oxidizing agents, such as sulphuric acid (H_2SO_4) and nitric acid (HNO_3), which effectively oxidizes metal catalyst impurities, carbon nanoparticles and the weak C-C bonds in the highly ordered CNS. Moreover, the use of this chemical modification technique creates more active sites on the surface of the CNS that will subsequently facilitate the homogeneity of metal

deposition on the surface by any conventional platinization methods. To compare the effect of acid-oxidation treatment, one sample of as-prepared CNS was only purified with HCl trace metal solution to investigate the available active sites without surface functionalization.

500 mg of CNS (Sample A) was soaked in 250 ml of HCl trace metal solution and stirred at room temperature for 1 h to remove metal impurities and amorphous carbon. The washed CNS was diluted with deionised water and filtered with 5 to 10 μm ceramic micro filter. Then, the filtrate was washed with deionised water until the pH becomes neutral. The precipitate in the ceramic micro filter was dried overnight at 120 °C under dry nitrogen. Filtrate scrapped from the ceramic filter (Sample B) was then characterized for experimental comparisons.

The CNS surface was chemically modified by refluxing 500 mg of Sample A under various concentrations and proportions of H_2SO_4/HNO_3 mixture (Samples D, E, F, G, H & I) at an optimized temperature of 120 °C for 3 h. The resultant dark-brown mixture was diluted with deionised water and filtered using 5 to 10 μm ceramic micro filter. The precipitate was washed to neutralize pH and dried overnight at 120 °C under dry nitrogen.

Table 5.1 Various Proportions and concentrations of H_2SO_4 and HNO_3 used as surface oxidizers.

Sample ID	D	E	F	G	H	I
$H_2SO_4 : HNO_3$	1 : 1	1 : 1	1 : 1	3 : 1	3 : 1	3 : 1
Molarity of H_2SO_4	3 M	5 M	7.5 M	5 M	10 M	15 M
Molarity of HNO_3	5 M	9 M	15 M	6 M	15 M	20 M
Percentage yield	41.88	41.43	41.55	43.69	40.02	31.45

Table 5.1 shows the proportions and concentrations of acids used for purification and functionalization of various CNS samples. Excluding Sample I, there is no much difference in the yield of functionalized CNS despite variations in concentration of the reflux solution. The yield shown in the above table was calculated based on the amount of pure nanostructures left after chemical oxidation with reference to the total mass of the contents fed inside the crucible for ball milling. All the samples presented in this thesis

were prepared using 50 wt.% of pre-treated CNS 201 as a precursor material. Therefore, the carbon yield of the purified material with reference to the precursor material was calculated as follows:

$$\text{Yield (\%)} = 100 * (m_{after}/m_{before}),$$

where m_{after} is the amount of CNS obtained after chemical functionalization and m_{before} is the initial mass of carbon material before ball milling. The calculated value of yield after CNS purification was approximately 83% (usually, it range between 80% and 90%). Since, the initial carbon material was only 50 wt.% of the ball mill content, the overall yield will be half the calculated value as shown in Table 5.1.

5.3.2 CHARACTERIZATION OF ACID-OXIDIZED CNS

5.3.2.1 XRD AND TEM

The X-ray powder diffraction patterns of CNS purified and functionalized after acid oxidation is shown in Figure 5.1. It can be seen that the intensity of the (002) graphite peak has decreased after 3 h of chemical treatment when compared with Figure 4.2. This suggests that sulphuric acid - nitric acid mixture used in the treatment of CNS has damaged their structures. Prolonging the reflux time over 3 h caused more damage to CNS, thus reducing the yield and purity of the carbon material. Shortening the reflux time to less than 3 h has retained some metal impurities after enrichment of CNS.

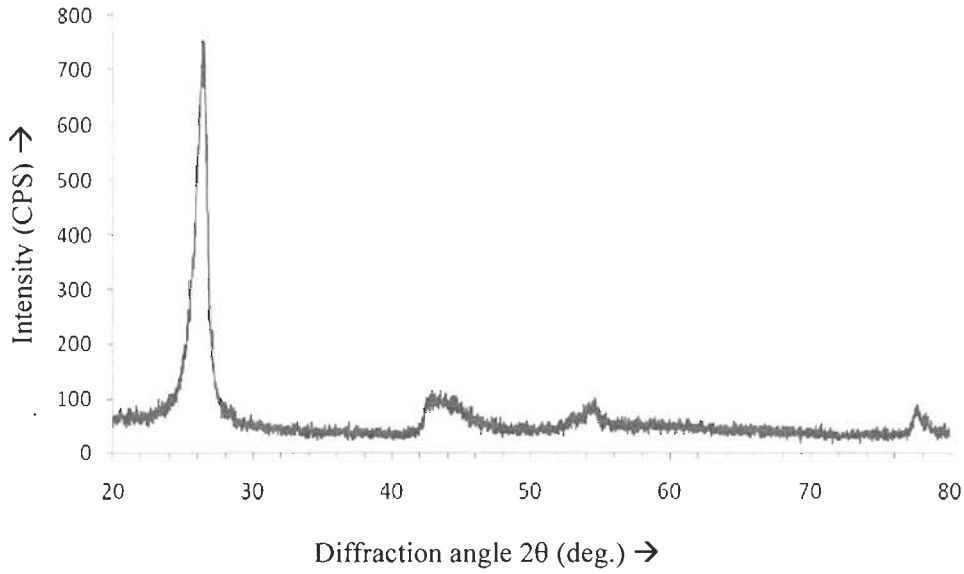

Figure 5.1 XRD pattern for an acid oxidized CNS.

To get detailed structure information, numerical analyses of diffraction patterns before and after chemical oxidation were done. Scherrer's formula,

$$L_c = \frac{0.9 \cdot \lambda}{\beta \cdot \cos\theta} \tag{5.1}$$

was used to calculate particle sizes L_c in the c-direction (002) from the X-ray diffraction patterns [λ = wave length, β = structural broadening (full width at half maximum intensity) and θ = diffraction angle]. The calculated particle sizes before and after chemical treatment was 130 Å and 100 Å, respectively. This reduction in the particle size is a factor of composition of the oxidation mixture, reflux time and temperature.

Figures 5.2 shows a TEM image of CNS after purification and functionalization. As shown in this figure, closed concentric spherical nanostructures can be detected. Furthermore, graphite layers can be observed, which are bent off up to 180°.

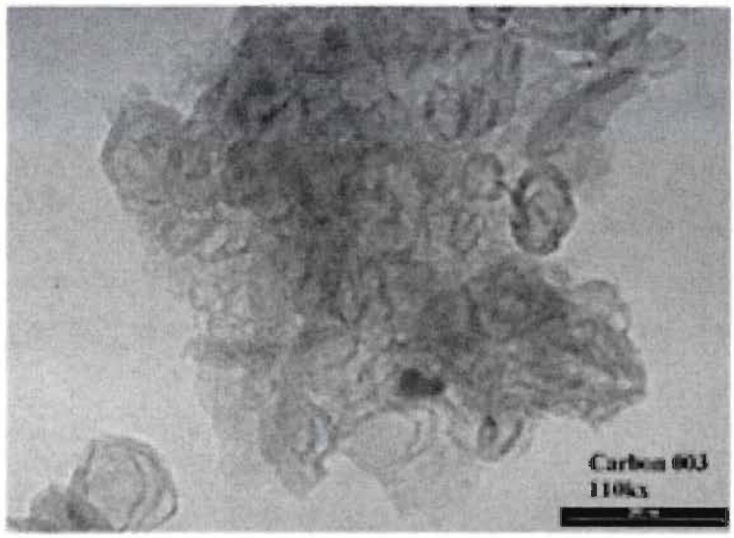

Figure 5.2 TEM image of CNS purified and functionalized after chemical oxidation.

5.3.2.2 THERMOGRAVIMETRIC ANALYSIS (TGA)

TGA is an analytical technique used to determine a material's thermal stability and its fraction of volatile components by monitoring the weight change that occurs as a specimen is heated. In this part of analysis, the measurement was carried out in oxygen atmosphere and the weight was recorded as a function of increasing temperature.

Figure 5.3 is a TGA graph of one purified CNS and shows a decomposition temperature centered at 738 °C for approximately 90 wt.% of the sample. The 10 wt.% loss between 20 °C and about 600 °C is attributed to water and amorphous carbon. As also shown in Figure 5.3 is a TGA curve of carbon nanotubes [76], which measured a decomposition temperature between 510 °C and 645 °C. However, there is no common burning temperature of carbon nanotubes since it is not only related to graphitization degree, but also to pre-treatment process.

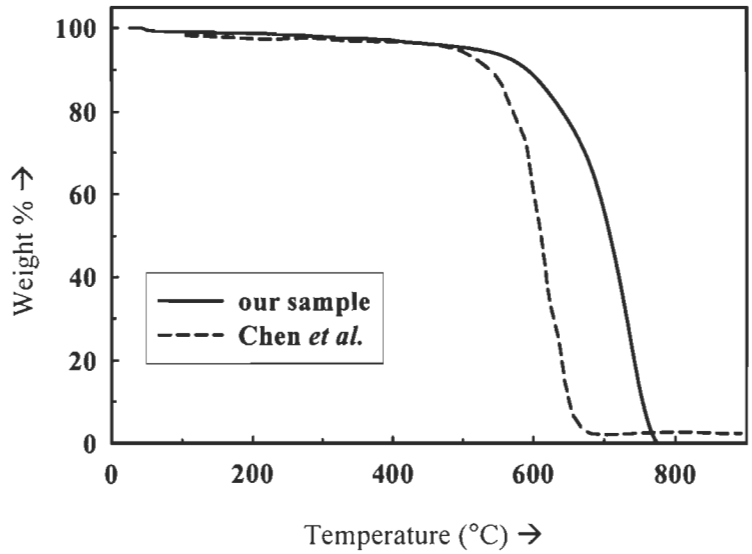

Figure 5.3 Typical TGA analysis results under O_2 atmosphere. Data from Chen *et al.* [76] are plotted for comparison.

It is known that atoms sheets in carbon nanotubes are formed by sp^3 hybridization; hence, they have a higher oxidation temperature than amorphous carbon. Since, the oxidation temperature of CNS is relatively high, we can only imply a high graphitization degree in our samples. Moreover, TGA provides further proof of the purity of CNS.

5.3.2.3 ELECTRICAL CONDUCTIVITY

Electrical conductivity was measured with a HP 4284A impedance meter. The carbon material was compressed between two aluminum electrodes inside an acrylic cylindrical cavity (plunger type). A calibrated spring compresses the powder to a maximum pressure of 40 atm. The electrical conductivity of the carbon material is strongly depended on the

compression pressure. It strongly increases upon compression. For comparison reasons, the conductivity of the samples measured in this thesis were held at a pressure of 40 atm.

With the conductance (G) measured with the impedance meter, the surface area of the electrodes (S = 19.6 mm^2) and the length of the sample (L = 0.3 cm), we calculated the conductivity (σ) using the following equation:

$$\sigma = GL/S. \tag{5.2}$$

The average electrical conductivity of CNS was found to be 0.9 S cm^{-1} against 1.0 S cm^{-1} for Vulcan XC-72, which is in close agreement with the value reported by Pantea *et al.* [77].

5.3.2.4 SURFACE AND POROSITY MEASUREMENTS

The total surface area and micropore volume of the porous CNS was obtained through BET measurement techniques from N_2 adsorption isotherms (77 K) measured with a Quantachrome AS-1-MP instrument. Before starting the BET measurements, the sample was degassed at T = 150 °C under vacuum for 5 h, and the mass was determined before and after degassing. The experimental results are: total surface area of 352.6 $m^2\ g^{-1}$; external surface area of 196.5 $m^2\ g^{-1}$; micropore volume of 0.14 $cm^3\ g^{-1}$ and an average width of micropore of 1.6 nm.

On the other hand, the macropore surface area, macropore volume, and macropore radius were obtained using Hg intrusion isotherms measured with a Quantachrome Autoscan porosimeter with a maximum pressure of 60 000 psi. The experimental results are: macropore cumulative surface area of 45.8 $m^2\ g^{-1}$ up to a pressure of 58 000 psi; total macropore volume of 635 $mm^3\ g^{-1}$, with one distinct peak at 120 $mm^3\ g^{-1}$ corresponding to a pore radius of 1 μm, as shown in Figure 5.4. Also plotted in the figure for comparison are the data from Passalacqua *et al.* [78] for Vulcan XC-72. It can be observed that CNS has a higher macropore volume over carbon black. If the peak from CNS at 1 μm is compared with the main peak at 5.5 μm from Passalacqua *et al.*, the shift in pore radius partly accounts for the higher pore volume in CNS.

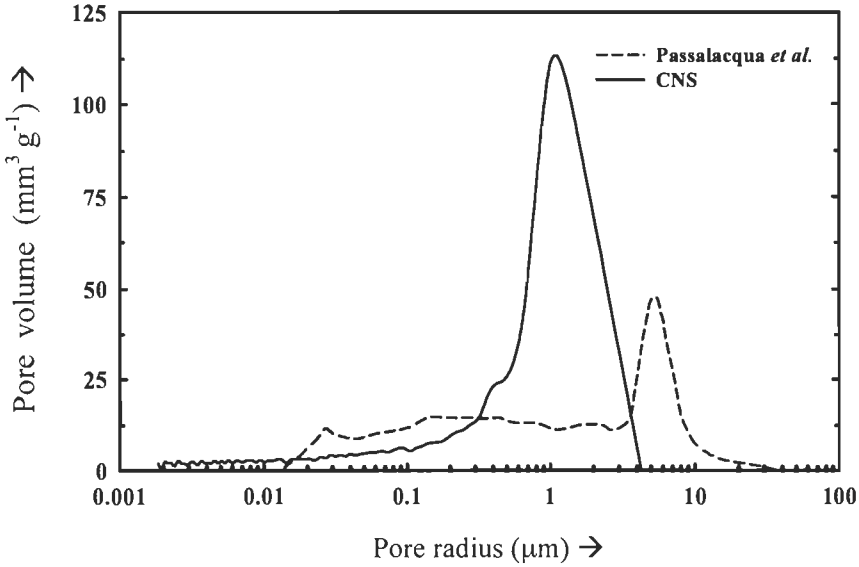

Figure 5.4 Pore volume as a function of pore radius from Hg intrusion data.

5.3.2.5 X-RAY PHOTOELECTRON SPECTROSCOPY (XPS)

In the Pt/CNS catalyst for use in PEMFCs, interactions between Pt and CNS, and the stability of the catalyst layers are related to the chemical nature of their interface. It is therefore important to recognize the role of the chemical nature of the CNS surface in the catalysts stabilization and the interaction between the Pt and carbon support. Mainly, oxygen surface groups are of greatest interest in the preparation of carbon-supported catalysts because the dispersion of Pt particles increases with increasing number of oxygen groups at the surface of the support. The oxygen groups are later used to anchor the Pt particles, thus enhancing the thermal stability of the catalyst under PEMFC operating conditions. Different proportions of functional groups were attached to the surface of the CNS by chemical treatment with different composition of oxidizing agents. It is the aim of this section to derive estimates for the relationships between acid purification (Sample B) and chemical functionalization (Sample F), not to derive a relationship between the functionalization treatment and the chemical nature of functional groups.

XPS was used to analyze and compare the elemental composition, chemical state and electronic state of the elements, carbon and oxygen composed in Samples, B and F. XPS spectra was obtained by irradiating both the samples, one by one with a beam of X-rays,

while simultaneously measuring the kinetic energy and number of electrons that escape from the top 1 to 10 nm of the material being analyzed. As shown in Figure 5.5b, our experimental results confirm the existence of surface functional groups such as hydroxyl, carbonyl and carboxyl groups generated through oxidation. The XPS studies clearly demonstrated that CNS treated with sulphuric acid – nitric acid mixture gave enhanced O_{1s} peaks compared with CNS washed with trace metal HCl (Figure 5.5a). In Sample B, only a small amount of oxygen is detected, which can be considered as adsorbed oxygen species. Furthermore, the ratio of O_{1s} peak area in Samples F and B is found to be about 2.21:1, indicating the higher efficiency of the acid oxidation treatment in the modification of CNS surface.

With reference to the XPS studies of surface-oxidized carbon fibers [79, 80], the present curve fittings of the O_{1s} peaks suggest the presence of new and additional surface functional groups with a binding energy of 533.00 eV in Sample F. Other peaks attributed to phenol (532.05 eV), carbonyl (530.95 eV) and carboxyl (533.76 eV) groups are also found in both the samples.

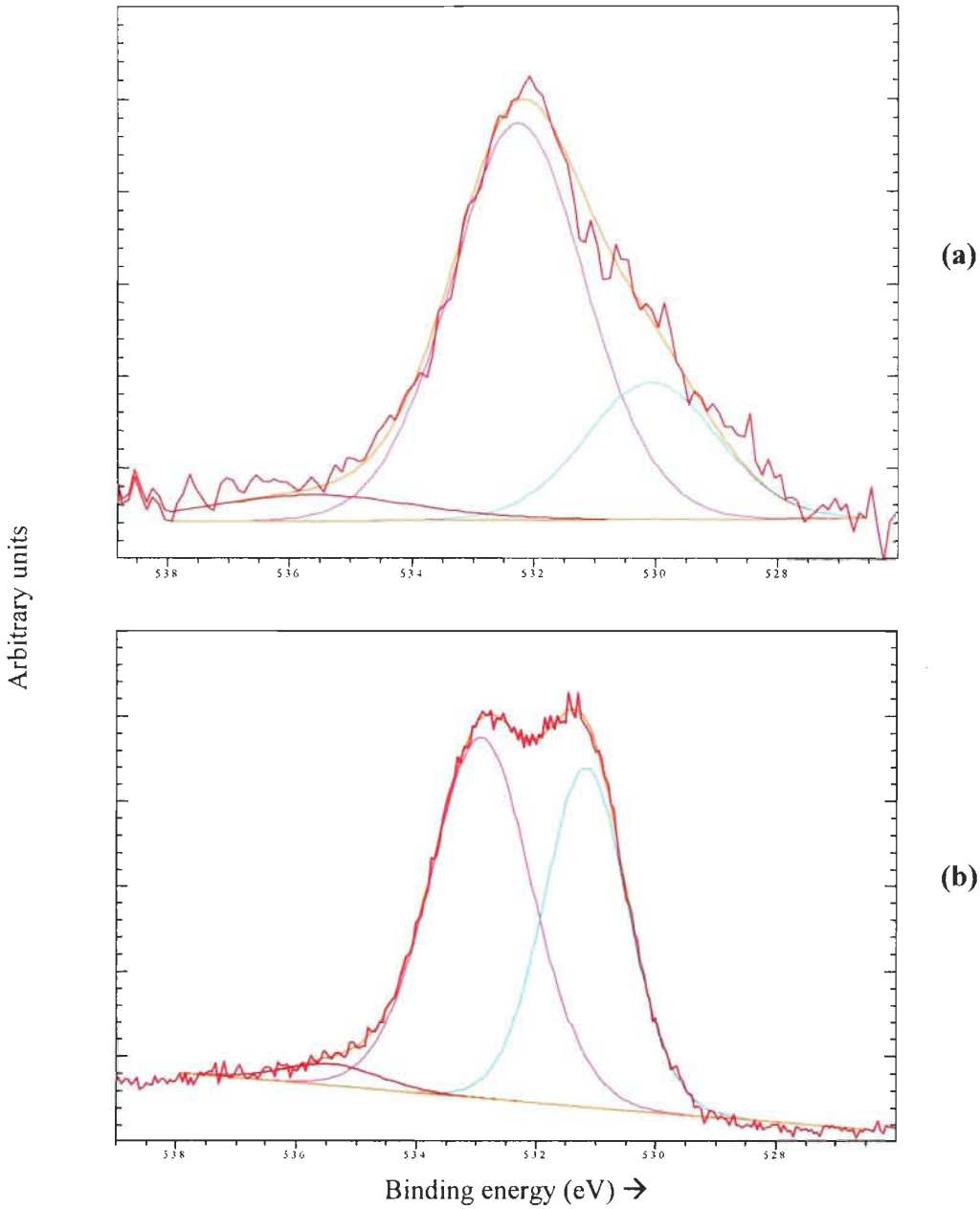

Figure 5.5 (a) CNS (Sample F) after surface modification (b) CNS (Sample B) before surface functionalization.

5.3.3 PLATINUM DEPOSITION ON CNS

5.3.3.1 INTRODUCTION

It is well known that the performance of PEMFC catalysts can be improved by achieving nanosized particles, uniform distribution and high loading of catalysts over large surface area carbon material support. Conventional preparation techniques used for the preparation of supported catalysts are based on wet impregnation followed by reduction in a hydrogen atmosphere at high temperatures or the chemical reduction of the metal precursors using reducing agents. Our technique involved mixing a solution of metal salt(s) with the carbon material. The resulting slurry was dried to remove the solvent and then usually heat-treated and/or reduced to decompose the salt to give the desired form of the catalyst. This method has the advantage that metal is only deposited within the pore structure of the carbon, but do not provide adequate control over the particle size and distribution.

We have used an alternative technique called colloidal method or polyol process in order to have sufficient control over the Pt particle size at higher loadings on CNS. The polyol process is a technique in which a polyol such as ethylene glycol is used as both solvent and reducing agent. Here, metal ions are reduced to form a metal colloid by receiving the electrons from the oxidation of ethylene glycol to glycolic acid. Glycolic acid is present in its deprotonated form as glycolate anion in alkaline solution. It is believed that the glycolate anion acts as a stabilizer by adsorbing the metal colloids. Furthermore, removal of these organics on the metal surface by heat treatment below 140 °C has been reported in this part of the work.

5.3.3.2 PLATINIZATION TECHNIQUE

A measured amount of CNS (400 mg) was suspended in 40 ml of ethylene glycol solution and stirred for 30 min to well disperse 10 mg of CNS/ml of ethylene glycol solution. In order to obtain smaller metal particles, 6.5 ml of hexachloro-platinic acid was added in drops followed by deionised water in 10 min intervals to constitute 5%, 10% and finally, 20% of water content in the bulk solution. It is the aim of this section to obtain metal loadings with smaller particle size, not to derive estimates for the relationship between the addition of water and average particle size. However, the

method described above was tuned in our laboratory to have sufficient control over the particle size. The hypothesis explaining the influence of water addition on the resulting Pt particle size is as follows; the absence of water favours metal formation while its presence favours oxide or hydroxyacetate formation. Therefore, the presence of a small amount of water in the solution may buffer the formation rate of the metal particle, and result in the size of the metal particles to be controlled at a specific value. The pH of the solution was adjusted to above 13 by appropriate addition of NaOH. The pH value of the initial Pt hydroxide colloidal solution is very important for obtaining stable Pt particles in glycol. If the pH value was lower than ~12, instead of a metallic colloidal solution, a precipitate was obtained during the subsequent heating process. The solution was heated in an oil bath at 140 °C to reduce Pt completely. Refluxing conditions were used in order to maintain water contents in the ethylene glycol - water system. A flow of argon was passed through the reaction system to eliminate oxygen and to remove organic by-products. After filtration, washing and drying (120 °C under dry nitrogen, 12 to 15 h) the Pt/CNS samples were obtained and designated B_{Pt}, D_{Pt}, E_{Pt}, F_{Pt}, G_{Pt}, H_{Pt} and I_{Pt} samples. Commercial sample of 20 wt.% Pt on Vulcan XC-72 (designated as C_{Pt}) was used for comparison.

5.3.3.3 XRD, HRTEM AND AAS MEASUREMENTS

The Pt/CNS samples were characterized by recording their XRD patterns, one such graphic is shown in Figure 5.6. XRD pattern identifies face centered cubic of the characteristic crystalline platinum peaks at Pt (111), Pt (200), Pt (220), Pt (311) and Pt (222).

The mean Pt particle sizes were calculated from Scherrer's formula (Equation 5.1) based on Pt (111) peak and listed in Table 5.2. Two HRTEM images of Pt/CNS (Sample F_{Pt}) are shown in Figure 5.7. The images with scale 20 nm and 5 nm represent a wide and uniform distribution of platinum metal clusters on the surface of functionalized CNS.

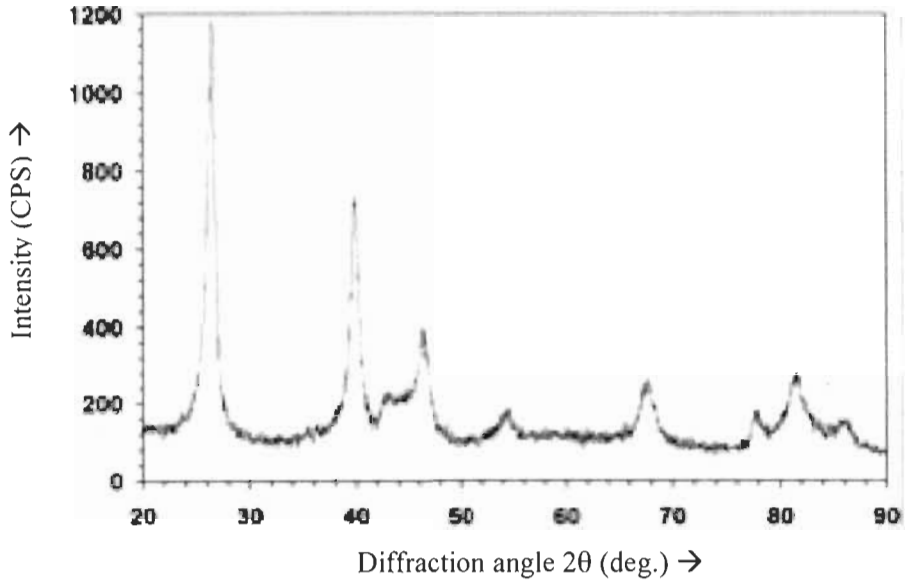

Figure 5.6 Powder XRD patterns of Pt/CNS (Sample F_{Pt}) platinized by EG method.

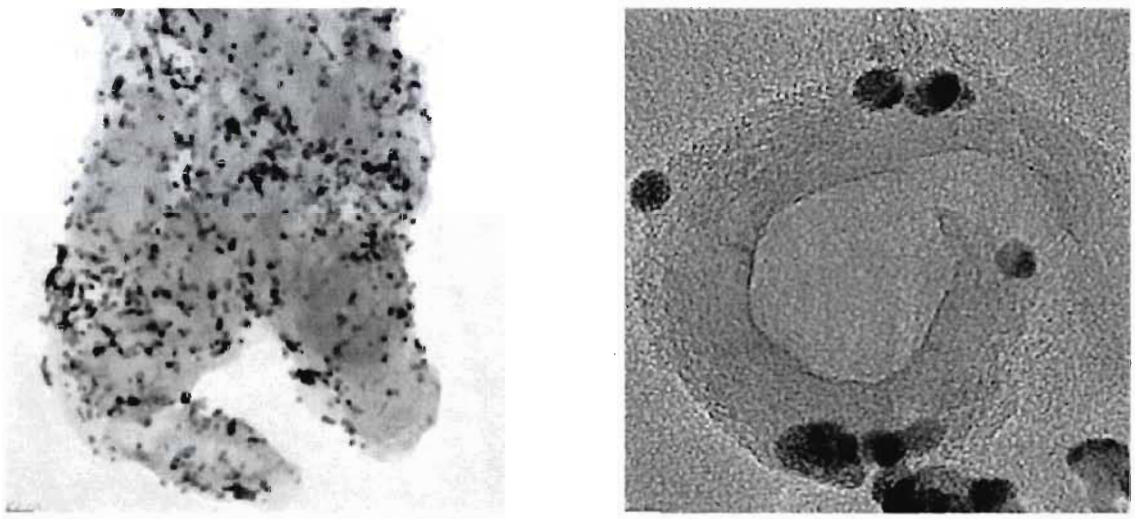

Figure 5.7 HRTEM images of Pt nanoparticles supported on functionalized CNS.

Figure 5.8a shows the particle size distribution of platinum clusters supported on CNS from randomly chosen particles in the HRTEM image (Figure 5.8b). It is evident from the histogram that these Pt particles are small (2.8 to 5.8 nm) and uniformly distributed, which is in near accordance with the value of 4 nm Pt supported on commercial Vulcan XC-72.

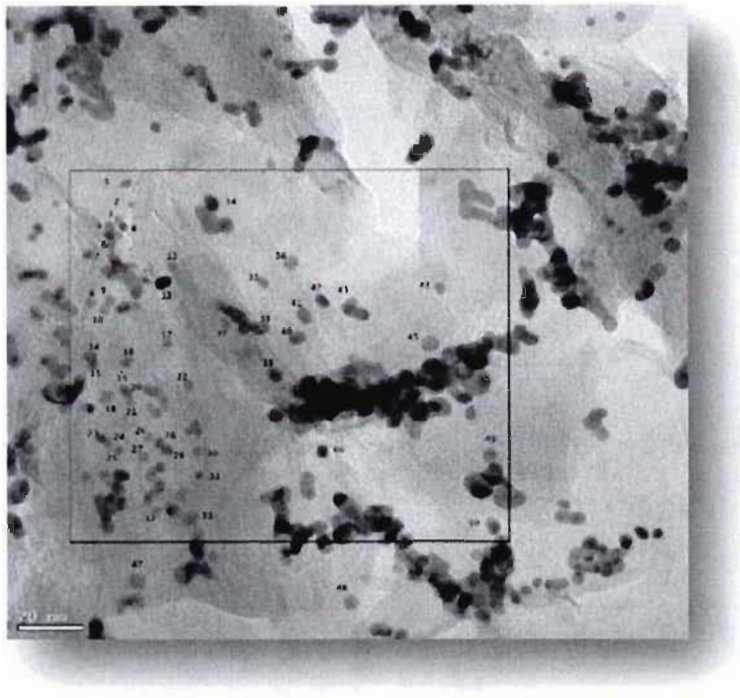

Figure 5.8a Pt particle count in a HRTEM image.

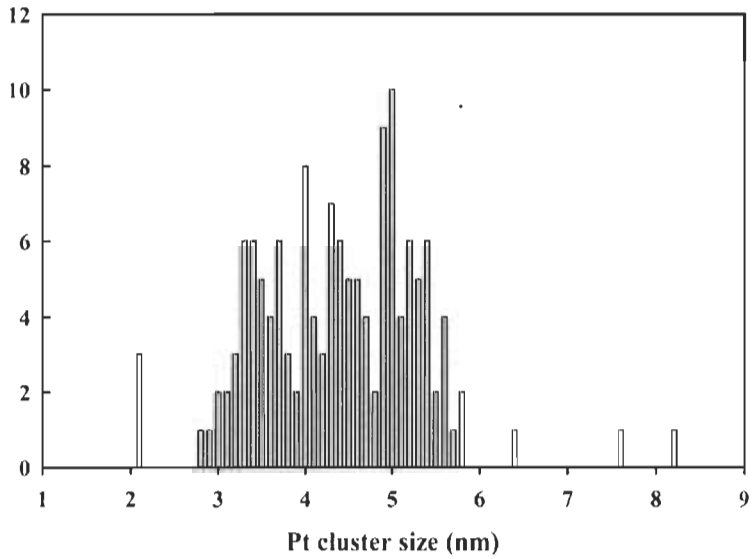

Figure 5.8b Pt cluster size distribution obtained from the above HRTEM image.

Atomic adsorption spectroscopy (AAS) was performed on all the platinized samples (as listed in Table 5.2) to evaluate the loading of platinum nanocrystals on the functionalized sites of CNS. It is evident that the sample treated with trace metal HCl (Sample B_{Pt}) had less oxides on its surface compared with acid-oxidized CNS samples. However, there are a few active sites on its surface that can support a Pt loading of 5.3 wt.%.

Table 5.2 Electrochemical active surface and platinum utilization for all Pt/CNS and for the sample of Pt/C Sample C_{Pt}).

Sample	B_{Pt}	C_{Pt}	D_{Pt}	E_{Pt}	F_{Pt}	G_{Pt}	H_{Pt}	I_{Pt}
Platinum loading in CNS (wt.%)	5.3	20	11.3	14.0	11.9	11.10	8.60	9.70
Electro adsorption (mC cm^{-2})	2.95	25.04	15.79	17.23	24.19	10.33	15.76	28.35
Electro desorption (mC cm^{-2})	1.85	28.60	15.19	15.38	24.94	7.47	12.05	23.23
Coulombic charge for H_2 desorption (mC cm^{-2})	2.40	26.82	15.49	16.31	24.57	8.90	13.91	25.79
Specific charge (mC g^{-1})	12.00	134.1	77.45	81.53	122.83	44.49	69.53	128.95
EAS (m^2 g^{-1})	5.71	63.86	36.88	38.82	58.49	21.19	33.11	61.41
Diameter of Pt crystallite (nm)	6.70	4.00	5.33	8.69	6.83	9.50	5.69	5.97
Geometrical surface area of Pt particles in GC (cm^2)	5.90	9.89	7.419	4.55	6.59	4.16	6.95	6.62
Platinum Utilization (%)	13.69	91.32	70.28	120.62	142.85	71.96	67.35	131.06

5.3.3.4 CYCLIC VOLTAMETRY (CV)

Cyclic voltammetry (CV) was employed to obtain the electrochemical active area of different samples prepared in this work. Here, CV was carried out in a conventional airtight three-electrode cell containing 1 M H_2SO_4 bulk solution at room temperature. The setup was comprised of a 2 mm diameter glassy carbon (GC) electrode, a platinum wire counter electrode, and Ag/AgCl (sat. KCl) reference electrode. Measurements were made at room temperature using a Zahner IMe6 electrochemical workstation. The coulombic charges exchanged during hydrogen adsorption and desorption on the active Pt sites was calculated with the procedure employed by Pozio *et al.* [81]. Thus obtained charge densities were found well in agreement with the results derived by the software - Thales Flink software, which controls all the functions of the IMe6 workstation. The

charge integration feature of the Thales Flink software plots I vs. t, which can be integrated to calculate the charge under the curve. Once this function is activated, the time interval over which the current is to be integrated is defined by selecting the time range of hydrogen adsorption and desorption peaks. Moreover, one of the major contributions to the background current for a cyclic voltammetry experiment is the current required to charge the double layer capacitance at the interface of the working electrode and the bulk solution. We have removed the background current charge contribution from the charges involved in hydrogen adsorption and desorption. The electrochemically active surface (EAS) area of the electrode was then obtained from the charged required for hydrogen desorption from the platinum electrocatalyst by

$$\mathrm{EAS} = \frac{Q_{\mathrm{M}}}{[\mathrm{Pt}] \times 0.21}, \tag{5.3}$$

where Q_{M} is the average charge exchanged during hydrogen adsorption and desorption (mC cm^{-2}), [Pt] represents the Pt loading (mg cm^{-2}) and the numerical value 0.21 represents the charge required to oxidize a monolayer of hydrogen [81]. However, if the initial scanning potential of CV was below the reversible potential for hydrogen desorption, then the measured charges exchanged during electro-desorption of hydrogen have some contribution from the charges involved in the re-oxidation of molecular hydrogen species. Although these measurements have limited absolute accuracy, they are useful for making comparison between catalysts. Since all the voltammograms were with the same operating parameters, then the measured hydrogen desorption charge is restricted to a monolayer only.

The percentage of platinum utilization was calculated by the ratio of electrochemically active platinum surface to the geometrical area of platinum estimated from the mean particle diameter. Particles were assumed to be spherical with a surface area of $4\pi r^2$ and a volume of $4\pi r^3/3$. The theoretical number of platinum nanoparticles in the catalyst layer coated on the GC electrode was calculated by dividing the total mass of loaded Pt on the GC with the mass of one platinum nanoparticle. Surface area of a spherical Pt nanoparticle multiplied by the number of Pt particles gives the theoretical surface area of

Pt supported on CNS. Although the sizes of particles are widely distributed, we approximated the results by assuming the size to be the mean particle diameter.

Figure 5.9 shows the cyclic voltammogram patterns for the platinized samples - D_{Pt}, G_{Pt} and B_{Pt}. This selected comparison was made in order to study the primary effects of chemical reflux on the inert surface of the CNS. All the potentials measured in this article are referred to Ag/AgCl (sat. KCl) reference electrode. The platinum loading was maintained constant (0.2 mg cm^{-2}) for all the CNS samples and also for Sample C_{Pt}. Table 5.2 shows the summary of the charges exchanged during electro-adsorption and electro-desorption for all the platinized CNS and Sample C_{Pt}. It is evident that treatment of CNS with trace metal solution of HCl has removed only the catalytic metal impurities and the amorphous carbon with very little impact on functionalizing CNS.

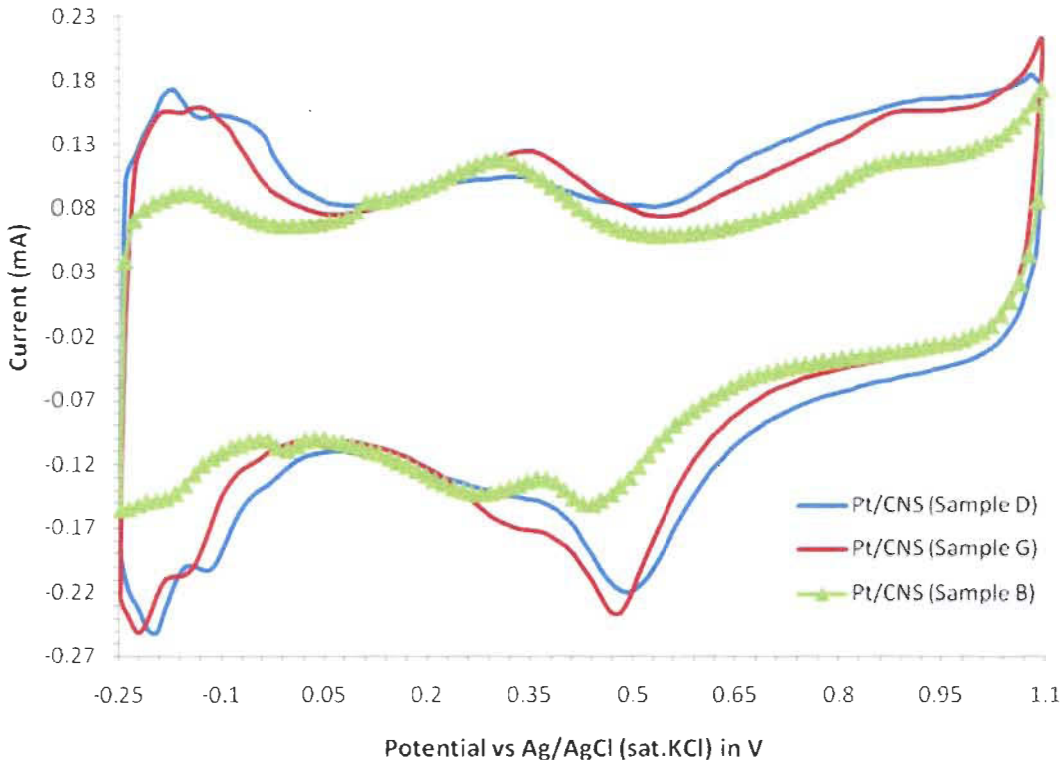

Figure 5.9 Cyclic voltammograms of GC electrode coated with Samples D_{Pt}, G_{Pt} and B_{Pt} scanned at 10 mV s^{-1} in nitrogen saturated 1M H_2SO_4.

The specific charge is defined as the ratio of the coulombic charge required to desorb one monolayer of hydrogen over the Pt loaded on the GC electrode. The calculated value is found to be lower for sample B_{Pt} than that of the nanostructures refluxed with the acidic

mixture. Sample D_{Pt}, treated for surface oxidation with equal proportion of 3 M H_2SO_4 and 5 M HNO_3 has higher specific charge than Sample G_{Pt} refluxed with 3:1 ratio of 5 M sulphuric acid and 6 M nitric acid is primarily due to the higher ratio of H_2SO_4, which intensifies the intermediate $-OSO_3H$ bonding with the carbon surface.

For a constant platinum loading in a GC electrode, the thickness of the electrode grows due to low platinum weight content in the catalyst. Some platinum particles remain inactive as they are hidden by the carbon substrate and are not exposed to the bulk solution. Hence, the EAS is too low for Sample B_{Pt} with low order functionalized CNS which facilitates low platinum loading forcing more quantity of platinized CNS on the small geometry of GC working electrode. As observed from Table 5.2, because of it low EAS, Sample B_{Pt} shows a low rate of Pt utilization when compared with other pre-functionalized Pt/CNS samples. A better rate was observed for Sample D_{Pt} than Sample G_{Pt} as the former covers more active surface with the presence of small diameter platinum clusters.

Figure 5.10 show the voltammograms of Samples H_{Pt} and I_{Pt} functionalized with higher concentrated of acid-oxidation mixture than the composition mixture used to treat Sample G_{Pt}. Although the catalytic metal impurities, iron and cobalt are readily dissolved in dilute nitric acid or dilute sulphuric acid mixture, the concentrated acid of which forms a metal oxide layer that protects (passivates) the metal from further oxidation. Conversely, a high molar concentration of the acid mixture readily modifies the surface of highly ordered inert nanostructures for platinum deposition better than the low concentrated ones.

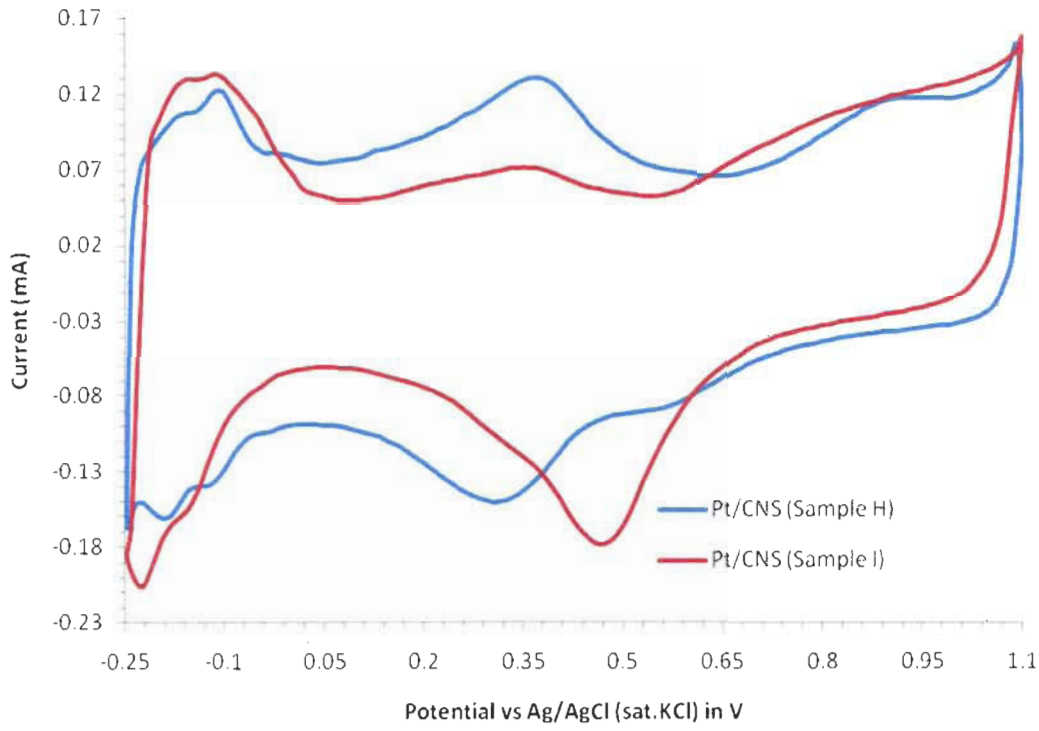

Figure 5.10 Cyclic voltammograms of GC electrode coated with Samples H_{Pt} and I_{Pt} scanned at 10 mV s^{-1} in nitrogen saturated 1M H_2SO_4.

High specific charge of Sample I_{Pt}, when compared to Sample H_{Pt} shows the presence of more electrochemically active sites available for hydrogen adsorption and desorption. This clearly indicates that the surface modification for Sample I_{Pt} is much effective than Sample H_{Pt}. Although, the dimension of platinum particles are similar for Sample H_{Pt} than Sample I_{Pt}, their distribution on functionalized sites and high loading results in higher rate of platinum utilization. The estimated value of platinum utilization for Sample I_{Pt} is greater than 100% is due to the influence of background current to the calculated hydrogen adsorption charge. Moreover, it is also because of the presence of bigger Pt nanoparticles with low theoretical platinum surface resulting in higher platinum efficiency. In fact, due to the practical measurement limitations, the platinum utilization cannot be measured accurately to study the electrochemical activity of catalysts. But, the approximated version of it can be used to make a secondary comparison between different catalysts. However, the performance studies of different catalysts in this thesis are primarily based on their specific charge or by their electrochemically active surface area.

Figure 5.11 compares the cyclic voltammograms of Sample F_{Pt} and Sample C_{Pt} obtained in a deaerated 1 M H_2SO_4. The Pt electrochemical surface areas for these two samples were estimated from the integrated coulombic charge required for desorption of hydrogen of the cyclic voltammogram shown in Figure 5.6. If we assume that the charge required to desorb one monolayer of adsorbed hydrogen to be 0.21 mC cm^{-2}, then the active surface of Pt/CNS and Pt/C were calculated as 58.49 and 63.86 $m^2 g^{-1}$, respectively. For the same Pt loading on the GC electrode, the thickness of the electrode coated with 11.9 wt.% Pt/CNS will be greater than the electrode coated with 20 wt.% Pt/C. As a result of variable thickness, some Pt particles supported on CNS were blocked in the carbon substrate and not exposed to the bulk solution as it would be the case for Sample F_{Pt}. This also applies for the catalyst layers coated on either gas diffusion layer or on the membrane (decal method) in a membrane electrode assembly (MEA). But, regardless of electrode thickness, Sample F_{Pt} with 11.9 wt.% of Pt supported on CNS showed similar electrochemical performances as Pt supported on Vulcan XC-72 carbon (Figure 5.11). This is primarily due to the highly porous structure of the CNS.

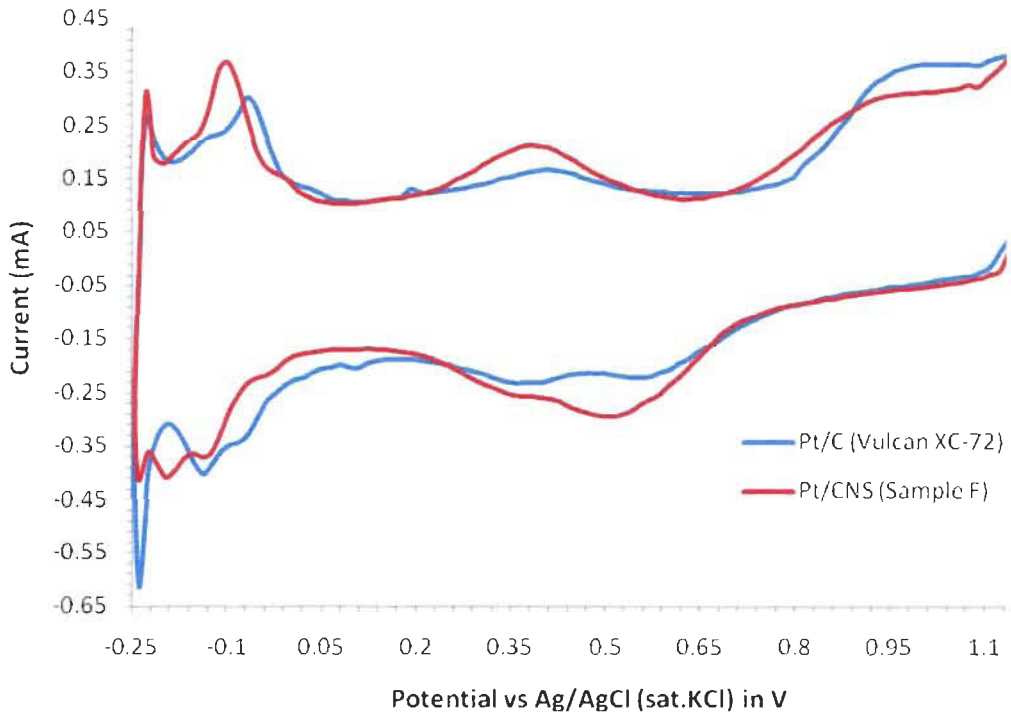

Figure 5.11 Cyclic voltammograms of GC electrode coated with Samples C_{Pt} (Pt/Vulcan) and F_{Pt} scanned at 10 mV s^{-1} in nitrogen saturated 1 M H_2SO_4.

The presence of more micro and macro porous structure in CNS should improve gas transport to the active Pt sites in the catalyst layers of MEAs, thus increasing the limiting current and consequently the maximum reachable power.

In comparison with Sample I, Sample F exhibits more active sites for platinum loading upon surface oxidation, which confirms the stability of the structure even after acid reflux. Hence, Sample I_{Pt} can accommodate only 9.7 wt.% of Pt when compared to 11.9 wt.% on Sample F_{Pt}, as the highly ordered structure of the latter was disrupted on treatment with high molar concentration of refluxed acid solution. The nanostructures are coated with a layer of amorphous carbon upon oxidation with high molar acids, showing that the surface of Sample I was damaged before platinization.

In summary, we conclude that the best ratio to purify and functionalize CNS is with a 1:1 volumetric mixture of 7.5 M of sulphuric acid and 15 M of nitric acid, which ended up showing similar electrochemical performances for Sample F_{Pt} as that of Sample C_{Pt} (ETEK's Pt/C) achieved because of the CNS porous structure. Moreover, the method we proposed in this work attached almost 50% of carbonyl groups with less than 5% of acidic functional groups. It is proposed elsewhere in the literature [6] that these C=O groups acting as anchoring sites for Pt nanoparticles hinder agglomeration and surface diffusion of catalyst particles across the graphene layers under oxidizing conditions of cathode.

6. ELECTROCATALYST DURABILITY MEASUREMENTS

6.1 INTRODUCTION

The durability of PEMFCs is a major barrier to the commercialization of these systems for stationary and transportation power applications. The catalyst degradation is due to dissolution and sintering of the Pt catalyst nanoparticles and corrosion of the carbon support as a result of electrochemical oxidation, with the latter being more pronounced at the cathode where the oxygen is being reduced. Recently, Kangasniemi *et al.* [33] investigated the electrochemical surface oxidation of Vulcan XC-72 at different potential and temperature ranges under PEMFC condition. Using various characterization techniques, they observed that the carbon support effectively undergoes oxide formation under simulated fuel cell environment. Despite its widespread use, carbon black undergoes electrochemical oxidation to surface oxides and eventually to CO_2 at the cathode of a PEMFC, where it is subjected to high acidity, high potential, high humidity and high temperature. So, when this carbon support is corroded away, Pt nanoparticles are lost from the electrode or aggregated to larger particles. The same group also studied the influence of Pt on the corrosion of the carbon support and found that Pt accelerated the corrosion rate of carbon black. One proposed generic stepwise mechanism of surface oxide formation and CO_2 evolution is shown schematically in reaction (6.4), wherein the subscript 's' denotes surface species (water is understood to be the source of oxygen [82-86]):

$$C_s \rightarrow C_s^+ + e^- \quad (6.1)$$

$$C_s^+ + \tfrac{1}{2} H_2O \rightarrow C_sO + H^+ \quad (6.2)$$

$$2C_sO + H_2O \rightarrow C_sO + CO_2 + 2H^+ + 2e^- \quad (6.3)$$

$$R\text{-}C_s\text{-}H \rightarrow R\text{-}C_s\text{-}OH \rightarrow R\text{-}C_s{=}O \rightarrow R\text{-}C_sOOH \rightarrow R\text{-}H + CO_2. \quad (6.4)$$

Early studies [50, 87] have concluded that the carbon material with more graphite component, such as carbon nanotubes, was proven to be more stable than carbon black. This is because carbon black has a turbostratic structure in which graphite crystallites mix with amorphous carbons with short-range order. These amorphous carbon and the more edges in the graphite component were easily attacked by oxyacids [88, 89]. Whereas,

carbon nanotubes have definite graphitic surfaces with no basal plane edges except at their extremities, excluding the defects in the tubular structure. Carbon nanostructures prepared in our laboratory have similar properties as carbon nanotubes, but with no well-defined shape. Therefore, CNS should exhibit very similar durability properties as carbon nanotubes for use as catalyst support in PEMFCs. It is the aim of this section to perform a comparative study on Pt/C and Pt/CNS catalysts following potentiostatic treatments up to 200 h under simulated conditions of a PEMFC cathode.

6.2 MEA AND TESTING

6.2.1 PREPARATION OF ELECTRODES AND MEA

Carbon cloth (ETEK) was used as a substrate for casting of a catalyst layer comprising of supported electrocatalyst and impregnated 5 wt.% Nafion (Aldrich) mixture. The amount of Pt catalyst coated on the anode gas diffusion layer (GDL) was 200 $\mu g\ cm^{-2}$, which is half the amount coated on the cathode GDL (400 $\mu g\ cm^{-2}$). The ratio of supported electrocatalyst to dry weight of Nafion during the ink preparation was maintained constant (2.5:1) for all the MEAs prepared in this work. The catalyst ink was mechanically stirred with a magnetic stir bar for at least 24 h. With an appropriate size camel brush, the ink was coated on one side of a teflonized carbon cloth referred to as gas diffusion media (GDM or GDL). Subsequently, the ink was dried in an oven preheated to 80 °C for 30 min. This procedure was repeated until a Pt loading 200 $\mu g\ cm^{-2}$ was reached at cathode. Finally, the ink coated GDM was dried in 80 °C drying oven for at least 12 h. The final drying done in this work after 12 h had an equivalent Pt loss of up to 10 $\mu g\ cm^{-2}$.

The type of polymer electrolyte membrane used in this work was a Nafion NRE212 (DuPont). This membrane is a non-reinforced dispersion-cast film based on perfluorosulfonic acid polymer in the acid form. This membrane performs as an electrode separator and a solid electrolyte that selectively transports protons (when properly humidified) across the cell junction. The membrane purchased from Fuel Cell Store, was cut into a desired size (5 cm × 5 cm) before pre-treatment process. Then, the membrane was cleaned by boiling it in a 3% hydrogen peroxide solution for 1 h, rinsed with deionised water and followed by boiling in deionised water for another hour. Finally, the

membrane was boiled in 0.5 M sulphuric acid for 1 h, rinsed with deionised water and boiled in deionised water for another hour. The hydrophilic regions around the clusters of sulphonated polymer chains can lead to the absorption of large quantities of water, increasing the dry weight of the material up to 50%. Therefore, the membrane needs to be dried prior to hot press. The drying was done by placing the wet membrane on a heated homemade vacuum table that was at room temperature, heated to 75 °C for 5 to 10 min, cooled to room temperature with vacuum still on, removed and stored in plastic bags for hot pressing.

The hand painted cathode, standard anode and the pre-treated membrane were hot pressed onto a 5 cm^2 MEA using a Carver press mounted with two hot platen set at a temperature of 120 °C and under a pressure of 700 psi for 3 min. The MEA was then allowed to cool at room temperature before being available for testing. The performance of the fabricated MEA was evaluated using a 5 cm^2 single cell hardware (Fuel Cell Technologies, Inc.) equipped with a reversible hydrogen electrode (RHE) and wired to a Zahner IMe6 workstation. The MEA was sealed between a 0.01 inch thick silicone rubber gasket at the anode and a 0.01 inch thick Furon gasket (Saint-Gobain) at the cathode and was assembled with a 10.5 Nm torque between two poco graphite plates with serpentine flow-field.

6.2.2 MEA TEST PROCEDURE

The single cell performance was characterized by feeding humidified hydrogen gas at 80 °C of 100% relative humidity (RH) at the anode and humidified air at 70 °C of 80 % RH at the cathode with a stoichiometric ratio of 1.5 and 2, respectively. The gas pressure at the electrodes was maintained at 30 psig using a back pressure regulators. Initially, the cell was conditioned with a constant load of 0.5 A cm^{-2} at 80 °C for 50 h. The steady state value of the cell potential at a load of 1 A cm^{-2} was the mean value calculated from the data logged over a runtime of 1 h. To help identify the rate of performance degradation between Pt/C and Pt/CNS, hydrated (100% RH) ultra high purity (UHP) nitrogen was passed through the working electrode (cathode compartment) and hydrated (100% RH) UHP hydrogen was passed through the counter electrode (anode compartment).

The anode serves as a counter electrode as well as reference electrode (RHE). The cell temperature was maintained constant at 80 °C throughout the process and the pressure is atmospheric at three-cell mode. Then, the Zahner workstation was switched to cyclic voltammetry mode and a constant potential of 1.2 V was applied between the working electrode and RHE to accelerate the oxidation of the carbon support at the cathode catalyst layer (CCL). The potentiostatic hold was maintained for a period of 15 h during repetitive cycles of this experiment.

Prior measuring the steady state values of open circuit voltage (OCV) and the cell voltage at 1 A cm^{-2}, the gas feed, the humidity conditions and the pressure were tuned back to the values mentioned above. Later, the MEA was briefly conditioned with a load of 0.5 A cm^{-2} at 80 °C for 30 min. This test cycle was repeated during the course of the experiment. Figure 6.1 summarizes the accelerated corrosion test procedure developed in our laboratory to evaluate the degradation of electrocatalyst layer in PEMFCs.

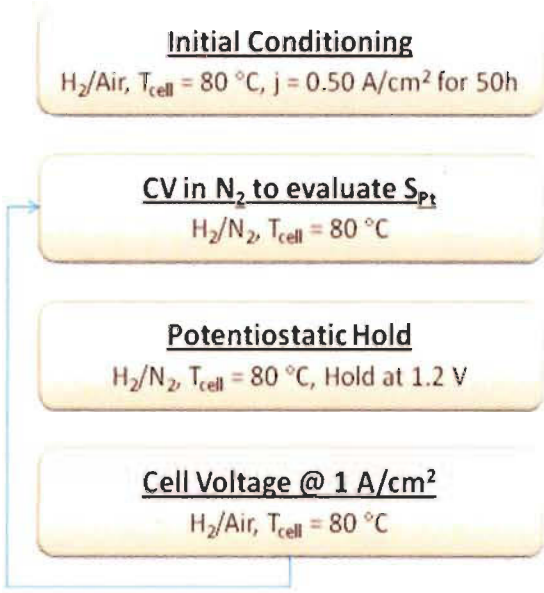

Figure 6.1 Accelerated corrosion test procedure to evaluate degradation of catalyst layer.

Figure 6.2 shows a steady decline in cell voltage under a constant load of 1 A cm^{-2} at different time intervals during accelerated electrochemical oxidation at cathodes fabricated with Pt/C and Pt/CNS, respectively.

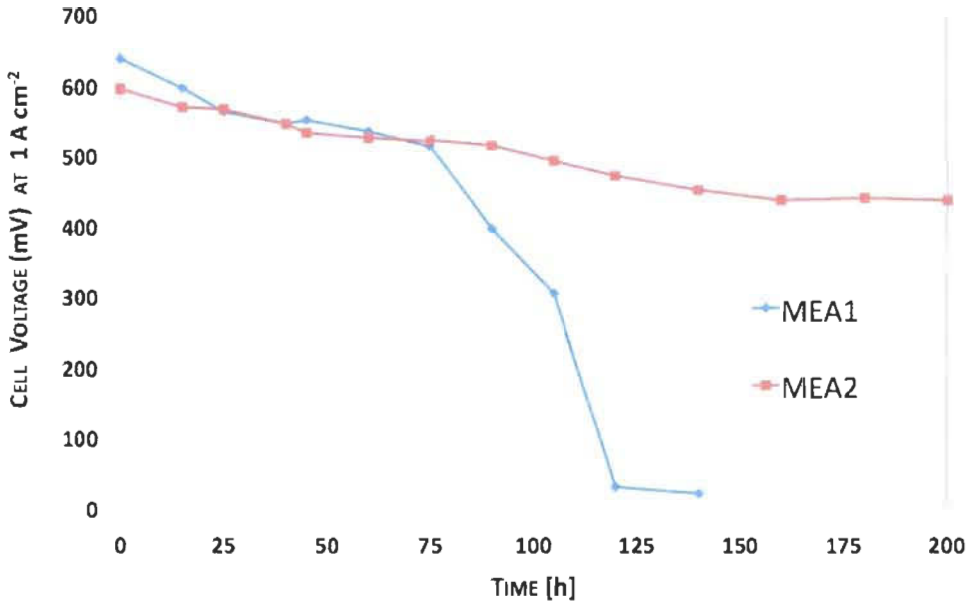

Figure 6.2 Measurements of cell voltage at 1 A cm^{-2}, showing a sudden drop in cell performance for MEA1 after 75 h of electrochemical oxidation.

The MEAs fabricated using Pt/C and Pt/CNS was designated as MEA1 and MEA2, respectively. The cell potential measurement values at 1 A cm^{-2} for both MEAs follow a steady linear downtrend over the operation of 60 h for the two cells, whose cathode is electrochemically oxidized at a potential of 1.2 V at 80 °C.

The fluctuation in the trend before 60 h of operation is ascribed to the process of wetting level in the electrolyte membrane and the ionomer in the catalyst layer. After 60 h a marked decrease in the cell potential is observed for MEA2, whereas a steep downward trend is observed for Pt/C. It can be seen that almost 95% of the cell voltage was lost for MEA1 after 140 h of accelerated oxidation treatment, while only 25% loss in cell voltage is observed for MEA2.

Furthermore, most of the potential drop for both MEAs occurred between 60 h and 140 h of oxidation treatment as shown in Figure 6.3. However, the rate of voltage drop is very small for MEA2 after 140 h. The drop was merely 2.36% after continuous oxidation for an additional 60 h. This indicates that CNS with high graphitic content and long range order is less prone to corrosion under oxidative conditions when compared with Vulcan. A similar trend was also observed on open circuit voltage measurement (Figure 6.4) indicating that degradation of the membrane caused loss in cell performance. On a long

run, MEAs prepared with Pt/CNS could potentially provide much higher durability than MEAs prepared with Pt/C.

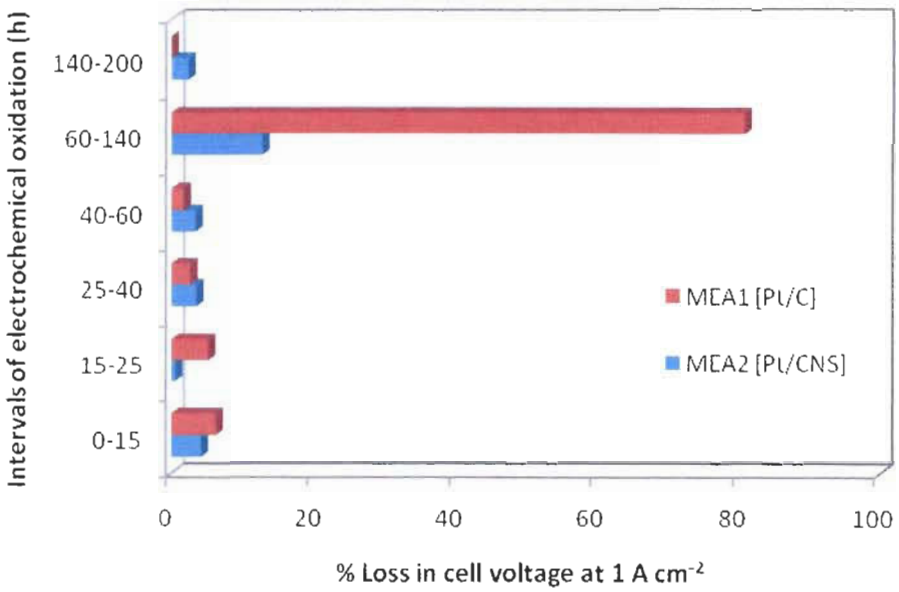

Figure 6.3 Percentage losses in cell potential at 1 A cm^{-2} at different time intervals,

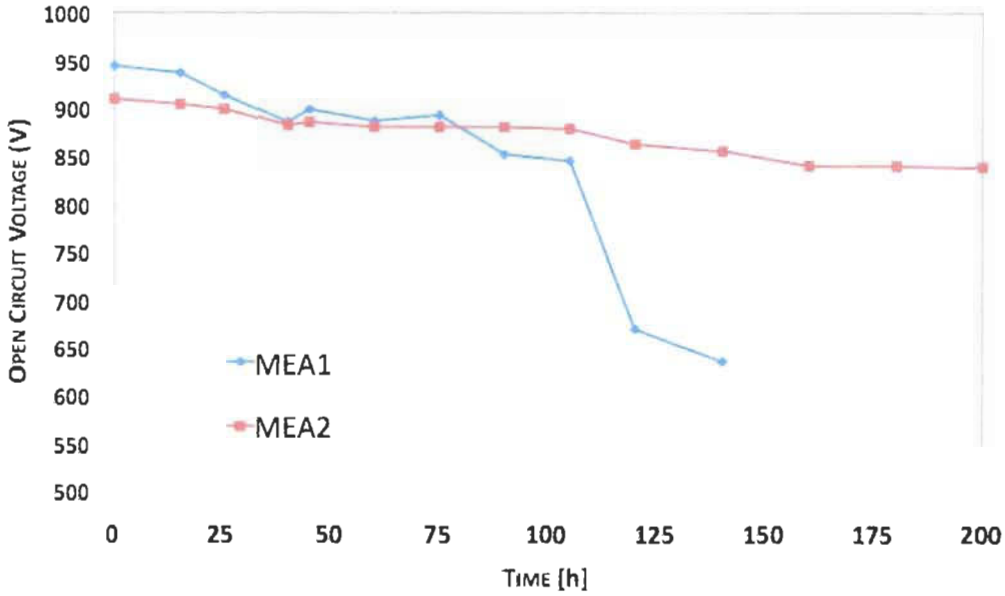

Figure 6.4 Measurements of OCV showing degradation of membrane in MEA1, which is accountable for poor performance after 75 h.

6.2.4 LOSS IN PT SURFACE AREA

6.2.4.1 PREPARATION OF WORKING ELECTRODE

Prior to CV electrochemical measurements, the Pt electrocatalyst supported on carbon black and CNS were conditioned in a tube furnace in order to remove surface contaminants and anneal the Pt crystallite, under an atmosphere of 10% hydrogen and 90% argon for 1 h at 300 °C. Glassy carbon (GC) disks (BASI, 3 mm, 0.07069 cm^2), polished to a 0.05 μm mirror finish (alumina, BASI) before each run, and served as substrate for the supported catalyst. An aqueous suspension of catalyst ink was prepared by ultrasonically dispersing 25 mg of catalyst in deionised water (Millipore) to a ratio of 2 $mg_{catalyst}$ mL^{-1}. A 20 μL aliquot of the ultrasonically redispersed suspension was then pipette onto the disk. In order to obtain a uniform distribution of the suspension, the GC electrode was dried at room temperature for an hour before leaving it inside a preheated (80 °C) oven for another hour. After complete evaporation of the water droplet, 20 μL of the diluted Nafion solution (5 wt.% Nafion, Aldrich) was pipetted onto the dried powder surface to enhance the adherence between the catalyst powder and the electrode. The cyclic voltammetries were carried out in a conventional airtight three-electrode thermo stated (80 °C) cell containing a 0.5M H_2SO_4 electrolyte. Potentials were measured using a Ag/AgCl (Sat. KCl) electrode, but all the potentials throughout this study are referenced to RHE. Measurements were made using an automated Zahner IMe6 electrochemical workstation. A potentiostatic hold of 1.2 V was applied to the working electrode and was held for 0, 15, 30, 45... and 175 h to electrochemically oxidize the support material. Voltammograms were recorded for each time period, to compute the rate and loss of the catalyst active surface due to electrochemical oxidation.

6.2.4.2 RESULTS AND DISCUSSION

To quantify the extent of loss in platinum surface area, cyclic voltammetry was conducted on Pt/C and Pt/CNS in N_2 purged 0.5 M H_2SO_4 electrolyte at different time intervals during their treatment at 1.2 V and 80 °C. The amount of columbic charge involved during hydrogen desorption was used to calculate the active platinum surface of the electrodes as described in Section 5.3.3.4, after correcting for double layer capacitance. Figure 6.5 shows the drop in electrochemical active surface area for the case

of Pt/C and Pt/CNS at different time intervals of potential hold. During the initial 15 h of oxidation, nearly 35% loss in Pt surface area was observed for Pt/C, while there is a considerable 20% loss for Pt/CNS as shown in Figure 6.6. For the next 40 h, dissolution of Pt particles was nearly three times less when the catalyst was supported with CNS over Vulcan. After 75 h of oxidation, a steady downward trend of surface area loss is observed for Pt/C, while the rate of Pt area loss is very small for Pt/CNS. The loss in active Pt surface area explains the drop in cell operating voltage as discussed earlier.

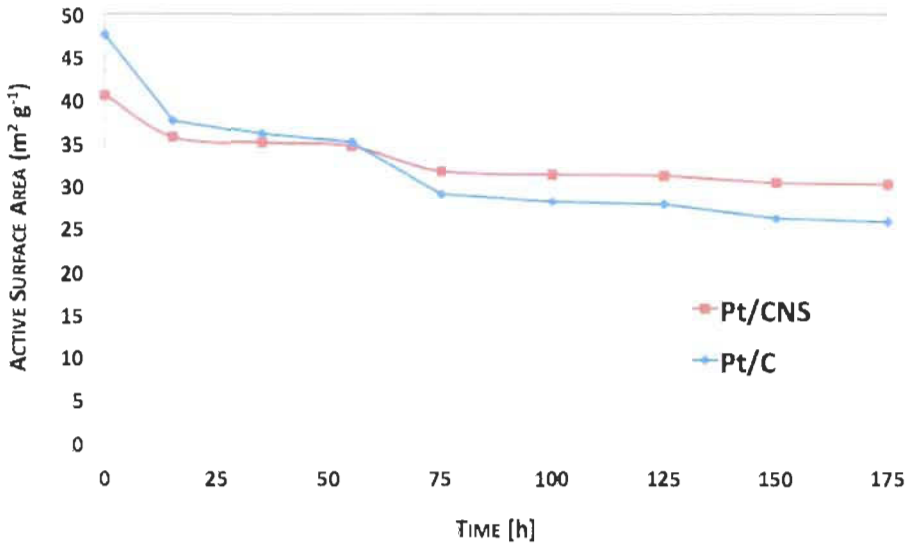

Figure 6.5 Comparison of Pt active surface area loss for the case of Vulcan XC-72 and CNS at different time intervals during oxidation treatment.

The sudden drop in cell voltage and also the OCV is explained by the following hypothesis: Two sintering mechanisms proposed on several studies to explain the loss of EAS of Pt in an aqueous electrolyte [90, 91]: dissolution/reprecipitation [92-94] and migration [95, 96] (surface diffusion of Pt particles). With the carbon black support corroding rapidly at cathode under simulating conditions for accelerated corrosion, it can be observed that both the above sintering mechanisms occur in MEA1. The loss in specific surface area explains the fact that some of the dissolved Pt ionic species were redeposited on other Pt particles, resulting in Pt particle growth (electrochemical Ostwald ripening). Some of the dissolved Pt ionic species diffuse out of the electrode and into the polymer electrode membrane. Generally, in a PEMFC, a small amount of the supplied oxygen in air can also transport across the membrane and so does hydrogen.

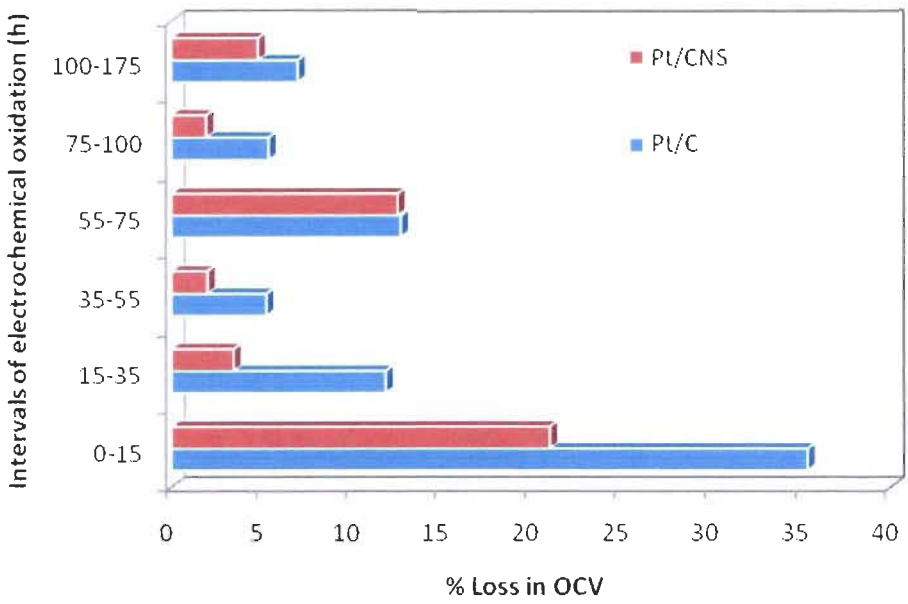

Figure 6.6 Percentage losses in OCV during different time intervals of electrochemical oxidation.

Therefore, there exists a concentration gradient of oxygen as well as hydrogen across the polymer electrolyte membrane. In the case of an air atmospheric cathode, the region near the cathode has a high oxygen concentration and a low hydrogen concentration. Under these conditions, a Pt nucleus is not easily generated by reduction with hydrogen because a very small Pt nucleus might be unstable with high potential (mixed potential composed of dissolved hydrogen and oxygen) under such oxygen-rich conditions. Therefore, nucleus generation on the Pt band occurs more easily closer to the anode as shown in Figure 6.7. The platinum nucleus generation in the membrane accelerated by hydrogen stimulates the degradation of the ionomer. The typical degradation of the membrane at higher potential holds close to OCV stems from hydrogen peroxide formation during the two-electron oxygen reduction reaction process near the anode layer catalyzed by the reduced platinum nucleus. The degradation of the membrane is reflected as a sudden performance drop in MEA1.

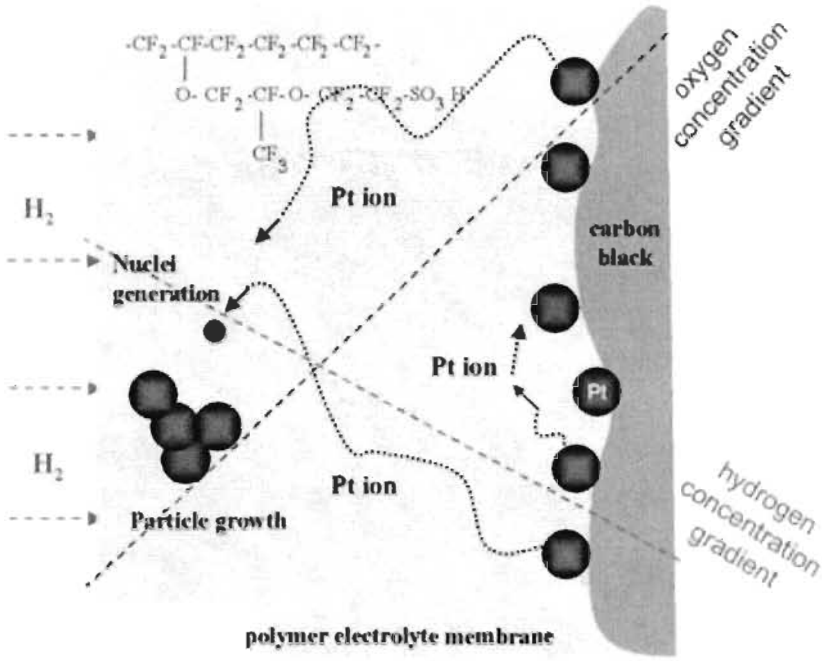

Figure 6.7 Schematic drawing of platinum deposition in a polymer electrolyte membrane.

Although, CNS prepared in our laboratory has nearly 50 % of C=O groups as Pt anchoring sites, we cannot exclude the possibility of Pt particles growth by migration like MEA1. Therefore, the decrease in electrochemically active surface area of Pt supported on CNS is caused mainly by the dissolution of Pt anchored on other functional groups. A part of the dissolved platinum ionic species gets aggregated on other platinum particles, resulting in platinum particle growth. A small proportion of diffused Pt ionic species remains in ionic form as a band close to cathode catalyst layer boundary minimizing the possibility of nucleation. Even though, we have no HRTEM image of MEA cross-section supporting the theory described above, but the steady performance of MEA2 after initial decline evidently proves our hypotheses.

6.2.5 CHANGES IN SURFACE FUNCTIONAL GROUPS AND PARTICLE SIZE

It is the aim of this section to derive estimates for the relationships between the loss in specific surface area and growth of Pt particles. In order to study the extent of surface electrochemical oxidation of Pt/C and Pt/CNS, the corresponding catalyst ink was coated over a 10 cm^2 nickel substrate, later exposed to 1.2 V vs. RHE at room temperature for different time intervals (0 h, 75 h and 150 h). The extent of oxidation at different time periods on electrochemically oxidized Vulcan and CNS was characterized by XRD

(particle size) and thermal gravimetric analysis (TGA to correlate functional groups based on oxidation temperature). Prior to TGA, the oxidized catalysts at different time periods was scrapped out from the substrate, washed with deionized water and dried in an oven at 65 °C at atmospheric pressure.

6.2.5.1 LOSS IN Pt PARTICLE SIZE

The oxidized catalyst layer was scrapped from the substrate, washed and dried prior measuring the size of Pt particles by powder XRD. The size of platinum particles in the dried catalyst power of electrochemically oxidized Pt/C and Pt/CNS was examined by powder X-ray diffraction (XRD). XRD measurements was performed with a Rigaku diffractometer using Cu Kα1 radiation (λ = 1.54051 Å) and $\theta/2\theta$ geometry. The XRD patterns for Pt/C and Pt/CNS electrochemically oxidized at 0 h, 75 h and 150 h are plotted in Figure 6.8 and Figure 6.9, respectively. The crystallite size of Pt nanoparticles (L_c) was estimated using Scherrer's equation as shown in Equation (5.1). It is observed that the characteristic Pt diffraction peak narrowed during the course of electrochemical oxidation indicating the growth of Pt particles when compared with the fresh Pt particles. The Pt particle growth stabilized on Pt/CNS after 75 h of potentiostatic hold, whereas a progressive behaviour was observed for Pt supported on carbon black. From the results obtained in this study in favour of Pt/CNS, we propose that CNS can be a durable catalyst support for PEMFCs.

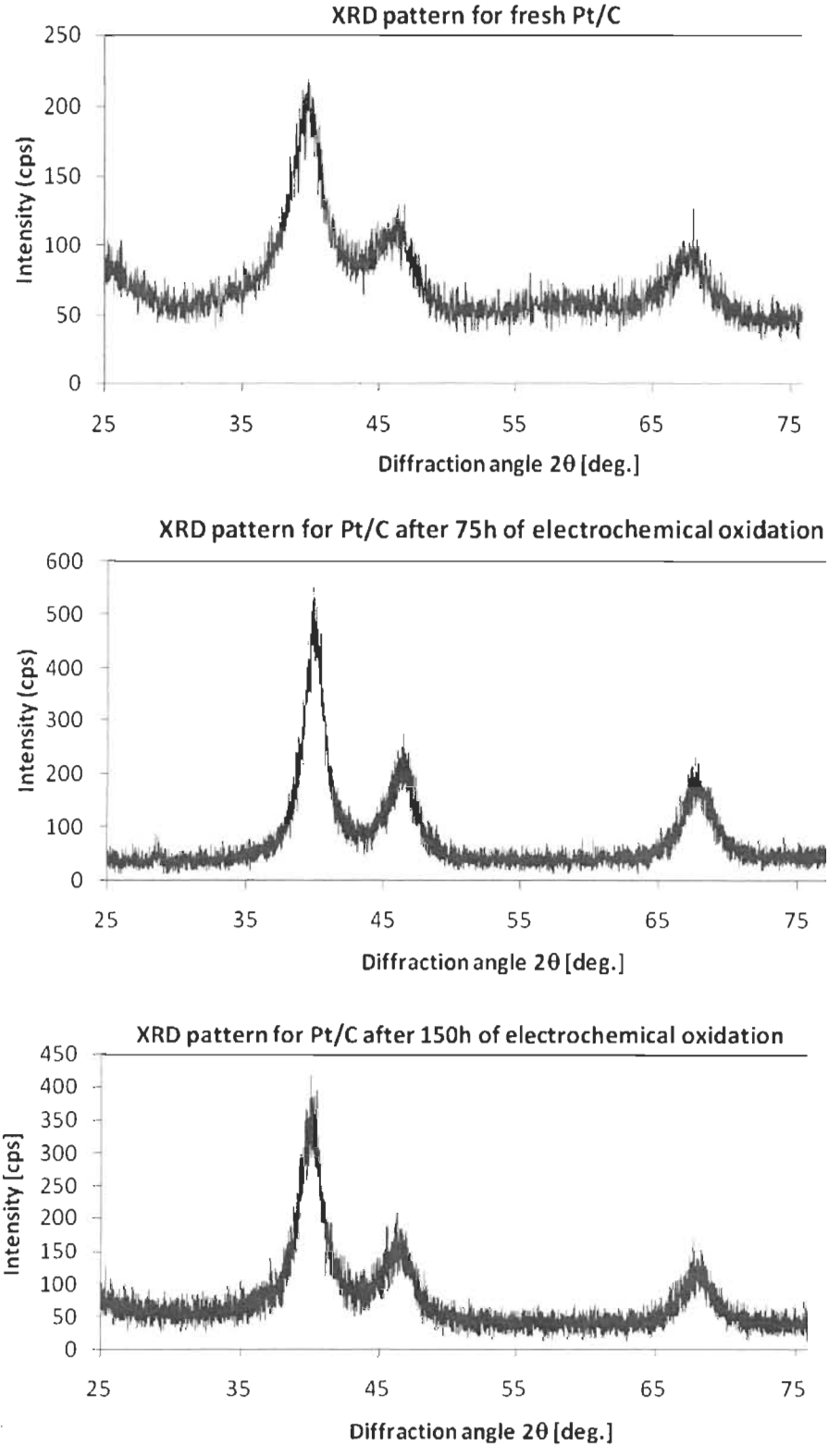

Figure 6.8 X-ray diffraction patterns for Pt/C after electrochemical oxidation at 1.2 V for different time intervals.

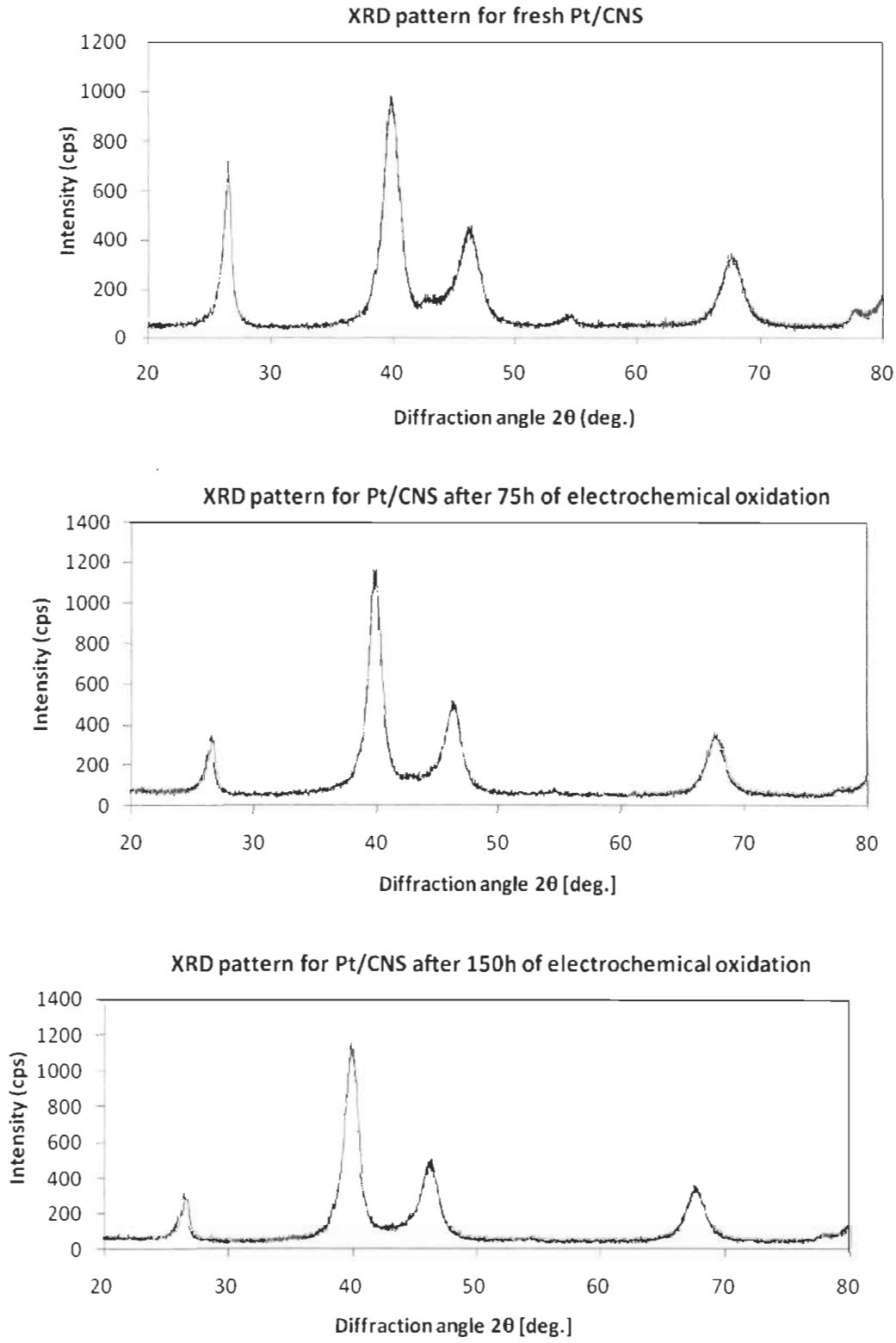

Figure 6.9 X-ray diffraction patterns for Pt/CNS after electrochemical oxidation at 1.2 V for different time intervals.

Figure 6.10 shows a 20% growth in platinum particle size from its original value for a period of electrochemical oxidation up to 150 h. The hypothesis of why a 40% loss in platinum surface area supported on CNS is caused mainly by dissolution and aggregation of Pt ions is considered as follows; Firstly, the percentage drop in operating cell potential is five times lesser for MEA2 compared with MEA1. This explains the fact that the apparent density of the Pt ion band formed close to the cathode layer in MEA2 is lower than MEA1. Secondly, the distance of the Pt band from the cathode is closer to the anode, which enhances the oxygen flux from the cathode, thanks to reduced pore size and better hydrophobicity properties of CNS. Thirdly, if the Pt band is reduced near the anode catalyst layer, then the performance of MEA2 would have dropped significantly due to membrane degradation. However, this is not the case of MEA2, where the rate of loss in operating cell potential is very less compared to MEA1.

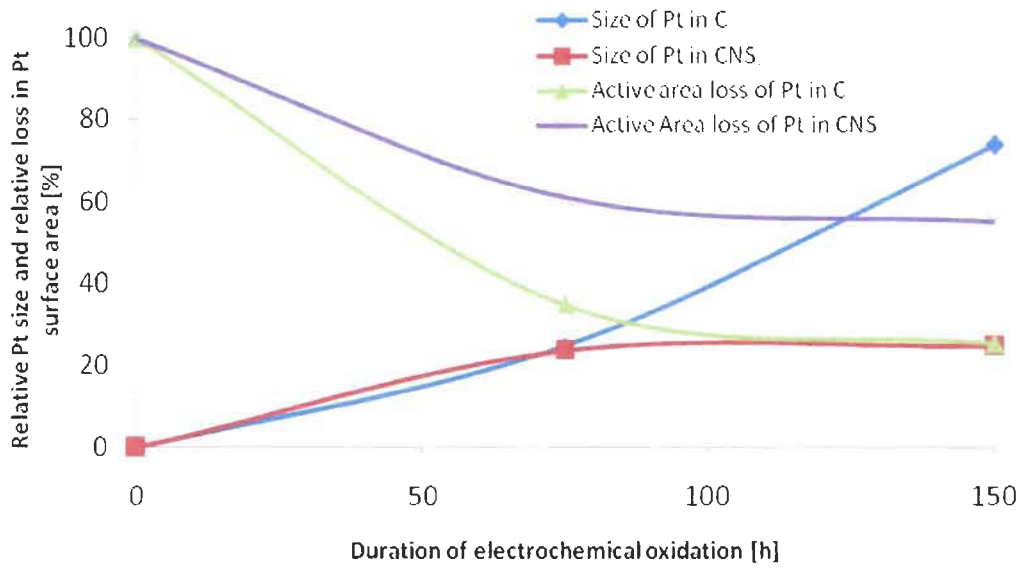

Figure 6.10 Growth of Pt particle size as observed by XRD related to the loss in active surface area of the catalyst during electrochemical oxidation of Pt/C and Pt/CNS.

6.2.5.2 ANALYSIS OF SURFACE FUNCTION GROUPS

Kangasniemi *et al.* [33] performed thermal desorption studies on carbon to assign decomposition temperature for different functional species and their thermal decomposition products. The same group estimated the amount of surface oxygen groups on carbon using a mass spectrometer by analyzing the volatile surface oxides from the

TGA instrument. We used the relationship between the surface functional groups and their oxidation temperature, which used in this thesis to get an idea about the functional groups at different intervals of electrochemical oxidation.

In our lab, TGA was performed using a TGA 7 PERKIN ELMER apparatus with an argon atmosphere at a purge rate of 30 sccm. The temperature was ramped as follows: room temperature to 50 °C at 5 °C min^{-1}, holds for 5 min at 50°C and heated from 50 °C to 850 °C at 5 °C min^{-1}.

In summary, evolution of CO_2 observed at low temperatures (approx. 250 °C) are usually assigned to acidic functional group, carboxylic acids and those at higher temperatures (approx. 625 °C) to lactones. At higher temperatures (600 °C to 900 °C), evolution of CO observed corresponds to ethers, phenols, carbonyls and quinones, while carboxylic anhydrides give rise to both CO and CO_2 peaks. Therefore, to characterize the surface functional groups during electrochemical oxidation of Pt/C and Pt/CNS, TGA was performed under argon on the dried samples at oxidation time periods of 0 h, 75 h and 150 h. Figure 6.11 and Figure 6.12 shows the TGA profiles of Pt/C and Pt/CNS after electrochemical oxidation at different time intervals. It is observed that on both the catalyst surfaces, the composition of –COOH intermediate for evolution of CO_2 remains almost unchanged. However, a huge variation in the composition of lactone was observed at different oxidation periods for the evolution of CO_2 between 350 °C and 400 °C.

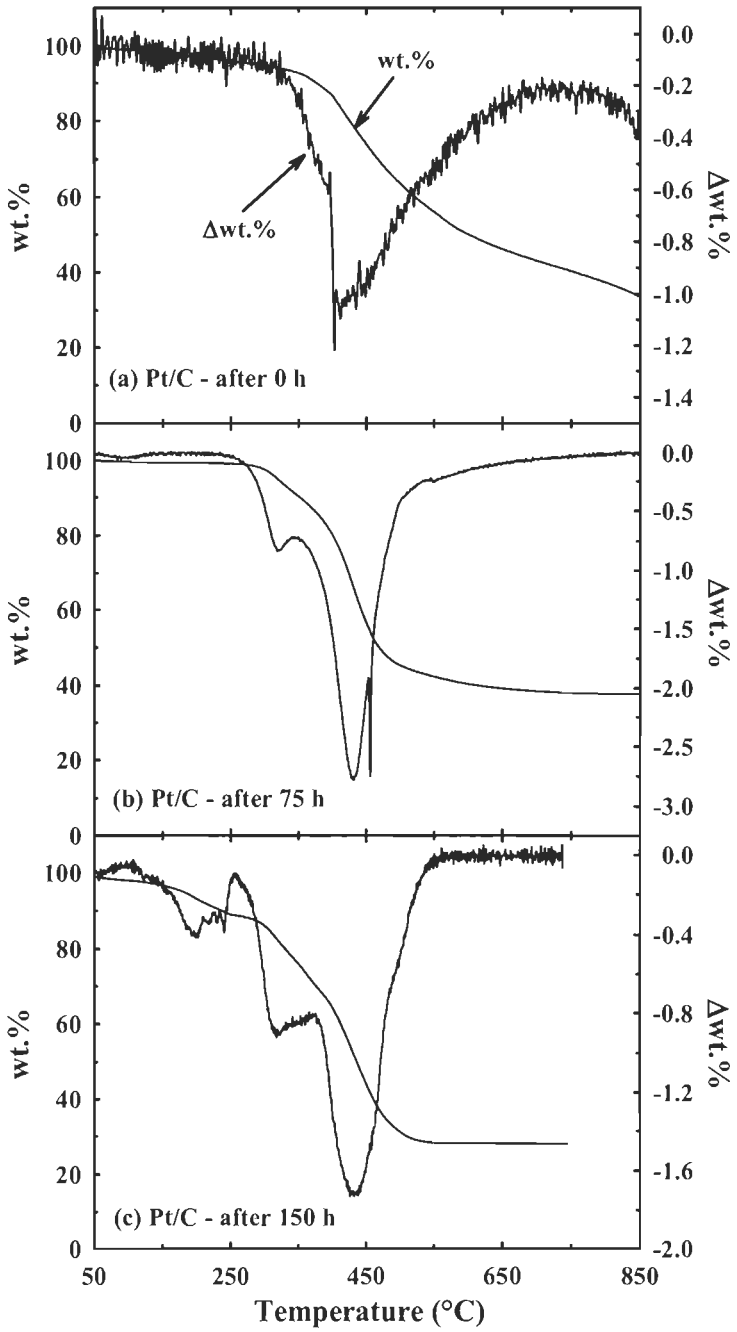

Figure 6.11 TGA profiles for Pt/C after electrochemical oxidation at 1.2 V for different time intervals.

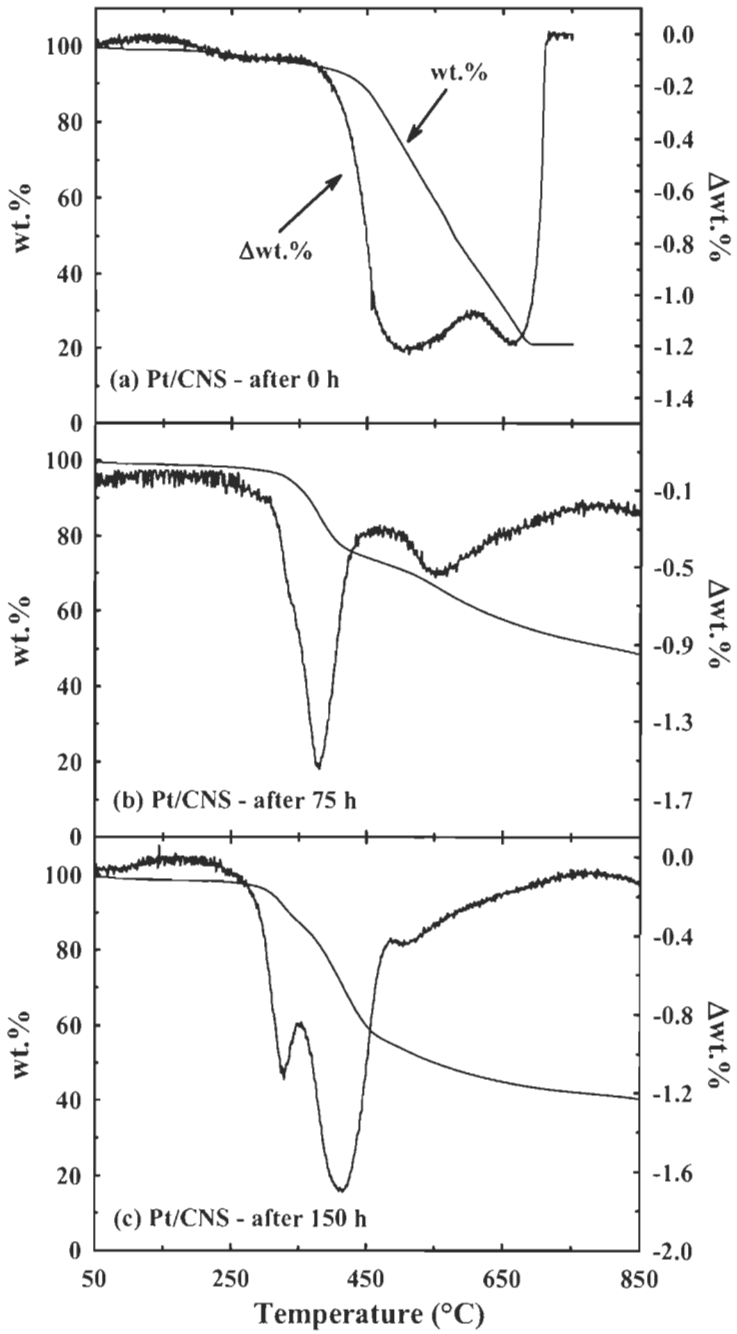

Figure 6.12 TGA profiles for Pt/CNS after electrochemical oxidation at 1.2 V for different time intervals.

Figure 6.11 shows an increase in density of surface oxides on carbon surface in the form of an intermediate, lactone over a period of electrochemical oxidation up to 150 h. Similarly, the CO_2 evolution from Pt/CNS was observed throughout the temperature

range, affirming the presence of different functional groups generated during the electrochemical oxidation of the catalyst. In addition to the functional groups involved for the evolution of CO_2, carbonyls and quinones, as well as phenols and ethers, decompose at temperatures higher than 700 °C to evolve CO. The apparent density of these functional groups responsible for the evolution of CO tend to decrease during the course of electrochemical oxidation, which is well in agreement with the generic mechanism of surface oxide formation proposed by Yue *et al.* [97] During the course of oxidation, an increase in surface oxygen content decreases the hydrophobic properties of the catalyst support, thus breaking down the surface oxides to CO_2. A similar decrease in density of surface functional groups for the evolution of CO is observed for Pt/C.

7. APPLICATION OF CNS

During the course of this work, we found a few applications to use CNS as a support material, which on demand generated good performance. Most of the work done in this section is confidential and what is disclosed here only reflects the perspective of the author, not any scientific information obtained during the course of the work.

A part of this work was done for SiM composites, Inc. [45]; a company specialize in manufacturing hydrocarbon membranes. We studied different methodologies to prepare anode catalyst layers with Pt loadings not greater than 50 $\mu g\, cm^{-2}$ dispersed homogeneously on CNS. Primarily, CV studies were performed on glassy carbon working electrodes to evaluate different platinization techniques that can be used at the anode catalyst layer to achieve higher Pt specific surface area. With our new approach and CNS as the substrate material, a catalyst loading of 50 $\mu g\, cm^{-2}$ was achieved using different methodologies selected using CV. It was observed that fuel cell tests performed on Pt supported on CNS with a very low platinum loading exhibited very similar results as that of a MEA prepared with standard 500 $\mu g\, cm^{-2}$ Pt/C based gas diffusion electrodes. However, a few research groups [98-100] have achieved a similar performance with even lower loadings of Pt using pulsed laser deposition and other sputtering techniques either on a membrane or on GDL's. Durability of as said methods has not been proved yet. Unlike other methods, the Pt deposition that was used in our technique involves carbon bonding with covalent-metallicity value close to 2.02, which approximates to 50% covalent and 50% metallic bonding between the surface carbon atoms and Pt. With the durability of CNS demonstrated as a part of this thesis work, we believe that our new methodology to prepare anode catalyst layers can contribute to research to come in the future. Kindly contact SiM Composites to avail this information, if it is made public. To follow up on this research work, we propose the following sequence;

a) Since, this work is done as a part to demonstrate/develop catalyst layer with low Pt loading, more understanding of the morphology of the catalyst layer (HRTEM, AFM…) and the interaction between Pt and C is necessary.

b) Not only to have control on Pt particle size, but also on the thickness of the catalyst layer.

c) To consider all the options yet another stable support material, carbon nanotubes can also be tried and with the aid of technical expertise from other research groups/companies, the alignment of these tubes cab be achieved, thus enhancing three-phase contacts.

d) Electrochemical Impedance Spectroscopy measurements must be performed to study the electrochemical responses of interfacial processes and structures.

e) Eventually, any catalyst support must be studied for its electrochemical durability under fuel cell operating conditions.

8. ONGOING AND FUTURE WORK

This section best describes the ongoing work and a few recommendations that come to mind when consider improving the porosity of CNS and electrode preparation techniques. At present, we are employing the decal technique [101], which has effectively proven to be one of the efficient methods for the fabrication of MEA. Given below is a step by step procedure of the same;

[1] **PREPARATION OF THE INK:** Measure out 1.0 g of 5 wt.% of Nafion solution into a vial and add 125 mg of supported electrocatalyst, so that the ratio of Pt carbon supported electrocatalyst to dry weight of Nafion is equal to 2.5:1 for the cathode. However, for the anode the ratio was maintained to 1:1. Stir the mixture with a magnetic stir bar for 1 h and add glycerol (half the amount of 5 wt.% Nafion) followed by stirring for at least 15 min. Now, cation exchange the solubilized Nafion to TBA^+ form by adding 50 mg of tetra butyl ammonium hydroxide (TBA-OH) in 1 M methanol using a micropipette or syringe. Stir the ink for 1 h. Add glycerol again, half the amount of 5 wt.% Nafion solution and stir for at least 24 h.

[2] **PAINT AND OVEN DRY DECALS:** Clean 5 cm^2 fiberglasses reinforced Teflon decal blanks with isopropanol and dry them. Paint a coat of catalyst ink on one side of decal material and dried in oven at 140 °C for 1 h. Subsequently, remove the dried decals from the oven and repeat the painting procedure until the desired loading is achieved. Usually, the paintings are done alternatively at 90 °angles to the previous coat direction. The final weighing is made after 24 h of drying.

[3] **MEMBRANE PRE-TREATMENT:** Clean Nafion NRE212 by boiling it in a 3% hydrogen peroxide solution for 1 h, rinsing with deionised water and boiling it in deionised water for another hour. The protonic form of the membrane is exchanged to Na^+ form by boiling in 1% NaOH solution for 1 h, rinsing with deionised water and boiling it again in deionised water for another hour. Dry the treated membrane by placing it on a heated vacuum table that is at room temperature, steadily heated to 130 °C for 5 to 10 min, cooled to room temperature with vacuum still on, removed and stored in a plastic cover.

[4] **HOT PRESSING:** The MEA is hot pressed with the procedure described earlier. However, the conditions of this step is changed due to the fact that the membrane with Na^+ form is more robust and can withstand higher temperature and pressure. The conditions are $T = 210$ °C, $P = 110$ lb cm^{-2} and holding time is 5 min.

[5] **MEMBRANE PROTONATION:** Peel the decals away from the membrane leaving the catalyst electrodes fused to the membrane. Boil the MEA in 0.5 M sulphuric acid for 1 h, rinse with deionised water and boil again in deionised water for another hour. Dry the MEA on a vacuum table at 60 °C for 15 min. Finally, with GDLs covered on both sides, assemble the MEA as described earlier.

We had no issues during painting the teflonized composite material or transferring the catalyst layer onto the membrane. However, a very low cell performance was obtained which may be due to one of the following reasons; (a) the proton group's membrane was not successfully exchanged into Na^+ form, which here can be resolved by increasing the treatment time or adjusting the concentration of NaOH, (b) the membrane exchanged with Na^+ group has physical properties similar to a plastic material, which makes it difficult to dry on a vacuum table, (c) if by any chance some of the sulfonic groups are not exchanged with Na^+ ions, the high temperature and pressure conditions used in this technique might have caused pinholes in the membrane leading to permanent damage in MEA, (d) if the degree of protonation of PEM with electrodes after hot pressing is not effective, this creates a voids with Na^+ groups resisting the transport of protons within the catalyst layer. The points listed above are some of our recommendations, which any researcher continuing this work can consider as an option to resolve as said problem.

During the course of this research work, we proposed a new technique called as decal platinization to disperse high density of Pt nanoparticles between the cathode catalyst layer and membrane interface. Essentially, the steps followed to fabricate MEA using decal technique will be repeated here with a few corrections,

(a) The catalyst ink is prepared with carbon support material and Nafion instead of Pt supported carbon and Nafion.

(b) The dried decal after step 2 is platinized using colloidal technique. By this way, the smaller Pt-OH molecules diffuse through the pores of the carbon support and get reduced on the functional groups that the electrolyte membrane has closer access to.

The loading after decal platinization was estimated to be 0.02 mg cm^{-2}. During the first cycle of this experiment, a polarization curve better than the one obtained during decal method is shown in Figure 8.1. However, a setback of this technique is preventing the solubility of dried catalyst layer under strong acidic conditions and the repeatability of these results was not successful. A quick recommendation to continue this work is to play with the viscosity of the ink mixture to enhance the adhesion or to modify this technique to platinize directly onto a microporous layer.

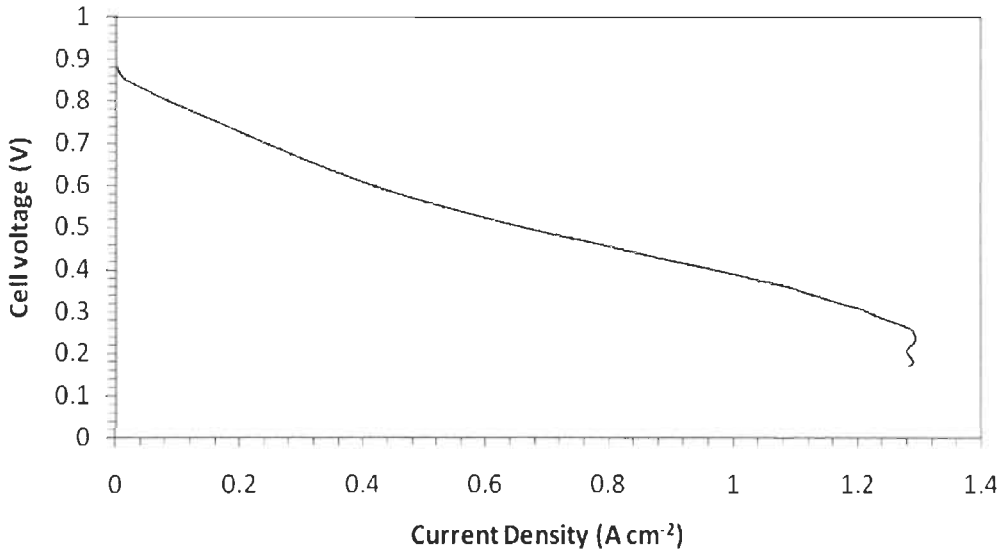

Figure 8.1 Polarization curve for the MEA prepared using decal platinization.

9. SUMMARY

Within the scope of this thesis a number of techniques have been developed in order to investigate CNS as suitable catalyst support material in PEMFCs. Moreover, electrode material durability is an important factor limiting the commercialization of PEMFCs. So, we examined this support material for loss in specific surface area and compared it with Pt/C. The summary of this thesis work is as follows;

- Ball milling of graphite or activated carbon with transition metal catalysts under hydrogen followed by heat treatment under argon is an effective tool to prepared nanostructured powders of carbon with tuneable properties.
- BET analyses on our CNS samples gave a specific surface area of 352.6 $m^2 g^{-1}$, a micropore volume of 0.14 $cm^3 g^{-1}$, and an average micropore width of 1.6 nm. The Hg intrusion data analysis gives a macropore size radius of 45.8 $m^2 g^{-1}$ and a total macropore volume of 635 $mm^3 g^{-1}$.
- The oxidation temperature of CNS was as high as carbon nanotubes indicating higher graphite component in both the samples.
- Chemical oxidation of CNS with 1:1 ratio of 7.5 M sulphuric acid and 15 M nitric acid showed significant improvement for the removal of impurities and generation of surface functional groups over other oxidation treatments.
- With half the amount of Pt supported on CNS when compared with Pt/C, the former catalyst exhibited similar electrochemical performance like the latter one indicating the influence of high porous structure favouring mass and concentration transports.
- During the durability studies on the electrocatalyst, the loss in specific surface area of Pt was due to the growth in particle size. However, diffusion of Pt ionic species into the membrane causing degradation over a period of operation was observed on MEA prepared with Pt/C.
- The loss in surface area of Pt was observed as a result of carbon support corrosion under cathode simulated conditions.
- Electrochemical characterizations showed that CNS prepared in our laboratory has improved corrosion resistance and better performance over Vulcan XC-72.

From the results obtained in this study, we conclude that CNS can be a good candidate for PEMFC catalyst support material exhibiting less Pt surface area loss without sacrificing catalytic activity.

This work has resulted in 3 articles, 2 published and 1 submitted (in appendix):

[1] Sadesh Kumar Natarajan and Jean Hamelin, "Electrochemical Durability of Carbon Nanostructures as Catalyst Support for PEMFCs", *Journal of the Electrochemical Society* 156(2), pp. B210-B215 (2009).

[2] Sadesh Kumar Natarajan, D. Cossement and J. Hamelin, "Synthesis and Characterization of Carbon Nanostructures as Catalyst Support for PEMFCs", *Journal of the Electrochemical Society* 154(3), pp. B310-B315 (2007)

[3] Sadesh Kumar Natarajan and Jean Hamelin, "Homogeneous Pt Deposition on Chemically Modified Carbon Nanostructures as Catalysts for PEMFCs", *Electrochimica Acta* 52(11), pp. 3741-3757 (2007).

10. REFERENCES

[1] P. Costamagna, S. Srinivasan, J. Power Sources 102 (2001) 242.

[2] P. Costamagna, S. Srinivasan, J. Power Sources 102 (2001) 253.

[3] K. Sopian, W.R. Wan Daud, Renew. Energy 31 (2006) 719.

[4] E. Auer, A. Freund, J. Pietsch, T. Tacke, Appl. Catal. A: Gen. 173 (1998) 259.

[5] S. Litster, G. Mclean, J. Power Sources 130 (2004) 61.

[6] F. Rodriguez-Reinoso, Carbon 36 (1998) 159.

[7] DOE FY 2002 & 2004 Annual Progress Reports.

[8] L. Zhang, J. Zhang, D.Wilkinson, H.Wang, J. Power Sources 156 (2006) 171.

[9] E. Antolini, J. Mater. Sci. 38 (2003) 2995.

[10] N. Alonso-Vante, H. Tributsch, Nature 323 (1986) 431–432.

[11] N. Alonso-Vante,W. Jaegermann, H. Tributsch,W. Honle, K. Yvon, J. Am. Chem. Soc. 109 (1987) 3251.

[12] R.W. Reeve, P.A. Christensen, A.J. Dickinson, A. Hamnett, K. Scott, Electrochim.Acta 145 (2000) 3463.

[13] M.C. Martins Alves, J.P. Melet, D. Guay, M. Ladouceur, G. Tourillon, J.Phys. Chem. 96 (1992) 10898.

[14] L.T.Weng, P. Bertrand, G. Lalande, D. Guay, J.P. Dodelet, Appl. Surf. Sci. 84 (1995) 9.

[15] Frederic Jaouen, Jean-Pol Dodelet, Electrochimica Acta, 52 (2007) 5975.

[16] H.A. Gasteiger, S.S. Kocha, B. Sompalli, F.T. Wagner, Appl. Catal. B: Environ. 56 (2005) 9.

[17] G. Liu, H. Zhang, Y. Zhai, Y. Zhang, D. Xu, Z. Shao, Electrochem.Commun. 9 (2007) 135.

[18] D. Thompsett, W. Vielstich, H.A. Gasteiger (Eds.), Handbook of Fuel Cells—Fundamentals, Technology and Applications, vol. III, JohnWiley & Sons, New York, 2003, pp. 467–480.

[19] O. Savadogo, P. Beck, J. Electrochem. Soc. 143 (1996) 3842.

[20] J. Shim, C. Lee, H. Lee, J. Lee, E. Cairns, J. Power Sources 102 (2001) 172.

[21] K. Ota, A. Ishihara, S. Mitsushima, K. Lee, Y. Suzuki, N. Horibe, T.Nakagawa, N. Kamiya, J. New. Mater. Electrochem. Syst. 8 (2005) 25.

[22] S. Mukerjee, S. Srinivasan, J. Electroanal. Chem. 357 (1993) 201.

[23] G. Tamizhmani, G.A. Capuano, J. Electrochem. Soc. 141 (1994) 968.

[24] M. Pourbaix, Altas of Electrochemical Equilibrium in Aqueous Solutions, Pergamon Press, New York, 1966.

[25] T. Okada, in: W. Vielstich, A. Lamm, H.A. Gasteiger (Eds.), Handbook of Fuel Cells: Fundamentals, Technology, and Applications, vol. 3, John Wiley & Sons, New York, 2003 (Chapter 37).

[26] K. Kinoshita and J. A. S. Bett, Carbon 11 (1973) 403.

[27] K. Kinoshita and J. Bett, Carbon 11 (1973) 237.

[28] K. Kinoshita and J. A. S. Bett, Carbon 12 (1974) 525.

[29] K. Kinoshita and J. A. S. Bett, Carbon 13 (1975) 405.

[30] K. Kinoshita and J. A. S. Bett, Corrosion Problems in Energy Conversion and Generation, C. S. Tedmon, Jr., Editor, PV 74-3, p. 273, The Electrochemical Society Proceedings Series, Princeton, NJ (1974).

[31] K. Kinoshita, Carbon Electrochemical and Physicochemical Properties, Chap. 6, John Wiley & Sons, New York (1988).

[32] J. Willsau and J. Heitbaum, J. Electroanal. Chem. 161 (1984) 93.

[33] K.H. Kangasniemi, D.A. Condit, T.D. Jarvi, J. Electrochem. Soc. 151 (2004) E125.

[34] N. M. Rodriguez, M.S. Kim, and R. T. K. Baker, J. Phys. Chem. 98 (1994) 13108.

[35] A. Chambers, N. M. Rodriguez, and K. T. R. Baker, Langmuir 11 (1995) 3862.

[36] K. P. De Jong and J. W. Geus, Catal. Rev. Sci. Eng. 42 (2000) 481.

[37] C. A. Bessel, K. Laubernds, N. M. Rodriguez, and R. T. K. Baker, J. Phys. Chem. B 104 (2000) 1115.

[38] E. S. Steigerwalt, G. A. Deluga, D. E. Cliffel, C. M. Lukehart, J. Phys. Chem. B 105 (2001) 8097.

[39] G. Che, B. B. Lakshmi, E. R. Fisher, and C. R. Martin, Nature 393 (1998) 346.

[40] W. Li, C. Liang, J. Qiu, W. Zhou, H. Han, Z. Wei, G. Sun, and Q. Xin, Carbon 40 (2002) 787.

[41] Z. Liu, X. Lin, J. Y. Lee, W. Zhang, M. Han, and L. M. Gan, Langmuir 18 (2002) 4054.

[42] Daniel Cossement, Richard Chahine, Tapan k. Bose, U.S. Patent 20050260117, 2005.

[43] Energy Efficiency and Renewable Energy, USDOE, http://www.eere.energy.gov

[44] http://electrochem.cwru.edu/ed/encycl/

[45] SiM Composites, 4925 Lionel-Groulx, suite 11, St-Augustin-de-Desmaures Quebec G3A 1V1

[46] E. Yeager, J. O'M Bockris, B. E. Conway and S. Sarangapani. Comprehensive Treatise of Electrochemistry 9 (1984) 24.

[47] G. Tremiliosi-Filho, G. Jerkiewicz and B. E. Conway, Langmuir 8 (1992) 658.

[48] H. Yoshitake, T. Mochizuki, O. Yamazaki and K. Ota.. J. Electroanaly. Chem., 361 (1993) 229.

[49] James P. Hoare, J. Electrochem. Soc. 132 (1985) 301.

[50] C. Wang, M. Waje, X. Wang, J.M. Tang, R.C. Haddon, Y.S. Yan, Nano Lett. 4 (2004) 345.

[51] Z. Paál and P. G. Menon, Hydrogen effects in catalysis: Fundamental and practical applications, Marcel Dekker (1987).

[52] M. Endo, K. Takeuchi, S. Igarashi, K. Kobori, M. Shiraishi and H. W. Kroto, J. Phys. Chem. Solids 54 (1993) 1841.

[53] S. B. Sinnott, R. Andrews, D. Qian, A. M. Rao, Z. Mao, E. C. Dickey and F. Derbyshire, Chem. Phys. Letters 315 (1999) 25.

[54] S. Bandow, A. M. Rao, K. A. Williams, A. Thess, R. E. Smalley and P. C. Eklund, J. Phys. Chem. B101 (1997) 8839.

[55] K. B. Shelimov, R. O. Esenaliev, A. G. Rinzler, C. B. Huffman and R. E. Smalley, Chem. Phys. Lett. 282 (1998) 429.

[56] G. S. Duesberg, M. Burghard, J. Muster, J. Philipp and S. Roth, Chem. Commun. 435 (1998)

[57] A. C. Dillon, K. M. Jones, T. A. Bekkedahl, C. H. Kiang, D. S. Bethune and M. J. Heben, Nature 386 (1997) 377.

[58] J. L. Zimmerman, R. K. Bradley, C. B. Huffman, R. H. Hauge and J. L. Margrave, *Chem. Mater.* 12 (2000) 1361.

[59] I. W. Chiang, B. E. Brinson, R. E. Smalley, J. L. Margrave and R. H. Hauge, *J. Phys. Chem.* B 105 (2001) 1157.

[60] I. W. Chiang, B. E. Brinson, A. Y. Huang, P. A. Willis, M. J. Bronikowski, J. L. Margrave, R. E. Smalley and R. H. Hauge, J. Phys. Chem. B105 (2001) 8297.

[61] A. Rinzler, Appl. Phys. A67 (1998) 29.

[62] J. Liu, Science 280 (1998) 1253.

[63] J. Zhang, H. Zou, Q. Qing, Y. Yang, Q. Li, Z. Liu, X. Guo and Z. Du J. Phys. Chem. B 107 (2003) 3712.

[64] R. M. Lago, S. C. Tsang, K. L. Lu, Y. K. Chen, M. L. H. Green, J. Chem. Soc., Chem. Commun. (1995) 1355.

[65] S. C. Tsang, Y. K. Chen, J. P. F. Harris, M. L. H. Green, Nature 372 (1994) 159.

[66] K. C. Hwang, J. Chem. Soc., Chem. Commun. (1995) 173.

[67] H. Hiura, T. W. Ebbesen, K. Tanigaki, Adv. Mater. 7 (1995) 275.

[68] L. Okhlopkova, A. Lisitsyn, V. Likholobov, M. Gurrath, H. Boehm, Appl.Catal. A 204 (2000) 229.

[69] M. Fraga, E. Jordao, M. Mendes, M. Freitas, J. Faria, J. Figueredo, J.Catal. 209 (2002) 355.

[70] M. Watanabe, M. Uchida, S. Motoo, J. Electroanal. Chem. 229 (1987) 395.

[71] J. Lobato, M. Rodrigo, J. Linares, K. Scott, J. Power Sources 157 (2006) 284.

[72] C. Huang, Z. Han, X. Li, Y. Chen, Chin. J. Power Sources 24 (2000) 243.

[73] T. Kodas, U.S. Patent 6,103,3392 (2000).

[74] Z. Liu, J.Y. Lee, M. Han,W. Chen, L.M. Gan, J. Mater. Chem. 12 (2002) 2453.

[75] Wenzhen Li, Changhai Liang, Weijiang Zhou, Jieshan Qiu, Zhenhua Zhou, Gongquan Sun, Qin Xin, J. Phys. Chem. 107 (2003) 6292.

[76] X. H. Chen, C. S. Chen, Q. Chen, F. Q. Cheng, G. Zhang and Z. Z. Chen, Materials Letters 57 (2002) 734.

[77] D. Pantea, H. Darmstadt, S. Kaliaguine, L. Sümmchen and C. Roy, Carbon 39 (2001) 1147.

[78] E. Passalacqua, G. Squadrito, F. Lufrano, A. Patti and L. Giorgi, J. Appl. Electrochem. 31 (2001) 449.

[79] U. Zielke, K. J. Huttinger, W. P. Hoffman Carbon 34 (1996) 983.

[80] W. K. J. Huttinger, S. Hohmann-Wien, M. Seiferling Carbon 29 (1991) 449.

[81] A. Pozio, M. De Francesco, A. Cemmi, F. Cardellini, L. Giorgi, J. Power Sources 105 (2002) 13.

[82] Z. R. Yue, W. Jiang, L. Wang, S. D. Gardner, and C. U. Pittman Jr., Carbon 37 (1999) 1785.

[83] D. Rivin, Rubber Chem. Technol. 36 (1963) 729.

[84] Y. Yang and Z. G. Lin, J. Appl. Electrochem., 25 (1995) 259.

[85] N. L. Weinberg and T. B. Reddy, J. Appl. Electrochem. 3 (1973) 73.

[86] B. W. Chun, C. R. Davis, Q. He and R. Gustafson, Carbon 30 (1992) 177.

[87] X. Wang, M. Waje, Y.S. Yan, Electrochem. Solid State Lett. 8 (2005) A42.

[88] J. M. Thomas, Adv. Catal., 19 (1969) 293.

[89] B. R. Puri, J. Indian Chem. Soc. 51 (1974) 62.

[90] A. Antolini, J. Mater. Sci. 38 (2003) 2995.

[91] S. Mukerjee, S. Srinivasan, 2: Electrocatalysis, in Handbook of Fuel Cells – Fundamentals, Technology and Applications, John Wiley & Sons (2003) 502.

[92] A. C. C. Tseung, S. C. Dhara, Electrochimica Acta 20 (1975) 681.

[93] A. Honji, T. Mori, K. Tamura , Y. Hishinuma, J. Electrochem. Soc. 135 (1988) 355.

[94] M. Watanabe, K. Tsurumi, T. Mizukami, T. Nakamura, P. Stonehart, J. Electrochem. Soc. 141(1994) 2659.

[95] K. F. Blurton, H. R. Kunz, D. R. Rutt, Electrochimica Acta 23 (1978) 183.

[96] J. A. Bett, K. Kinoshita, P. Stonehart, J. Catal. 41 (1976) 124.

[97] Z.R. Yue, W. Jiang, L. Wand, S.D. Gardner, C.U. Pittman, Carbon 37 (1999) 1985.

[98] N. Cunningham, E. Irissou, M. Lefevre, M. C. Denis, D. Guay, J. P. Dodelet, Electrochem. Solid State Lett. 6 (2003) A125.

[99] Ryan O'Hayre, Sang-Joon Lee, SukWon Cha, Fritz. B. Prinz, J. of Power Sources 109 (2002) 483.

[100] Chieh-Hao Wan, Meng-Tsun Lin, Qing-Huang Zhuang, Chien-Heng Lin, Surface & Coatings Technology 201 (2006) 214.

[101] Mahlon S. Wilson, Judith A. Valerio, Shimshon Gottesfeld, Electrochimica Acta 40 (1995) 355.

11. APPENDIX I: FIRST PAPER

Sadesh Kumar Natarajan, Daniel Cossement, Jean Hamelin, *Synthesis and Characterization of Carbon Nanostructures as Catalyst Support for PEMFCs*, Journal of Electrochem. Soc. 154 (2007) B310.

Journal of The Electrochemical Society, **154** (3) B310-B315 (2007)
0013-4651/2007/154(3)/B310/6/$20.00 © The Electrochemical Society

Synthesis and Characterization of Carbon Nanostructures as Catalyst Support for PEMFCs

Sadesh Kumar Natarajan,* Daniel Cossement, and Jean Hamelin,z**

Institut de Recherche sur l'Hydrogène, Université du Québec à Trois-Rivières, Trois-Rivières, Quebec, Canada G9A 5H7

A detailed procedure for synthesis, characterization, and possibility of carbon nanostructures (CNS) as support for catalysts in polymer electrolyte membrane fuel cells (PEMFCs) is presented. The fabrication process is two-staged ballmilling of carbon graphite in the presence of hydrogen and transition metals (Fe, Co) followed by heating of the milled carbon initially in an argon atmosphere. The milling induces amorphous forms of carbon and metal, as well as C-H bonds. During the second stage, the production of methane by catalytic reaction of the bonded carbon and hydrogen is first observed, followed by the formation of metallic nanocrystals, and, finally, the formation of carbon structures on the metallic nanocrystals at a temperature of 700°C. Subsequently, metals and carbon nanoparticles are removed from the as-prepared sample. The purified samples are platinized after surface treatment by either air or chemical oxidation. Material characterization results obtained by X-ray diffraction, transmission electron microscopy, thermogravimetric analysis, X-ray photoelectron spectrocopy, and atomic adsorption spectroscopy are presented. In addition, we also report their measured electrical conductivity, specific surface, and porosity. The real electrochemical active surface area was evaluated by cyclic voltammetry on a thin porous coated electrode.
 [DOI: 10.1149/1.2409867]

Manuscript submitted July 20, 2006; revised manuscript received October 13, 2006. Available electronically January 17, 2007.

Polymer electrolyte membrane fuel cells (PEMFCs) are considered as one of the potential alternative power source for stationary and automotive applications because of their high efficiency, high power density, low noise, and low emissions. The cathodic overpotential is strongly influenced by several physical and operating parameters such as the cell current density, electrochemically active catalyst surface area, conductivity and thickness of the electrode, the concentration and diffusion coefficient of air or O_2, and so on. At relatively high current densities, PEMFCs are characterized by high water production at the cathode. As a result, water gets agglomerated in the diffusion and catalyst layer pores and drastically slows down the diffusion of O_2 to the active catalyst sites; the electrode is then said to be flooded. Consequently, the anode voltage drops.[1]

A proposed solution is to replace the commercial catalyst support, Vulcan XC-72, E-TEK, with a carbon containing nanostructure such as nanotubes. Since the discovery of carbon nanotubes in 1991 by Iijima,[2] carbon nanostructures have continued to fascinate the scientific community. Their mechanical and electrical properties make their use in industries such as electrochemistry and electronics very promising. Yoshitake et al.[3] have shown the use of carbon nanostructures (CNS), such as single-wall nanohorns, as catalyst support for PEMFCs with higher power densities than standard carbon black. According to the authors, increase in power is strongly influenced by homogenous dispersion of the catalyst over the carbon support.

Generally, three different techniques are used to prepare CNS-arc discharge,[4] laser ablation,[5] and chemical vapor deposition (CVD).[6,7] This last technique is the most widely used, as it has the advantage to produce a large quantity of nanostructures at a relatively low cost. In this study, we present a new technique to produce CNS similar to CVD, with CNS forming on Fe/Co metallic nanocrystals, and is composed of two distinct steps. The first step is the mechanical milling (ballmilling) of carbon graphite in the presence of hydrogen and transition metals (Fe and Co). Ballmilling creates an amorphous solid from the carbon and the transition metals, forms C-Fe and C-H bonds and produces methane (CH_4). The second step is the heating of the milled carbon in an argon atmosphere. It is during this step that the production of methane due to a catalytic reaction between the carbon and the bonded hydrogen is observed, followed by the formation of metallic nanocrystals (Fe, FeCo, and Fe_7Co_3), and at 700°C, the CNS were formed on the nanocrystals with evolution of H_2 gas.

To characterize the physical properties of these carbon powders, we have performed a series of analyses: X-ray diffraction (XRD) to confirm the presence of the carbon structure, the presence of Pt after platinization, and to calculate the average Pt cluster diameter; thermogravimetric analysis (TGA), to give us a clue about the type of nanostructures present in our carbon samples; X-ray photoelectron spectroscopy (XPS) to identify the chemical bonds (C and O) at the surface of our samples and inform us about the degree of functionalization of the carbon surfaces; atomic adsorption spectroscopy (AAS) to measure the exact amount of Pt in Pt/CNS, transmission electron microscopy (TEM) to obtain a 2D picture of CNS and Pt/CNS, to study the Pt distribution and also to corroborate the average Pt cluster diameter obtained from XRD.

CNS has relatively high pore volume, which extends the upper limit of current density that a PEMFC could achieve before the cathode gets flooded.[8,9] The high external surface of CNS facilitates homogenous distribution of catalyst over their external surface, thus leading to more efficient catalyst utilization.

Electrical conductivity is important to ensure sufficient electron transfer within the catalyst layer. In addition, CVs were performed on Pt/CNS to study the surface electrochemistry of the catalyst layer. Most of our results were compared with standard 20 wt % Pt/Vulcan XC-72, manufactured by E-TEK.

Theory

X-ray analysis of the milled graphite showed the formation of Fe, Fe_3C, and Fe_7C_3. Gas chromatography of the residual gases in the crucible indicate the presence of CH_4 and traces of heavier hydrocarbons. Activated amorphous carbon produced by high-energy ballmilling under H_2 atmosphere induces the formation of metallic carbons by mechanical synthesis, such as Fe_3C, Fe_7C_3, and hydrogenation of carbon, eventually releasing methane. The chemistry of methanation can be described with[10]

$$Fe - C + 4Fe - H \rightarrow CH_4 + 5Fe \qquad [1]$$

which involves the following sequence of elementary steps:

1. The following reaction involves the reversible dissociative adsorption of hydrogen on the iron surface,

$$H_2 + 2Fe \rightleftharpoons 2Fe - H(ads) \qquad [2]$$

2. During the mechanical synthesis, the carbon gets adsorbed on the metallic iron surface

* Electrochemical Society Student Member.
** Electrochemical Society Active Member.
z E-mail: Jean.Hamelin@UQTR.ca

$$Fe + C \rightarrow Fe - C(ads) \quad [3]$$

which is hydrogenated by the adsorbed atomic hydrogen in the following steps

$$Fe - C_{ads} + Fe - H_{ads} \rightarrow Fe - CH_{ads} + Fe \quad [4]$$

$$Fe - CH_{ads} + Fe - H_{ads} \rightarrow Fe - CH_{2ads} + Fe \quad [5]$$

$$Fe - CH_{2ads} + Fe - H_{ads} \rightarrow Fe - CH_{3ads} + Fe \quad [6]$$

$$Fe - CH_{3ads} + Fe - H_{ads} \rightarrow CH_4 + 2Fe \quad [7]$$

The milled sample is transferred under an inert atmosphere to a quartz tube for heating. The process of methane formation is similar to that occurring during ballmilling, except here, the required energy comes from heating. The hydrocarbon catalytic decomposition over metallic precursors (or CVD) and the subsequent graphitic nanostructure conversion was extensively studied and modeled by Endo et al.[6] and Sinnott et al.[7] During the heating process, the following reactions take place, desorption of the H_2 and hydrocarbon formation over the transition metals, then, catalytic decomposition of these hydrocarbons over the transition metals, thus resulting in formation of ordered CNS with evolution of H_2.

Experimental

Production process: ballmilling and heating.— In a hardened steel crucible, a sample of commercial activated carbon previously heated in a vacuum to 1000°C to rid it of impurities was mixed with a certain quantity of Fe and Co (99.9% pure). Typical proportions are, respectively, 50, 44, and 6 wt % for C, Fe, and Co. Three balls were used during milling, with a relative mass of balls to sample of 35 to 1. Hydrogen was then introduced to the crucible at a pressure of 1.4 MPa and the sample was milled for 12 h. The mill was an SPEX, which produces more mechanical energy than a planetary mill, but has the disadvantage of contaminating the sample with Fe by attrition.

During the second stage, the milled sample was transferred under an inert atmosphere to a quartz tube that is heated to 700°C for 1.5 h. The quartz tube was connected to a sampling cylinder for gas analysis.

The catalytic impurities and the amorphous carbon were removed by soaking the as-prepared sample in HCl trace metal solution, mechanically stirred for 35 min. Then, the solution is poured through a 5–10 μm filter. The precipitate is washed with ultrapure water and then dried in air at 200°C for 1.5 h. This procedure was used to obtain pure nanostructures (sample A) for characterization such as XRD, TGA, and TEM.

To compare the nanostructures with nanofibres, an X-ray diffractometer (Rigaku Co., Japan) with Co Kα1 (λ = 1.788965 Å) as radiation source was used. Platinized CNS were analyzed by a different X-ray diffractometer (Rigaku Co., Japan) with Cu Kα1 radiation (λ = 1.54051 Å). The TGA analysis was performed using a TGA 7 Perkin Elmer apparatus at a rate of 4°C min^{-1} from room temperature to 900°C and under O_2 atmosphere.

Surface functionalization.— Grafting of platinum catalyst is essential to prevent its leaching from PEMFC and to achieve a homogenous metal dispersion. Yu et al.[11] used chemical modification methods involving HNO_3 or HNO_3/H_2SO_4 mixtures and they found better dispersion of Pt clusters on the CNS surface is accomplished solely by the high density of O-containing groups.

To improve surface oxidation, i.e., functionalization, we tested the following methods; (a) ballmilling the purified CNS at 50 psig for a period of 30 min (sample B) and 1 h (sample C) under air. The functionalized samples were purified with the washing procedure described in the previous subsection, to remove Fe and Co added by attrition from the crucible and balls, (b) the as-prepared sample was refluxed with optimized 1:1 proportion of 7.5 M H_2SO_4 and 15 M HNO_3 mixture at 120°C for 3 h. The resultant dark-brown mixture was diluted with deionized water, filtered using 5 to 10 μm ceramic microfilter and finally washed with deionized water until the pH of the filtrate becomes neutral. The ceramic microfilter with the precipitate (sample D) was dried overnight at 120°C under dry nitrogen. XPS analysis was performed to characterize the chemical species at the surface of the sample, hence enabling us to determine the increase in C-O bonds after surface modification. The XPS apparatus was a Kratos Axis Ultra spectrometer using a Vision2 software for data analysis.

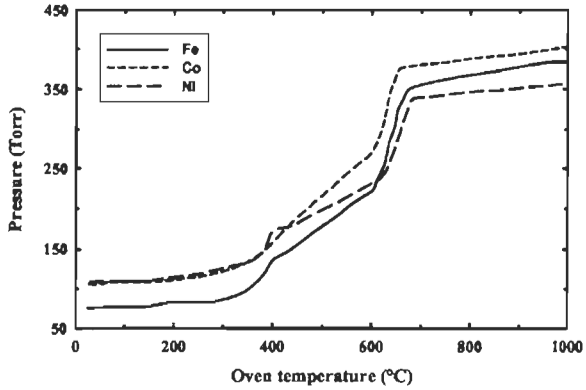

Figure 1. Pressure evolution during heating process with samples containing Fe, Co or Ni.

Surface and porosity measurements.— The total surface area and micropore volume of the porous CNS was obtained through Brunauer-Emmett-Teller (BET) measurement techniques from N_2 adsorption isotherms (77 K) measured with a Quantachrome AS-1-MP device. The macropore surface, pore volume, and pore radius were obtained from Hg intrusion isotherms measured with a Quantachrome Autoscan porosimeter with a maximum pressure of 60,000 psi.

Electrical conductivity measurement.— Electrical conductivity was measured with a Hewlett Packard 4284A impedance meter. The samples were compressed between two aluminum electrodes in an acrylic cylindrical cavity. A calibrated spring compresses the powder to a maximum pressure of 40 atm. With the conductance (G) mea-

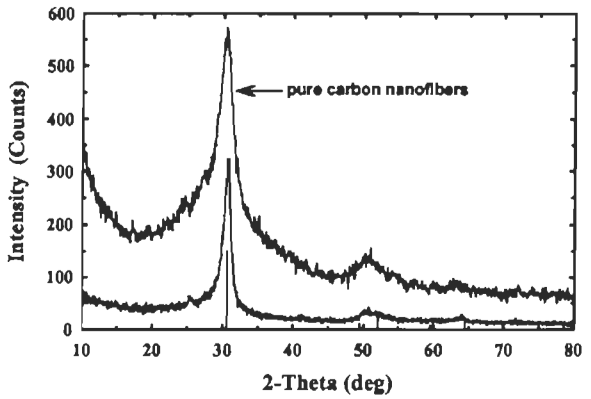

Figure 2. Typical XRD pattern of a carbon sample where the peaks correspond to graphite structures (Co source). The XRD pattern from a sample of pure nanofibers is also plotted for comparison.

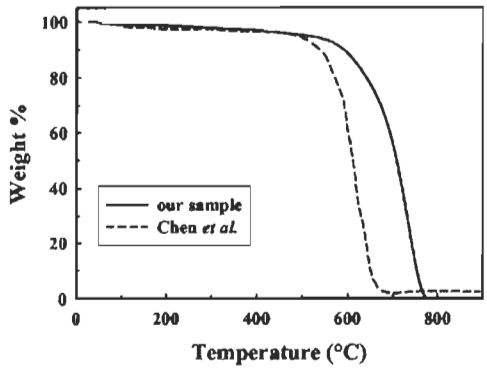

Figure 3. Typical TGA analysis results under O_2 atmosphere. Data from Chen et al.[13] are plotted for comparison.

sured from the impedance meter, the surface area of the electrodes (S) and the length of the sample (L), we calculate the conductivity (σ) using

$$\sigma = \frac{GL}{S} \quad [8]$$

During the measurements, samples of length $L = 0.3$ cm were placed in the cylindrical cavity, while the electrodes at either end had surface areas $S = 19.6$ mm^2.

Platinization.— A well-adopted method more like the one used by Li et al.[12] was employed to control the size of platinum particles. 400 mg of surface functionalized carbon nanostructures (sample D) was suspended in 40 mL of ethylene glycol (EG) solution and stirred for 30 min to well disperse 10 mg of CNS/mL of EG solution. 6.5 mL of Hexachloro-platinic acid (H_2PtCl_6, 10 wt % Pt) was added in drops followed by deionized water in steps to meet 20% of the bulk solution. The pH of the solution was adjusted above 13 by appropriate addition of NaOH in EG solution. A precipitate instead of metallic colloidal solution will result in case of pH less than 12. The amount of added water controls the size of intermediates, platinum hydroxide or hydroxyl acetate clusters,[12] which later reduces to platinum metal colloidal in the subsequent heating process. Reflux was carried out in an oil bath at 140°C for 3 h to reduce platinum completely and prevent escaping water contents in EG-water system. The platinized sample D (sample D_{Pt}) was filtered, washed, and dried overnight at 120°C in dry nitrogen. AAS analyses were performed on sample D_{Pt} with Varian spectra AA 55. There again, XRD and HRTEM 2D images were made to study the size and size distribution of Pt clusters in sample D_{Pt}.

Voltammetry measurements.— Sample D_{Pt} was weighed into a small vial to obtain a load of 0.2 mg/cm^2 along with 0.67 mg/cm^2 loading of Nafion (5 wt % Aldrich Nafion solution). A proportion of lower aliphatic alcohols were added to balance the platinum loading followed by ultrasonication in a bath for 1 h to give a homogeneous suspension. Viscosity of the suspension was altered with addition of 5 mg of 99% glycerol. 0.0707 cm^2 glassy carbon electrode was coated evenly with 1.5 to 2.0 μL of this suspension and sintered at 60°C for 15 min.

The CV was carried out in a conventional airtight three-electrode cell containing 1 M H_2SO_4 bulk solution at room temperature. The setup comprises of a 2 mm diam glassy carbon electrode, a platinum wire counter electrode, and Ag/AgCl (sat. KCl) reference electrode. Measurements were made at room temperature using Zahner IMe6 electrochemical workstation.

Results and Discussion

Production process.— Figure 1 shows the pressure evolution in the cylinder during heating of the hydrogenated sample, which contained Fe, Co, or Ni. In all three cases, the pressure evolution is identical. A first rise in pressure is seen from a temperature of about 300°C, which corresponds with the release of hydrogen and the production of methane on the catalysts. At just over 600°C, there is a further sharp rise in pressure. Many hypotheses can explain this phenomenon, such as the sudden release of hydrogen covalently bonded to the carbon or the decomposition of methane on the metallic particles. In this last case, one mole of methane produces two moles of molecular hydrogen (H_2), which is consistent with the sharp rise in pressure.

The X-ray pattern in Fig. 2 (Co source) shows the primary peak at 30.6°, associated with the piling of 002 graphite sheets, for a typical purified sample and the diffraction peaks of a sample of pure carbon nanofibers for comparison. It is clear that there is a perfect fit between the two curves. X-ray analysis also leads us to conclude that the addition of a small quantity of Co to the crucible before milling favors the formation of Fe-Co alloys during heating as opposed to Fe-C compounds. X-ray analyses also show that the formation of Fe-Co crystals begins at temperatures as low as 500°C during the heating process. The hypothesis governing the formation of nanostructures could therefore be that during heating of the sample, metallic crystals begin forming at approximately 500°C and at just over 600°C methane starts decomposing on the crystals with carbon diffusion leading to the formation of nanostructures if the

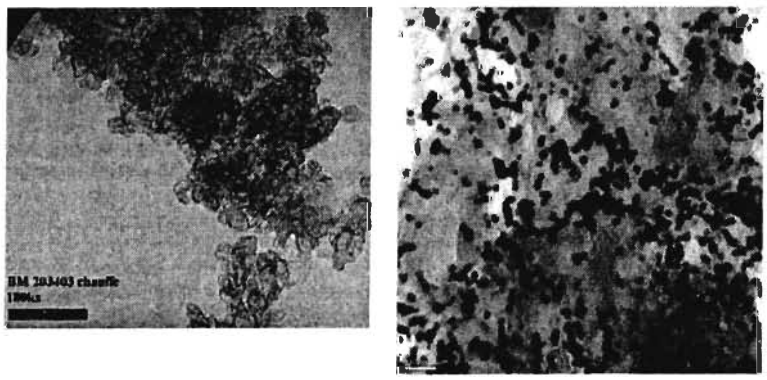

(a) (b)

Figure 4. TEM of (a) the carbon structures and (b) a platinized sample.

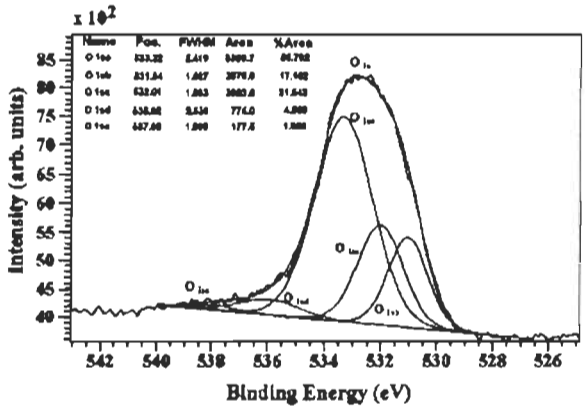

Figure 5. O 1s peak from XPS analysis of CNS sample ball milled under air for 1 h.

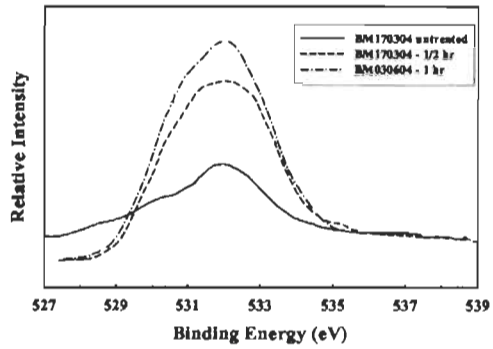

Figure 6. XPS results showing the increase in the O 1s peak as a function of milling time under air at 50 psig.

metallic crystal size is sufficiently small. If the crystal formations are too large, graphite layers are formed around them instead.

Figure 3 is the TGA graph of one typical sample and shows a decomposition temperature centered at 738°C for ~90 wt % of the sample. The 10 wt % loss between 20°C and about 600°C is attributed to water and amorphous carbon. As also shown in Fig. 3 is the result from Chen et al.,[13] which measured a decomposition temperature between 510 and 645°C for their multiwalled carbon nanotubes. However, as they mentioned in their paper, there is no common burning temperature of carbon nanotubes because it is not only related to graphitization degree, but also to pretreatment process. It is known that atoms sheets in carbon nanotubes are formed by sp^2 bond hence they have a higher oxidation temperature than amorphous carbon. Therefore, a higher oxidation temperature implies a higher graphitization degree in the sample. Because the oxidation temperatures is relatively high, we can only imply a high graphitization degree in our samples.

Figure 4a and b are HRTEM images of functionalized CNS and platinized CNS, showing homogeneous and high distribution of metal particles on the carbon surface. The structure of our CNS resembles a chain of onion rings with highly ordered graphitic structure.

Surface functionalization.— To assess the degree of surface functionalization, XPS analysis was performed on the samples A, B, C, and D. The binding energy peak reference was set as that of C 1s at 284.6 eV. Oxidation generates surface functional groups such as carbonyl, hydroxyl and carboxyl groups on the surface of CNS. XPS analysis shown in Fig. 5 for sample C reveals that the surface O 1s bonding is mainly composed of 17.1% carbonyl, 21.5% hydroxyl, and 55.7% carboxyl functional groups. We found that this method for oxidizing the carbon's surfaces increased the relative amount of O_{1s} liaisons by 5.72% for sample B and 6.43% for sample C, with a comparable decrease in C 1s liaisons for both samples, as shown in Fig. 6.

Chemical oxidation by acid reflux, generates the same surface functional groups but in different proportions. XPS analysis shown in Fig. 7 for sample D reveals that the surface O 1s bonding is composed of 48.8% carbonyl, 46.4% hydroxyl, and 4.8% carboxyl functional groups. These results indicate that high density of oxygen containing species is generated more on the surface of CNS after chemical oxidation. Moreover, the ratio of O 1s peak areas for sample C and sample D was found to be 1:1.73, which indicates the higher efficiency of chemical treatment to modify the inert surface of CNS. Primarily, this is due to high reactivity and elevated temperature of reflux with strong oxidizers H_2SO_4 and HNO_3 than air oxidation which physically modifies the surface carbon atoms in CNS.

Surface and porosity measurements.— BET adsorption isotherm analysis of a purified sample A with nitrogen at 77 K gives a total surface area of 196.5 $m^2\ g^{-1}$, an external surface estimated at 196.5 $m^2\ g^{-1}$, a micropore volume of 0.14 $cm^3\ g^{-1}$, and an average micropore width of 1.6 nm.

The Hg intrusion analysis gives a macropore cumulative surface area of 45.8 $m^2\ g^{-1}$ up to a pressure of 58,000 psi, a total macropore volume of 635 $mm^3\ g^{-1}$ with one distinct peak at 120 $mm^3\ g^{-1}$ corresponding to pore radius of 1 μm, as plotted in Fig. 8. Also plotted in Fig. 8 for comparison are the data from Passalacqua et al.[8] for Vulcan XC-72. It is clearly seen that our CNS sample as a higher macropore volume. If we compare the peak from our sample at 1 μm, with the main peak from Passalacqua et al., at 5.5 μm, this shift in pore radius partly accounts for the higher pore volume of our sample. The higher CNS pore volume, attributed to the space between the CNS, along with surface functionalization is directly responsible for a better platinum cluster distribution.

Electrical conductivity.— The average electrical conductivity of Pt/CNS was found to be to 0.9 S cm^{-1}. The variations in the conductivity between samples was due to differences in proportions of amorphous to nanostructured carbons and also the variations of

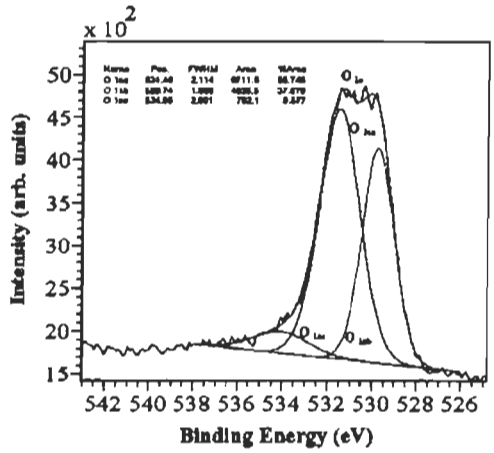

Figure 7. O 1s peak from XPS analysis of CNS sample oxidized by acid reflux.

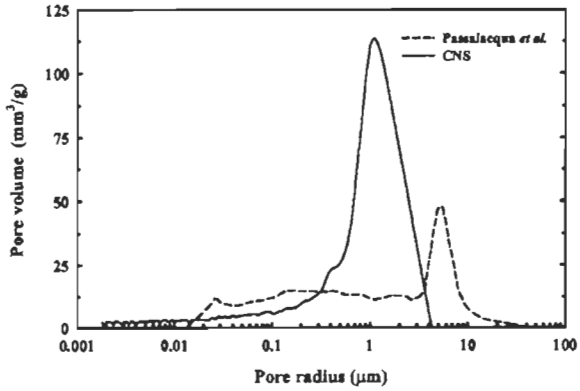

Figure 8. Pore volume as a function of pore radius from Hg intrusion data.

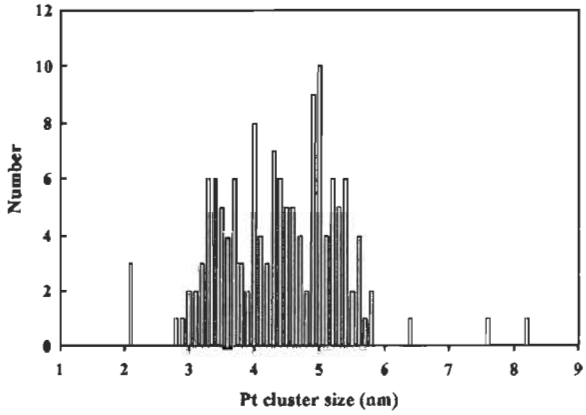

Figure 10. Pt cluster size distribution from HRTEM pictures.

spring pressure in the measurement cell electrode strongly influences the contact resistance. The electrical conductivity of Vulcan XC-72 as a function of the compression pressure has been reported by Pantea et al.,[14] which is in agreement with our measurement of 1.0 S cm^{-1}.

Platinization.— Figure 9 shows the XRD pattern of one platinized CNS sample, with platinum peaks Pt(111), Pt(200), Pt(220), Pt(311), and Pt(222). From the well defined Pt(220) peak, using Scherrer's formula

$$t = (0.9 \cdot \lambda)/(B \cos \theta) \quad [9]$$

where λ is the wavelength of the Cu Kα spectral line, B is the width at midheight of the main peak, and θ is its diffraction angle, we find a mean crystallite diameter t of 7 nm. This value does not take into account the strain on the sample. A more accurate t value is obtained in the next paragraph from TEM images.

Figure 10 shows the particle size distribution of platinum clusters in the supported CNS from randomly chosen particles in the HR-TEM image (Fig. 4b). It is evident from the histogram that these Pt particles are small (2.8–5.8 nm) and more uniformly distributed on CNS, which is in near accordance with the value of 4 nm Pt supported on commercial Vulcan XC-72 from Schmidt et al.[15] Generally, the size of the platinum cluster is controlled by the rate of reduction of platinum precursor, i.e., platinum hydroxide, the cluster size of which depends on the percentage content of deionized water in EG solution. The presence of 20% of deionized water in EG buffers the formation rate of metal particle, which resulted in the desired size (2.8–5.8 nm) of metal colloidal in the organic media, ready to be reduced on the catalyst support. The mode of addition of the buffer solution has no impact on the size of Pt crystallites as our results are in good agreement with Li et al. Platinum hydroxide colloidal interacts with the surface functional groups of the oxidized CNS, then deposit on its surface. Platinum loading onto CNS is also determined by the surface functional groups. AAS studies show 11.9 wt % Pt was supported by CNS.

Cyclic voltammetry results.— Figure 11 compares the voltammograms of sample D_{Pt} and E-TEK Vulcan XC-72 in deaerated 1 M H_2SO_4 scanned at 10 mV s^{-1}. The electrochemical study on these voltammograms indicate that the Pt/CNS with a low platinum weight loading of roughly 12% showed nearly equal performance with the 20 wt % Pt/Vulcan XC-72. Primarily, this is due to wide and homogenous distribution of Pt clusters on chemically activated sites of CNS. The electrochemically active platinum surface for E-TEK Vulcan and platinized CNS was found to be 63.86 and 58.49 m^2 g^{-1}, respectively.

Conclusions

We have presented a carbon nanostructure production technique based on ballmilling of carbon graphite in a hydrogen atmosphere. Samples analyzed by XRD, TGA, and TEM imaging showed the presence of highly ordered graphitic nanostructures. Although our CNS resembles the one of Park et al.[16] (nanocoils), we cannot show clear evidence of it. CNS samples electrical conductivities averages to 0.9 S cm^{-1}, which compare well to the 1 S cm^{-1} of Vulcan

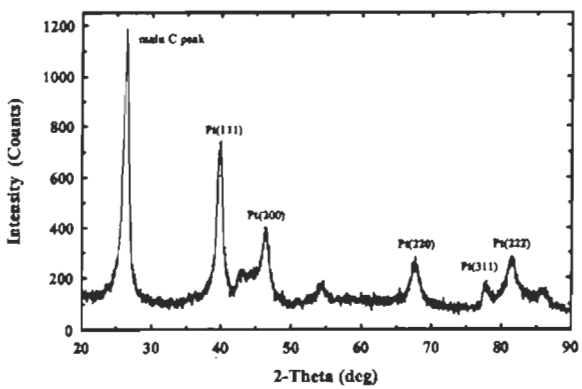

Figure 9. Typical XRD pattern of a platinized CNS sample (Cu source).

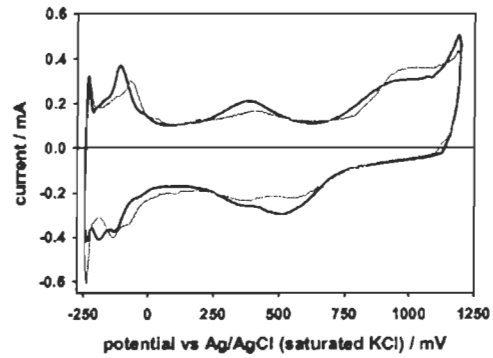

Figure 11. CVs [50 mV s^{-1} in N_2 saturated 0.5 M H_2SO_4 (aq.)] of glassy carbon electrodes coated with 20 wt % Pt/Vulcan (0.2 mg Pt cm^{-2}, light line) and 10 wt % Pt/CNS (0.2 mg Pt cm^{-2}, heavy line).

XC-72 carbon black as measured by Pantea et al.[14] BET analyses on our CNS samples gave a specific surface area of 352.6 $m^2 g^{-1}$, a micropore volume of 0.14 $cm^3 g^{-1}$, and an average micropore width of 1.6 nm. The Hg intrusion data analysis gives a macropore size radius of 45.8 $m^2 g^{-1}$ and a total macropore volume of 635 $mm^3 g^{-1}$. Thus, we believe that the major advantage of using nanostructured carbon as a catalytic support in PEMFC is their broken surfaces, micro and macro porosity. The broken surfaces allows for a plurality of sites for oxidation, responsible for the wide dispersion and small diameter sizes of the Pt clusters, which in turn creates a larger catalytic surface area and therefore superior reaction kinetics, and consequently more power. Also, the large macropore volume increases the availability of sites for platinization. The presence of a microporous structure would lead to better gas diffusion at the electrodes and reduces the risk of poor performance linked to poor mass transfer.

The inert surface of CNS were modified conveniently by two methods, air oxidation and chemical oxidation. The latter is significantly more effective in surface modification, leading to well dispersed 4.5 nm (average diameter, assuming spherical particles) Pt particles on CNS. Finally, CV studies showed similar electrochemical activity as Pt/Vulcan is achieved with Pt/CNS with almost half the percentage weight loading of Pt.

Acknowledgments

We thank the Natural Sciences and Engineering Research Council of Canada and Hydro-Québec for their financial aid. Additionally, we thank M.-A. Leduc, F. Fouda-Onana, and M.-H. Bégin.

The Physics Department of the Universite du Quebec assisted in meeting the publication costs of this article.

References

1. K. Kordesch and G. Simader, *Fuel Cells and Their Applications*, John Wiley & Sons, Mississauga, ON, Canada (1996).
2. S. Iijima, *Nature (London)*, **354**, 56 (1991).
3. T. Yoshitakea, Y. Shimakawaa, S. Kuroshimaa, H. Kimuraa, T. Ichihashi, Y. Kuboa, D. Kasuyad, K. Takahashic, F. Kokaic, M. Yudasaka, and S. Iijima, *Physica B*, **323**, 124 (2002).
4. T. W. Ebbesen and P. M. Ajayan, *Nature (London)*, **358**, 220 (1992).
5. S. H. Jung, M.-R. Kim, S.-H. Jeong, S.-U. Kim, O.-J. Lee, K.-H. Lee, J.-H. Suh, and C.-K. Park, *Appl. Phys. A*, **76**, 285 (2003).
6. M. Endo, K. Takeuchi, S. Igarashi, K. Kobori, M. Shiraishi, and H. W. Kroto, *J. Phys. Chem. Solids*, **54**, 1841 (1993).
7. S. B. Sinnott, R. Andrews, D. Qian, A. M. Rao, Z. Mao, E. C. Dickey, and F. Derbyshire, *Chem. Phys. Lett.*, **315**, 25 (1999).
8. E. Passalacqua, G. Squadrito, F. Lufrano, A. Patti, and L. Giorgi, *J. Appl. Electrochem.*, **31**, 449 (2001).
9. L. R. Jordan, A. K. Shukla, T. Behrsing, N. R. Avery, B. C. Muddle, and M. Forsyth, *J. Appl. Electrochem.*, **30**, 641 (2000).
10. Z. Paál and P. G. Menon, *Hydrogen Effects in Catalysis: Fundamental and Practical Applications*, Marcel Dekker, New York (1987).
11. R. Yu, L. Chen, Q. Liu, J. Lin, K.-L. Tan, S. C. Ng, H. S. O. Chan, G.-Q. Xu, and T. S. A. Hor, *Chem. Mater.*, **10**, 718 (1998).
12. W. Li, C. Liang, W. Zhou, J. Qiu, H. Li, G. Sun, and Q. Xin, *Carbon*, **42**, 436 (2004).
13. X. H. Chen, C. S. Chen, Q. Chen, F. Q. Cheng, G. Zhang, and Z. Z. Chen, *Mater. Lett.*, **57**, 734 (2002).
14. D. Pantea, H. Darmstadt, S. Kaliaguine, L. Sümmchen, and C. Roy, *Carbon*, **39**, 1147 (2001).
15. T. J. Schmidt, H. A. Gasteiger, G. D. Stäb, P. M. Urban, D. M. Kolb, and R. J. Behm, *J. Electrochem. Soc.*, **145**, 2354 (1998).
16. K.-W. Park, Y.-E. Sung, S. Han, Y. Yun, and T. Hyeon, *J. Phys. Chem. B*, **108**, 939 (2004).

12. APPENDIX II: SECOND PAPER

Sadesh Kumar Natarajan, Jean Hamelin, Homogeneous Pt Deposition on Chemically Modified Carbon Nanostructures as Catalysts for PEMFCs, Electrochimica Acta, 52 (2007) 3751.

Available online at www.sciencedirect.com
ScienceDirect
Electrochimica Acta 52 (2007) 3751–3757
ELECTROCHIMICA Acta
www.elsevier.com/locate/electacta

Homogeneous platinum deposition on chemically modified carbon nanostructures as catalysts for PEMFCs

Sadesh Kumar Natarajan, Jean Hamelin *

Institut de recherche sur l'hydrogène, Université du Québec à Trois-Rivières, 3351 Boul. des Forges, C.P. 500, Trois-Rivières, Que., Canada G9A 5H7

Received 20 July 2006; received in revised form 23 October 2006; accepted 24 October 2006
Available online 28 November 2006

Abstract

Carbon nanostructures (CNS) with high specific surface and porosity prepared by high energy ball milling of graphite is considered as one of the potential alternatives to Vulcan as catalyst support for polymer electrolyte membrane fuel cells. Purification and functionalization of as-prepared CNS were carried out in a single-stage reflux with different proportions and concentrations of the oxidizing mixture, H_2SO_4 and HNO_3. The density of the generated surface functional groups were investigated by XPS based on the activity of platinum dispersed on the specific sites of CNS. Cyclic voltammetry studies revealed that the electrochemical performance for some of the surface modified Pt/CNS were found to be similar to commercial ETEK® with 20 wt.% Pt supported on Vulcan XC-72 carbon black. XRD and HRTEM were also used to investigate the shape, size and distribution of Pt clusters on the functionalized surface of these CNS.

Keywords: Carbon nanostructures; Surface modification; Platinum; Catalyst; Voltammetry

1. Introduction

Polymer electrolyte membrane fuel cells (PEMFCs) are regarded as one of the efficient and environmentally clean electrical generators that are developed for stationary as well as mobile applications. When fed with hydrogen-rich gas, it achieves relatively high power density even at low temperatures (70–90 °C). The shape, size and distribution of platinum nanoparticles supported on carbon black (Pt/C) commonly used in the catalyst layers of PEMFCs greatly influence their performance [1]. The Pt/C powder, prepared mostly by established procedures based on colloid chemistry, has to be intimately mixed with recast ionomer to provide sufficient ionic conductivity within the catalyst layer. Previous studies have shown that the platinum supported on carbon nanotubes (CNTs) exhibit comparable [2] and even sometimes better [3] electrochemical performance compared to carbon black (Vulcan XC-72). Our previous studies on CNS [4] have attracted much interest as support material, owing to their good mechanical and unique electrical properties. A modified chemical vapor deposition technique [5] was used to synthesize CNS with less resource at a relatively low cost.

There have been several studies over the past few years to deposit platinum or its alloys as catalysts on CNTs either through electrochemical deposition or by impregnation [6–9]. The main objective of the current work therefore is to investigate and modify the electrochemical properties of the inert CNS developed in our laboratories and compare the electrochemical performance of platinized CNS with commercial 20 wt.% Pt on Vulcan XC-72, ETEK®.

The unwanted impurities such as metal or metal oxides, amorphous carbon and other carbon nanoparticles result in with the as-prepared raw CNS sample [4]. Several methods have been proposed to remove these impurities categorized by the following four techniques: acid oxidation [10,11], gas oxidation [12,13], filtration [14,15] and chromatography [16]. Combinations of acid reflux with modified solvent mixtures and fine tuned reflux period were used in this context not only to purify the CNS from impurities, but also to generate functional groups on the surface of CNS. These functional groups facilitate the deposition and dispersion of platinum clusters on CNS via chemically specific nucleation mechanism [17].

The size of platinum nanoparticles and its distribution on the carbon support are the key factors that influence the performance

* Corresponding author. Tel.: +1 819 376 5108; fax: +1 819 376 5164.
E-mail address: Jean.Hamelin@uqtr.ca (J. Hamelin).

0013-4686/$ – see front matter © 2006 Elsevier Ltd. All rights reserved.
doi:10.1016/j.electacta.2006.10.049

of the Pt/C catalyst [18]. Polyol synthesis method [19–22] is more widely in use to distribute platinum nanoparticles in colloidal form. Li et al. [18] devised a modified form of polyol synthesis method to control the size of platinum particles by adjusting the ratio of water to ethylene glycol (EG) during the preparation process. The method adopted in this work have performed pretests to control the platinum size by using nearly pure EG, with subsequent addition of pre-estimated water content in sequence whilst drop wise addition of hexachloro-platinic acid (H_2PtCl_6).

PEMFC assembly and testing will be time consuming and it would therefore be expensive to compare various catalysts at each sequence of their modifications. Hence, cyclic voltammetry was employed to study and compare the active electrochemical surface, rate of platinum utilization and the entire surface processes involved in the redox reaction.

In this paper, we also investigate and compare the electrochemical activity of nanostructures functionalized with different proportions and concentrations of oxidizing acids. The investigation is solely based on interpretation of cyclic voltammograms for the charges exchanged during electro-adsorption and electro-desorption of hydrogen, thus estimating the real electrochemical active surface area. By applying Scherrer's equation on powder X-ray diffraction patterns of platinized CNS, we estimate the size of the platinum crystallites. Assuming the particles are spherical, we calculate the real surface area, which is therefore used to estimate the rate of platinum utilization.

2. Experimental

Soft polymorph of graphite (50 wt.%) was transferred into a ball mill under argon atmosphere along with transition metal catalysts, iron and cobalt (44 wt.% and 6 wt.%). The powder mixture was then milled by a SPEX mill (SPEX is a trademark of SPEX Industries, Edison, NJ) for 12 h with a constant mass ratio of powder to balls (1:35). Prior to milling, argon is removed by a vacuum pump and hydrogen was introduced inside the crucible at a pressure of 1.4 MPa. Subsequently, the mechanically ground sample was transferred into a quartz tube in an argon filled glove box. The contents inside the quartz tube was heated to 700 °C for 90 min under argon atmosphere during which CNS (sample A) were formed on the metallic nanocrystals. A detailed description of the above procedure was discussed in our previous work [4]. X-ray powder diffraction (XRD) measurements was used to characterize the structural changes of the graphite powder and also to identify the impurities in the as-prepared sample, which are found to coexist with catalytic metal or metal oxides, amorphous carbon and carbon nanoparticles. XRD was performed with a Rigaku diffractometer using Cu $K\alpha_1$ radiation ($\lambda = 1.54051$ Å) and $\theta/2\theta$ geometry.

The as-prepared sample A serves as the starting material to support platinum nanoparticles via chemically specific nucleation mechanism. Since, the surface of generated nanostructures are rather inert, it is difficult to control the homogeneity of Pt deposition on the surface by conventional methods. In this article, we explored feasible techniques whereby surface modification and then Pt deposition on CNS can take place. The generation of functional groups on the surface of CNS can be accomplished by chemical modification techniques with variable proportions of strong oxidizing agents sulfuric acid (H_2SO_4) and nitric acid (HNO_3), which oxidizes metal impurities, carbon nanoparticles and the weak C–C bonds in the highly ordered CNS. Moreover, it opens active sites on CNS, which therefore facilitates homogeneous metal deposition on its surface by any conventional platinization techniques.

To compare the effect of acid-oxidation treatment, the as-prepared CNS was primarily washed with HCl trace metal solution to investigate the available active sites without surface functionalization. Five hundred milligrams of sample A was soaked in 250 ml of HCl trace metal solution and stirred at room temperature for 1 h to remove metal impurities and amorphous carbon [5]. The washed CNS was diluted with deionized water and filtered with 5–10 μm ceramic micro-filter. The filtrate was washed with deionized water until the pH of the filtrate becomes neutral. The precipitate in the ceramic micro-filter was dried overnight at 120 °C under dry nitrogen. Scrapped filtrate (sample B) from the ceramic filter was platinized (sample B_{Pt}) and characterized for experimental comparisons. Commercial sample of 20 wt.% Pt on Vulcan XC-72 carbon (sample C_{Pt}), ETEK® was used as a primary reference to compare the electrochemical activity of CNS before and after surface modification.

The as-prepared CNS is chemically modified by refluxing 500 mg of sample A under various concentrations and proportions of H_2SO_4/HNO_3 mixture (samples D–I) at an optimized temperature of 120 °C for 3 h. The resultant dark-brown mixture was diluted with deionized water and filtered using 5–10 μm ceramic micro-filter. The precipitate was washed to neutralize pH and dried overnight at 120 °C under dry nitrogen.

A well-adopted method more like the one used by Li et al. [18] was employed to control the size of platinum particles. Four hundred milligrams of surface functionalized carbon nanostructures (samples D–I) were suspended in 40 ml of EG solution and stirred for 30 min to well disperse 10 mg CNS/ml of EG solution. 6.5 ml of H_2PtCl_6 acid (10 wt.% Pt) was added in drops followed by deionized water in 30 min intervals to constitute 5%, 10% and 20% of water content in the bulk solution. The volume of the platinum precursor was adjusted to obtain a Pt loading of 15 wt.% on the CNS. The pH of the solution was adjusted above 13 by appropriate addition of NaOH in EG solution. A precipitate instead of a metallic colloidal solution will result in case where the pH is less than 12. The amount of added water controls the size of intermediates, platinum hydroxide or hydroxyl acetate clusters, which later gets reduced to platinum metal colloidal in the subsequent heating process. Hydrogen was reduced by reflux at 140°C for 3 h. The time interval for the subsequent H_2PtCl_6 acid and water addition will have a considerable effect on the size of platinum particles on the surface of CNS, when the cluster sizes are sorted for samples treated with 3:1 ratio of H_2SO_4 and HNO_3. The platinized CNS (samples D_{Pt}–I_{Pt}) was filtered, washed and dried overnight at 120 °C under dry nitrogen. Atomic adsorption spectroscopy analyses were performed on Pt loaded CNS with Varian spectra AA 55. XRD and cyclic voltammetry patterns were studied to characterize and compare

the influence of surface modification under different operating conditions.

The platinum supported CNS was weighed into a small vial to obtain a load of 0.2 mg cm^{-2} along with a Nafion (5 wt.% Aldrich Nafion® solution) loading of 0.67 mg cm^{-2}. A proportion of lower aliphatic alcohols were added to balance the platinum loading followed by ultrasonication in a bath for 1 h to give a homogeneous suspension. Viscosity of the suspension altered with an addition of 5 mg of 99% glycerol aids to coat the homogenous catalyst ink uniformly on the surface of a glassy carbon (GC) electrode. A 0.07069 cm^2 GC electrode was coated evenly with 1.7 μl of this suspension and sintered at 60 °C for 15 min.

Cyclic voltammetry was carried out in a conventional air-tight three-electrode cell containing 1 M H_2SO_4 bulk solution at room temperature. The setup comprises of a 2 mm diameter GC electrode, a platinum wire counter electrode, and Ag/AgCl (sat. KCl) reference electrode. Measurements were made at room temperature using Zahner IMe6 electrochemical workstation. The coulombic charges exchanged during hydrogen adsorption and desorption on the active Pt sites was calculated with the procedure employed by Pozio et al. [3]. Thus, obtained charge densities were found well in agreement with the results generated by Thales Flink, which controls all the functions of IMe6 workstation. The charge integration feature in the Thales Flink software plots I versus t, which can be integrated to calculate the charge under the curve. Once this function is activated, the time interval over which the current is to be integrated is defined just by selecting the left and right time limits of hydrogen adsorption and desorption peaks. Moreover, one of the major contributions to the background current for a cyclic voltammetry experiment is the current required to charge the double layer at the interface of the working electrode and the bulk solution. We eliminated the charge contribution from this background current on the charges involved in hydrogen adsorption and desorption, according to Ref. [3]. The electrochemically active surface (EAS) area of the electrode was obtained from the charged required for hydrogen desorption from the platinum electrocatalyst:

$$\mathrm{EAS} = \frac{Q_\mathrm{M}}{[\mathrm{Pt}] \times 0.21}$$

where Q_M is the mean of charges exchanged during hydrogen adsorption and desorption (mC cm^{-2}), [Pt] the platinum loading (mg cm^{-2}) and the numerical value 0.21 represents the charge required to oxidize a monolayer of hydrogen. However, if the initial scanning potential of CV was below the reversible potential for hydrogen desorption, then the measured charges exchanged during electro-desorption of hydrogen have some contribution from the charges involved in reoxidation of molecular hydrogen species. Although these measurements have limited absolute accuracy, they are useful for making comparison between catalysts. Since all the voltammograms were with the same operating parameters, we assume that the measured hydrogen desorption charge is restricted to a monolayer only.

The rate of platinum utilization was calculated by the ratio of electrochemically active platinum surface to the geometrical area of platinum estimated from the mean particle diameter. Particles were assumed to be spherical with surface area $4\pi r^2$ and volume $4\pi r^3/3$. The theoretical number of platinum nanoparticles in the catalyst layer coated on GC electrode was calculated by dividing the total mass of platinum loaded on GC with the mass of one platinum nanoparticle. Surface area of a spherical Pt nanoparticle multiplied by the number of Pt particles gives the theoretical surface area of Pt supported on CNS. Although the size of particles are widely distributed, we approximate the results by assuming the estimated size to be the mean particle diameter.

3. Results and discussion

The highly ordered carbon structures prepared by high energy ball milling under hydrogen atmosphere followed by heat treatment under argon atmosphere were inevitably accompanied by highly disordered structures of amorphous carbon with many active dangling atomic sites, carbon nanoparticles and catalytic impurities. Table 1 shows the proportion and concentration of acids used as chemical oxidizers to remove catalytic impurities, carbon nanoparticles and amorphous carbon. Excluding sample I, there is not much difference in the yield of functionalized CNS despite variations in molarity of the reflux solution.

X-ray photoelectron spectroscopy (XPS) was used to analyze and compare elemental composition, chemical state and electronic state of the elements carbon and oxygen composed in non-oxidized sample B and acid oxidized sample F. XPS spectra was obtained by irradiating samples B and F one by one with a beam of X-rays while simultaneously measuring the kinetic energy and number of electrons that escape from the top 1–10 nm of the material being analyzed. Chemical oxidation by acid reflux generates surface functional groups such as carbonyl, hydroxyl and carboxyl groups on the surface of CNS. XPS analysis was performed on untreated and surface modified samples to study the influence of chemical modification on the nanostructures. XPS spectra on surface modified CNS (Fig. 1a) clearly show the presence of enhanced O 1s peaks

Table 1
Proportion and concentration of H_2SO_4 and HNO_3 as surface oxidizers

	Sample					
	D	E	F	G	H	I
H_2SO_4:HNO_3	1:1	1:1	1:1	3:1	3:1	3:1
Molarity of H_2SO_4 (M)	3	5	7.5	5	10	15
Molarity of HNO_3 (M)	5	9	15	6	15	20
Percentage yield	41.88	41.43	41.55	43.69	40.02	31.45

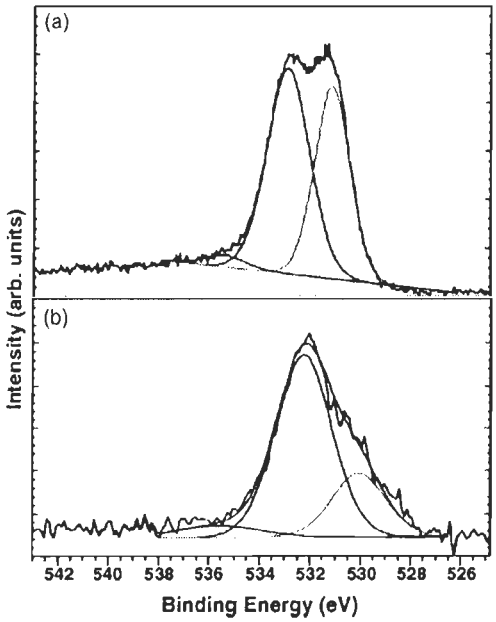

Fig. 1. (a) CNS (sample F) after surface modification and (b) CNS (sample B_{Pt}) before surface functionalization.

when compared with the spectra of untreated CNS (Fig. 1b). Fig. 1b show traces of oxygen bonded with orderly structure of carbon that are considered as adsorbed oxygen species. The spectra of functionalized nanostructures show the formation of high density oxygen species on the surface of CNS after chemical oxidation. With reference to XPS studies on surface modified carbon nanofibers [23], the curve-fittings of O 1s peaks were made. The ratio of O 1s peak area in the samples B and F was found to be 2.21:1, which indicates the higher influence of 1:1 mixture of 7.5 M H_2SO_4 and 15 M HNO_3 for the surface modification of CNS. The other peaks are attributed to 48.8% carbonyl (530.95 eV), 46.4% hydroxyl (532.05 eV) and 4.8% carboxyl (533.76 eV) functional groups [23].

The functionalized nanostructures were platinized with the method described in the experimental section. X-ray powder diffraction shown in (Fig. 2) identifies the face centered cubic of the characteristic crystalline platinum peaks for Pt(1 1 1), Pt(2 0 0), Pt(2 2 0), Pt(3 1 1) and Pt(2 2 2). The particle size of the characteristic platinum crystals (d) was estimated using Scherrer's equation:

$$d = \frac{k\lambda}{\beta \cos\theta}$$

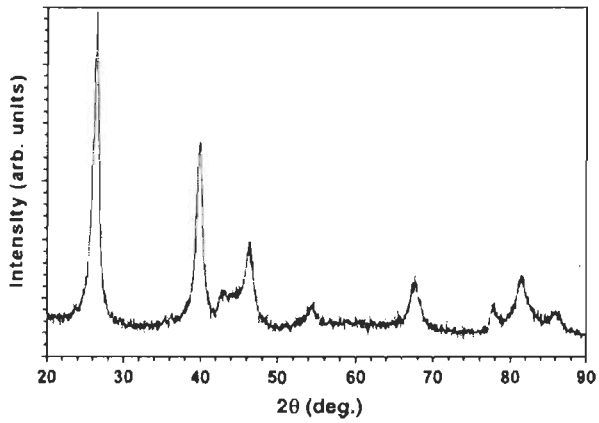

Fig. 2. Powder XRD patterns of Pt/CNS sample F_{Pt}, platinized by EG method.

where k is the coefficient, generally taken as 0.9, λ the wavelength of X-ray radiation equal to 1.54051 Å, β the full width at half-maximum (FWHM) measured in radians, and θ is the angle measured at the position of platinum peaks.

Some of the HRTEM images of sample F_{Pt} are shown in Fig. 3. The images show the wide and uniform distribution of platinum metal clusters on the surface of functionalized nanostructures. Atomic adsorption spectroscopy was performed on all platinized samples to evaluate the loading of platinum nanocrystals on functionalized sites of CNS. Table 2 shows the weight percentage of Pt supported on the surface modified CNS samples. It is evident that the sample treated with trace metal HCl has less oxides on its surface compared to acid-oxidized nanostructures. However, there are a few active sites on its surface which supports platinum clusters only up to 5.3 wt.%.

Fig. 4 compares the cyclic voltammograms of platinized samples D_{Pt}, G_{Pt} and B_{Pt}. This selected comparison was made in order to study the primary effects of chemical reflux on the inert surface of CNS. The coulombic charges accumulated during hydrogen adsorption and desorption can be used to calculate the electrochemically active platinum surface on the electrode. All the potentials measured in this article are referred to Ag/AgCl (sat. KCl) reference electrode. The platinum loading was main-

Table 2
Electrochemical active surface and platinum utilization for all the Pt supported CNS and Vulcan XC-72 (C_{Pt})

	Sample							
	B_{Pt}	C_{Pt}	D_{Pt}	E_{Pt}	F_{Pt}	G_{Pt}	H_{Pt}	I_{Pt}
Platinum loading in CNS (wt.%)	5.3	20	11.3	14.0	11.9	11.10	8.60	9.70
Electro adsorption (mC cm^{-2})	2.95	25.04	15.79	17.23	24.19	10.33	15.76	28.35
Electro desorption (mC cm^{-2})	1.85	28.60	15.19	15.38	24.94	7.47	12.05	23.23
Coulombic charge for H_2 desorption (mC cm^{-2})	2.40	26.82	15.49	16.31	24.57	8.90	13.91	25.79
Specific charge (mC g^{-1})	12.00	134.1	77.45	81.53	122.83	44.49	69.53	128.95
EAS (m^2 g^{-1})	5.71	63.86	36.88	38.82	58.49	21.19	33.11	61.41
Diameter of Pt crystallite (nm)	6.70	4.00	5.33	8.69	6.83	9.50	5.69	5.97
Geometrical surface area of Pt particles in GC (cm^2)	5.90	9.89	7.419	4.55	6.59	4.16	6.95	6.62
Platinum utilization (%)	13.69	91.32	70.28	120.62	142.85	71.96	67.35	131.06

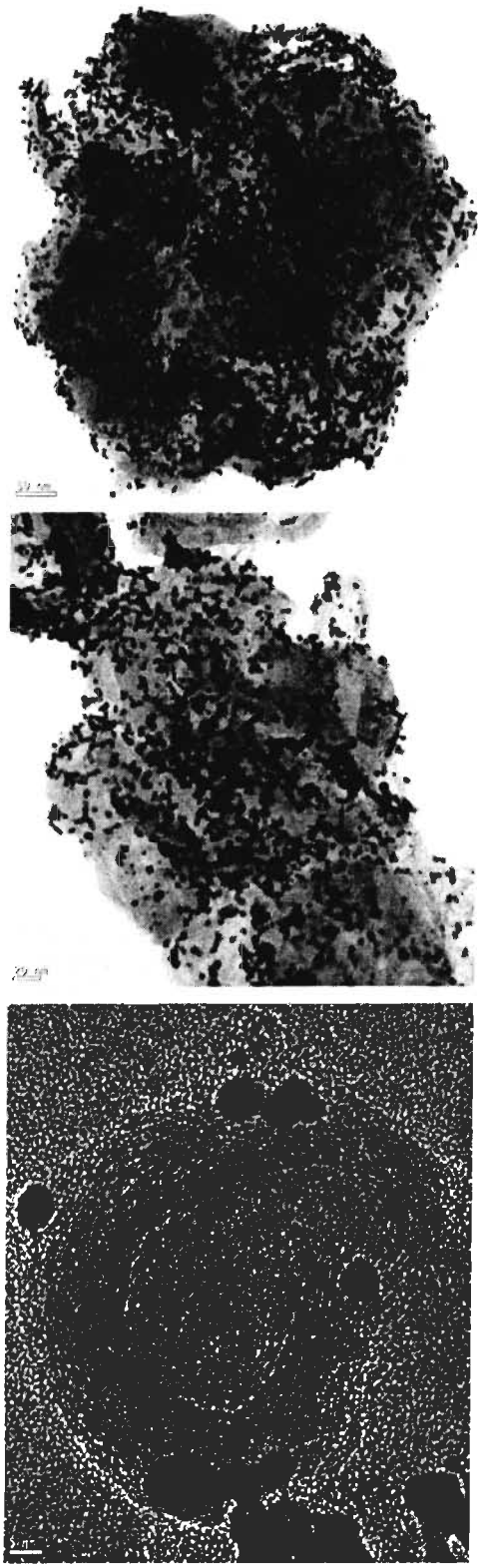

Fig. 3. HRTEM images of Pt nanoparticles supported in functionalized CNS sample F.

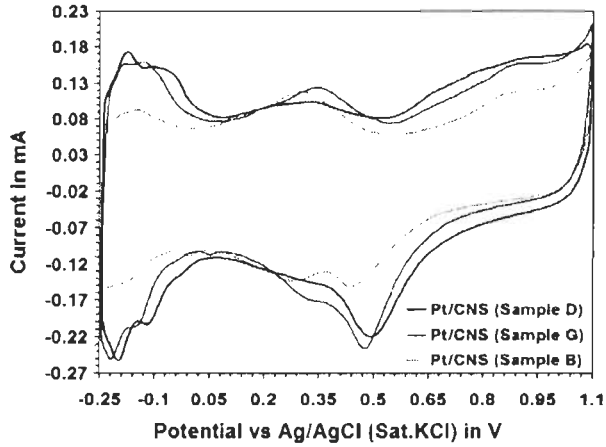

Fig. 4. Cyclic voltammograms of GC electrode coated with samples D_{Pt}, G_{Pt} and B_{Pt} scanned at 10 mV s^{-1} in nitrogen saturated 1 M H_2SO_4.

tained constant (0.2 mg cm^{-2}) for all the CNS samples and also for 20 wt.% Pt on Vulcan XC-72, ETEK® (C_{Pt}). Table 2 shows the summary of the charges exchanged during electro-adsorption and electro-desorption for all the platinized CNS and sample C_{Pt}.

Treatment of CNS with trace metal solution of HCl removes only the catalytic metal impurities and amorphous carbon. Analysis of voltammogram show that trace metal HCl has very little impact on the highly ordered nanostructures to modify its inert surface for deposition and dispersion of platinum nanoclusters. Specific charge is defined as the ratio of coulombic charge required to desorb one monolayer of hydrogen over the Pt loaded on the GC electrode. It is found to be lower for sample B_{Pt} than that of the nanostructures refluxed with acidic mixture.

Sample D_{Pt}, treated for surface oxidation with equal proportion of 3 M H_2SO_4 and 5 M HNO_3 has higher specific charge than sample G_{Pt} refluxed with 3:1 ratio of 5 M sulfuric acid and 6 M nitric acid is due to the higher ratio of H_2SO_4, which intensifies the intermediate $-OSO_3H$ bonding with the surface carbon. This result indicate that hydrolysis of $-OSO_3H$ group during platinization with the aid of EG is not as effective than H_2 gas reduction [17]. For a constant platinum loading in either a fuel cell electrode or a GC electrode, the thickness of the electrode grows due to low platinum weight content in the catalyst. Some platinum particles remain inactive as they are hidden by the carbon substrate and are not exposed to the bulk solution. Hence, the EAS is too low for sample B_{Pt} with low order functionalized CNS which facilitates low platinum loading forcing more quantity of platinized CNS on the small geometry of GC working electrode. As observed from Table 2, because of it low EAS, sample B_{Pt} shows a low rate of Pt utilization when compared with other pre-functionalized Pt/CNS samples. A better rate was observed for sample D_{Pt} than sample G_{Pt} as the former covers more active surface with the presence of small diameter platinum clusters.

Fig. 5 show the voltammograms of samples H_{Pt} and I_{Pt}, which are functionalized with highly concentrated version of the reflux mixture used to treat sample G_{Pt}. Although the catalytic metal impurities, iron and cobalt are readily dissolved in dilute nitric acid/dilute sulfuric acid mixture, the concentrated acid of which

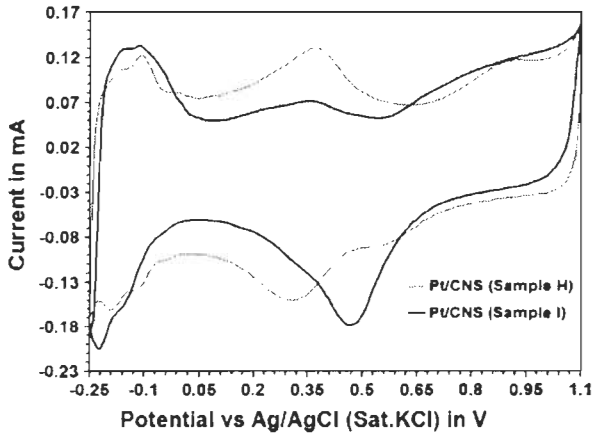

Fig. 5. Cyclic voltammograms of GC electrode coated with samples H_{Pt} and I_{Pt} scanned at 10 mV s^{-1} in nitrogen saturated 1 M H_2SO_4.

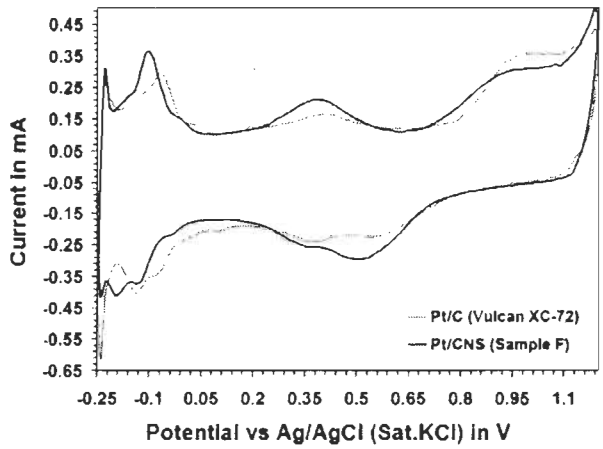

Fig. 6. Cyclic voltammograms of GC electrode coated with samples C_{Pt} and F_{Pt} scanned at 10 mV s^{-1} in nitrogen saturated 1 M H_2SO_4.

forms a metal oxide layer that protects (passivates) the metal from further oxidation. Conversely, high molar concentrations of the acid mixture readily modifies the surface of highly ordered inert nanostructures for platinum deposition better than the low concentrated ones. High specific charge of sample I_{Pt}, when compared to sample H_{Pt} shows the presence of more electrochemically active sites available for hydrogen adsorption and desorption. This clearly indicates that the surface modification for sample I_{Pt} was more pronounced than sample H_{Pt} at higher concentrations of reflux mixture. Although, the dimension of platinum particles are similar, the distribution of platinum nanoclusters on functionalized sites and high Pt loading results in higher rate of platinum utilization for sample H_{Pt} than sample I_{Pt}. The estimated value of platinum utilization for sample I_{Pt} is greater than 100% is due to the influence of background current to the calculated hydrogen adsorption charge. Moreover, it is also because of the presence of bigger size Pt nanoparticles with low theoretical platinum surface resulting in higher platinum efficiency. In fact, due to the practical measurement limitations, the platinum utilization cannot be measured accurately to study the electrochemical activity of catalysts. But, the approximated version of it can be used to make a secondary comparison between different catalysts. However, the performance studies of different catalysts in this article are primarily based on their specific charges or on their electrochemically active surface area.

Fig. 6 compares the cyclic voltammograms of sample F_{Pt} and sample C_{Pt} obtained in deaerated 1 M H_2SO_4. The real electrochemical surface area of platinum for these samples were estimated from the integrated coulombic charge required for desorption of hydrogen of the cyclic voltammogram shown in Fig. 6. If we assume the charge required to desorb one monolayer of adsorbed hydrogen to be 0.21 mC cm^{-2} [3], the active surface of Pt on CNS and Vulcan were calculated as 58.49 and 63.86 $m^2\,g^{-1}$. For the same Pt loading on the GC electrode, the thickness of the electrode coated with 11.9 wt.% Pt/CNS will be greater than the electrode coated with 20 wt.% Pt/C. As a result of variable thickness, some Pt particles supported on CNS were blocked in the carbon substrate and not exposed to the bulk solution. This also applies for the catalyst layers coated on either gas diffusion layer or on the membrane (decal method) in a membrane electrode assembly (MEA). Regardless of electrode thickness, Pt supported on CNS showed similar electrochemical performance like Pt supported on Vulcan Carbon, which was primarily due to the highly porous structure of the nanostructures. The presence of more micro- and macro-porous structure in CNS should improve efficient gas transport to the active Pt sites in MEA, thus minimizing the transport and concentration overpotentials. A BET surface area of 352.6 $m^2\,g^{-1}$ for sample F obtained from N_2 adsorption isotherms [4] showed a micropore volume of 0.14 $cm^3\,g^{-1}$ and a pore width of 1.6 nm. A meso/macro-pore surface of 45.8 $m^2\,g^{-1}$ and a meso/macropore volume of 0.64 $cm^3\,g^{-1}$ was observed from Hg intrusion isotherms. Thus, the presence of a high porosity on CNS strongly influences the availability of reactants on the active sites of platinum.

In comparison with sample I, sample F exhibits more active sites for platinum loading upon surface oxidation, which confirms the stability of the structure even after acid reflux. Hence, sample I_{Pt} can accommodate only 9.7 wt.% of Pt when compared to 11.9 wt.% on sample F_{Pt}, as the highly ordered structure of the latter was disrupted on treatment with high molar concentration of reflux solution. The nanostructures are coated with a layer of amorphous carbon upon oxidation with high molar acids, showing that the surface of sample I was damaged before platinization.

4. Conclusion

In summary, chemical oxidation of CNS with 1:1 proportion of 7.5 M H_2SO_4 and 15 M HNO_3 had showed significant improvement in its electrochemical performance, which is almost equivalent to Vulcan XC-72, ETEK®. Although the sample I_{Pt} treated with 3:1 proportion of 15 M H_2SO_4 and 20 M of HNO_3 showed even better electrochemical activity than sample F_{Pt}, increasing the ratio and concentration of sulfuric acid intensifies the $-OSO_3H$ peak, which is not efficiently hydrolyzed with the technique used in this research work [17]. XPS analysis of sample F have demonstrated the effective modification of its sur-

face which permits to well distribute Pt clusters on the oxidized sites, which was later confirmed with XRD, TEM and cyclic voltammetry results. In our previous article [4], we reported the combustion temperature of a typical CNS was centered at 738 °C for 90% of the sample measured by TGA. This clearly indicates that with the presence of highly ordered and stable structure, CNS used as catalyst support in PEMFCs should improve their durability. Because of its relatively high porous structure, the nanostructures should reduce mass transport losses of hydrogen to the inner nanolayers of the catalyst. Hence, with a highly ordered and stable structure, high porosity and a similar electrochemical activity, these Pt/CNS (10–15 wt.%) are considered as a potential replacement for PEMFC electrode catalyst support, 20 wt.% Pt/C Vulcan XC-72. As observed from Table 2, the mean particle size of Pt particles are comparatively bigger than the state-of-art catalysts. Studies on controlling the Pt particle size, corrosion and durability tests, improvement on Pt loading for use in cathodes are currently in progress.

Acknowledgements

The authors acknowledge the financial aid from Natural Sciences and Engineering Research Council of Canada and Hydro-Quebec. We are grateful to Daniel Cossement, Marie-Hélène Bégin, Marie-Andrée Leduc, Agnes Lejeune and Lyubov Lafi for their technical expertise.

References

[1] I.S. Armadi, Z.L. Wang, T.C. Green, A. Henglein, M.A. El-Sayed, Science 272 (1996) 1924.
[2] M.M. Waje, X. Wang, W. Li, Y. Yan, Nanotechnology 16 (2005) S395.
[3] A. Pozio, M. De Francesco, A. Cemmi, F. Cardellini, L. Giorgi, J. Power Sources 105 (2002) 13.
[4] S.K. Natarajan, D. Cossement, J. Hamelin, J. Electrochem. Soc., in press.
[5] J. Hamelin, M.-A. Leduc, S.K. Natarajan, International Conference on Processing & Manufacturing of Advanced Materials (THERMEC' 2006), Vancouver, Canada, July 4–8, 2006.
[6] H. Tang, J.H. Chen, Z.P. Huang, D.Z. Wang, Z.F. Ren, L.H. Nie, Y.F. Kuang, S.Z. Yao, Carbon 42 (2004) 191.
[7] W.Z. Li, C.H. Liang, J.S. Qiu, W.J. Zhou, H.M. Han, Z.B. Wei, G.Q. Sun, Q. Xin, Carbon 40 (2002) 791.
[8] Z.L. Liu, X.H. Lin, J.Y. Lee, W. Zhang, M. Han, L.M. Gan, Langmuir 18 (2002) 4054.
[9] R.Q. Yu, L.W. Chen, Q.P. Liu, J.Y. Lin, K.L. Tan, S.C. Ng, H.S.O. Chan, G.Q. Xu, T.S.A. Hor, Chem. Mater. 10 (1998) 718.
[10] A.G. Rinzler, J. Liu, H. Dai, P. Nikolaev, C.B. Huffman, F.J. Rodríguez-Macías, P.J. Boul, A.H. Lu, D. Heymann, D.T. Colbert, R.S. Lee, J.E. Fischer, A.M. Rao, P.C. Eklund, R.E. Smalley, Appl. Phys. A 67 (1998) 29.
[11] J. Zhang, H. Zou, Q. Qing, Y. Yang, Q. Li, Z. Liu, X. Guo, Z. Du, J. Phys. Chem. B 107 (2003) 3712.
[12] A.C. Dillon, K.M. Jones, T.A. Bekkedahl, C.H. Kiang, D.S. Bethune, M.J. Heben, Nature 386 (1997) 377.
[13] I.W. Chiang, B.E. Brinson, A.Y. Huang, P.A. Willis, M.J. Bronikowski, J.L. Margrave, R.E. Smalley, R.H. Hauge, J. Phys. Chem. B 105 (2001) 1157.
[14] S. Bandow, A.M. Rao, K.A. Williams, A. Thess, R.E. Smalley, P.C. Eklund, J. Phys. Chem. B 101 (1997) 8839.
[15] K.B. Shelimov, R.O. Esenaliev, A.G. Rinzler, C.B. Huffman, R.E. Smalley, Chem. Phys. Lett. 282 (1998) 429.
[16] G.S. Duesberg, M. Burghard, J. Muster, J. Philipp, S. Roth, Chem. Commun. 3 (1998) 435.
[17] R. Yu, L. Chen, Q. Liu, J. Lin, K.-L. Tan, S.C. Ng, H.S.O. Chan, G.-Q. Xu, T.S.A. Hor, Chem. Mater. 10 (1998) 718.
[18] W. Li, C. Liang, W. Zhou, J. Qiu, Z. Zhou, G. Sun, Q. Xin, J. Phys. Chem. 107 (2003) 6292.
[19] G.A. Capuano, G. Thamizhmani, J. Electrochem. Soc. 141 (1994) 968.
[20] A.S. Arico, A.K. Shukla, H. Kim, S. Park, M. Min, V. Antonucci, Appl. Surf. Sci. 172 (2001) 33.
[21] M. Neergat, A.K. Shukla, K.S. Gandhi, J. Appl. Electrochem. 31 (2001) 373.
[22] P.J. Britto, K.S.V. Santhanam, A. Rubio, J.A.A. Alonso, P.M. Ajayan, Adv. Mater. 11 (1999) 154.
[23] U. Zielke, K.J. Huttinger, W.P. Hoffman, Carbon 34 (1996) 983.

13. APPENDIX III: THIRD PAPER

Sadesh Kumar Natarajan, Jean Hamelin, *Electrochemical Durability of Carbon nanostructures as Catalyst Support for PEMFCs*, *Journal of the Electrochemical Society* 156(2), pp. B210-B215 (2009).

Journal of The Electrochemical Society, **156** (2) B210-B215 (2009)
0013-4651/2008/156(2)/B210/6/$23.00 © The Electrochemical Society

Electrochemical Durability of Carbon Nanostructures as Catalyst Support for PEMFCs

Sadesh Kumar Natarajan and Jean Hamelin*,z

Institut de recherche sur l'hydrogène, Université du Québec à Trois-Rivières, 3351, Trois-Rivières, Quebec, Canada G9A 5H7

Electrochemical surface oxidation of platinum supported on carbon black (Vulcan XC-72, Pt/C) and carbon nanostructures (Pt/CNS) was studied to understand and compare the durability as catalyst support in polymer electrolyte membrane fuel cells (PEMFCs). The subsequent electrochemical characterization at different treatment time intervals suggests that CNS is more electrochemically stable than carbon black due to its higher degree of graphitization. Furthermore, the reported membrane electrode assembly durability measurements suggest that highly ordered CNS would be a better catalyst support than turbostratic Vulcan XC-72.
 [DOI: 10.1149/1.3033517]

Manuscript submitted May 20, 2008; revised manuscript received October 29, 2008. Published December 4, 2008.

In recent years, polymer electrolyte membrane fuel cell (PEMFC) technology has been claimed to be the most promising and highly efficient technology for stationary and mobile applications. In the development of PEMFCs, durability of the membrane electrode assembly (MEA) is one of the most important issues that has to be addressed prior to commercialization.[1-3] The present state of the art PEMFC technology is based on nanosized platinum particles as a catalyst supported on high surface area carbon black (CB) for both the anodic oxidation of hydrogen as well as the cathodic reduction of air/oxygen. An ideal carbon support should possess the following characteristics: (*i*) high surface area to deposit nanosized Pt catalysts, thus increasing the reaction sites for electrochemical reaction, (*ii*) exhibit sufficient electrode porosity for the mass transport of reactants to the active sites and removal of products at demanding high current densities, (*iii*) stable under cathode environment, where it is subjected to a high potential (>0.85 V vs reversible hydrogen electrode), high acidity (low pH < 1), high humidity (relative humidity, RH 80%), and high temperature (60–90°C), and (*iv*) should possess very good electrical properties ($\sigma > 0.8$ S cm^{-1}) to move the electrons produced at the anode via an external circuit to the active sites at the cathode, where air/oxygen along with the protons conducted through the membrane from the anode is reduced to water. However, due to its turbostratic structure, the amorphous carbon and short-range graphitic crystallites in CB are easily attacked by acid, followed by hydrolysis and, on further oxidation, the attacked broken carbon sites are gasified to CO_2, predominantly catalyzed by Pt.[4-7] The corrosion of the carbon support as a result of electrochemical oxidation will lead to the dissolution and sintering of Pt nanoparticles, resulting in a reduced active surface area, thus considerably affecting the MEA performance over a prolonged period of usage. Furthermore, the oxidation of the carbon support can affect the surface hydrophobicity of the support, resulting in water flooding and gas transport limitations. Many research groups[8-12] have investigated the degradation mechanism behind the corrosion of the support, which strongly influences the performance of the PEMFC system. In brief, the proposed three-step mechanism initiates with the oxidation of the carbon surface, followed by the formation of transient oxygen radicals either by hydrolysis or due to the catalytic activity on air/oxygen, and finally, the evolution of CO or CO_2 breaking the graphitic plane for further oxidation. CB is more easily attacked than a graphitized carbon as there are more edges in the former support, which are vulnerable to surface oxidation under the cathode environment.

To overcome corrosion problems of CB and to reduce the performance degradation of PEMFCs, an alternative support with a long-range graphitic order such as carbon nanofibers, carbon nanotubes, etc., was investigated and found to be more durable than CB.[8] In a previous paper,[13] we proposed carbon nanostructures (CNS), developed in our laboratory, as a promising support material rather than CB for PEMFC catalyst due to its superior graphitic structure (oxidation temperature >700°C), an equivalent electrical conductivity (>1 S cm^{-1}), and a highly porous structure (BrunauerEmmett–Teller, BET, surface area of 352.6 m^2 g^{-1}, micropore volume of 0.14 cm^3 g^{-1}, macropore volume of 635 mm^3 g^{-1}, and an average micropore width of 1.6 nm) that minimizes mass transport losses. In this investigation, the durability of Pt electrocatalysts supported on CNS (Pt/CNS) were examined by measuring the losses in the electrochemical surface area, grain growth of agglomerated Pt nanoparticles, and a decline in the performance of the PEMFC system at a different period of time under conditions simulating the cathode environment. These results have been compared with similar tests performed on a commercially available platinum electrocatalyst supported on a Vulcan XC-72 (Pt/C).

Experimental

Carbon nanostructures with a BET surface area of 352.6 m^2 g^{-1} and a pore width as low as 1.6 nm were prepared in our laboratory by a modified chemical vapor deposition technique that was described elsewhere.[13,14] A platinum electrocatalyst was supported on CNS with a Pt loading of approximately 20 wt % and was prepared by a reported ethylene glycol method. The particle size distribution of the platinum clusters in the supported CNS from a randomly chosen 100 particles in a high-resolution transmission electron microscope image showed a range between 3 and 6 nm.[14] For comparison reasons, a platinum catalyst supported on Vulcan XC-72 prepared by E-TEK has been used as a reference material. Platinum metal loading of the Pt/C catalyst was also 20 wt % with an average particle width of 2.2 nm.

Carbon cloth (E-TEK) was used as a substrate for casting of a catalyst layer comprised of a supported electrocatalyst and impregnated 5 wt % Nafion (Aldrich) mixture. The amount of Pt catalyst coated on the anodic gas diffusion layer (GDL) was 200 μg cm^{-2}, which is half the amount coated on the cathode GDL (400 μg cm^{-2}). The electrodes and the pretreated membrane (Nafion NRE212, DuPont) were hot pressed into a 5 cm^2 MEA using a press at a temperature of 120°C under 700 psi for 3 min. The MEA was then allowed to cool at room temperature before testing. The performance of the fabricated MEA was evaluated using a 5 cm^2 single-cell hardware (Fuel Cell Technologies, Inc.) equipped with a reversible hydrogen electrode (RHE) wired to a Zahner IMe6 workstation. The MEA was sealed between a 0.01 in. thick silicone rubber gasket at the anode and a 0.01 in. thick Furon gasket (Saint-Gobain) at the cathode, and was assembled with 10.5 Nm torque between two Poco graphite plates with serpentine flow fields.

* Electrochemical Society Active member.
z E-mail: jean.hamelin@uqtr.ca

The single-cell performance was characterized by feeding humidified hydrogen gas at 80°C and 100% RH at the anode and humidified air at 70°C and 80% RH at the cathode with a stoichiometric ratio of 1.5 and 2, respectively. The gas pressure at the electrodes was maintained at 30 psig using a back-pressure regulator. Initially, the cell was conditioned with a constant load of 0.5 A cm^{-2} at 80°C for 50 h. The steady-state value of the cell potential at a load of 1 A cm^{-2} was calculated by the mean values of the data logged over a runtime of 1 h. To help identify the rate of performance degradation between Pt/C and Pt/CNS, hydrated (100% RH) ultrahigh-purity (UHP) nitrogen was passed through the working electrode (cathode compartment) and hydrated (100% RH) UHP hydrogen was passed through the counter electrode (anode compartment). The anode serves as a counter electrode as well as reference electrode (RHE). The cell temperature was maintained constant at 80°C throughout the process and the pressure was reduced to atmospheric at the two-electrode potentiostatic circuit mode. Then, the Zahner workstation was switched to cyclic voltammetry mode, and a constant potential of 1.2 V was applied between the working electrode and RHE to accelerate the oxidation of the carbon support at the cathode catalyst layer. The potentiostatic hold was maintained for a period of 15 h during repetitive cycles of this experiment. Prior to measuring the steady-state values of the open-circuit voltage (OCV) and cell voltage under a load of 1 A cm^{-2}, the gas feed, the humidity conditions, and the pressure were tuned back to the values mentioned above. Later, the MEA was briefly conditioned with a load of 0.5 A cm^{-2} at 80°C for 30 min. This test cycle was repeated over the course of the experiment, which was 200 h.

Prior to electrochemical measurements, the Pt electrocatalyst supported on CB and CNS was conditioned in a tube furnace to remove surface contaminants and anneal the Pt crystallite, under an atmosphere of 10% hydrogen and 90% argon for 1 h at 300°C. Glassy carbon (GC) disks (BASI, 3 mm, 0.07069 cm^2), polished to a 0.05 μm mirror finish (alumina, BASI) before each run, served as the substrate for the supported catalyst. An aqueous suspension of catalyst ink was prepared by ultrasonically dispersing 25 mg of catalyst in deionized (DI) water (Millipore) to a ratio of 2 $mg_{catalyst}$ mL^{-1}. A 20 μL aliquot of the ultrasonically redispersed suspension was then pipetted onto the disk. To obtain a uniform distribution of the suspension, the GC electrode was dried at room temperature for an hour before leaving it inside a preheated (80°C) oven for another hour. After complete evaporation of the water droplet, 20 μL of the diluted Nafion solution (5 wt % Nafion, Aldrich) was pipetted onto the dried powder surface to enhance the adherence between the catalyst powder and the electrode. The cyclic voltammetries were carried out in a conventional airtight three-electrode thermostatted (80°C) cell containing a 0.5 M H_2SO_4 electrolyte. Potentials were measured using a Ag/AgCl (Sat. KCl) electrode, but all the potentials throughout this study are referenced to RHE. A potentiostatic hold of 1.2 V was applied to the working electrode and was held for 0, 15, 30, 45, and 175 h to electrochemically oxidize the support material. Voltammograms were recorded for each time period to compute the rate and loss of the catalyst active surface due to electrochemical oxidation. The electrochemically active surface area was evaluated from the hydrogen desorption charge of a cyclic voltammogram. To study the extent of surface electrochemical oxidation of Pt/C and Pt/CNS under simulated conditions of a cathode environment, the 0.07069 cm^2 GC substrate, replaced by a 10 cm^2 nickel substrate, was exposed to 1.2 V at room temperature for various times (0, 75, and 150 h). The extent of oxidation at different time periods on electrochemically oxidized Vulcan and CNS was characterized by thermal gravimetric analysis (TGA). Prior to TGA, the oxidized catalysts at different time periods were scraped out from the substrate, washed with DI water, and dried in an oven at 65°C at atmospheric pressure. TGA was performed using a TGA 7 Perkin-Elmer apparatus with an argon atmosphere at a purge rate of 30 sccm. The temperature was ramped as follows: room temperature to 50°C at 5°C min^{-1}, holds for 5 min at 50°C, and heated from 50 to 850°C at 5°C min^{-1}. The chemical nature and the distribution of the surface functional groups during the course of oxidation at different time intervals was defined based on a study done by Kangasniemi et al.[5]

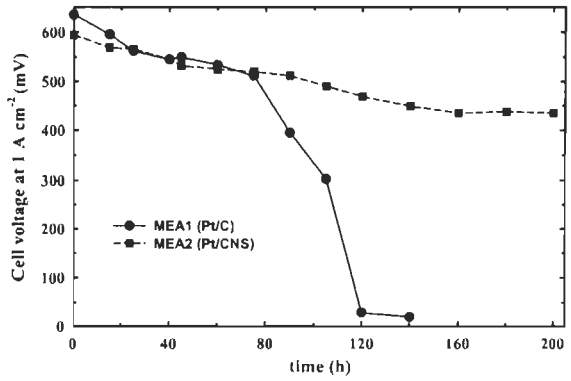

Figure 1. Measurements of cell voltage at 1 A cm^{-2}, showing a sudden drop in cell performance for MEA1 after 75 h of electrochemical oxidation at 1.2 V.

The size of the platinum particles in the dried catalyst powder of electrochemically oxidized Pt/C and Pt/CNS was examined by powder X-ray diffraction (XRD). XRD measurements were performed with a Rigaku diffractometer using Cu Kα1 radiation (λ = 1.54051 Å) and θ/2θ geometry.

Results and Discussion

As described in our previous publication,[14] CNS was functionalized with a 1:1 concentrated acid mixture of 7.5 M H_2SO_4 and 15 M HNO_3. Thus, strong anchoring sites at the interface of Pt and the surface of CNS were achieved through carbon surface modification. These acidic oxygen groups introduced by the chemical modification method decreases the hydrophobicity of CNS and increases the dispersion of platinum particles with an increase in surface oxygen groups. Studies have shown that C=O groups acting as anchoring sites hinder agglomeration and surface diffusion of platinum particles across the graphene layers.[15] X-ray photoemission spectroscopy studies performed on CNS functionalized using the conditions mentioned above showed 48.8% of carbonyl, 46.4% of hydroxyl, and 4.8% of carboxyl groups attached to the carbon surface.[14] The influence of unused acidic functional groups after platinization during hydrolysis is therefore considered negligible. However, the 0 h sample of CNS showed the presence of surface oxides prior to electrochemical oxidation.

Figure 1 shows a steady decline in cell voltage under a constant load of 1 A cm^{-2} at different time intervals during accelerated electrochemical oxidation at cathodes fabricated with Pt/C and Pt/CNS, respectively. The MEAs fabricated using Pt/C and Pt/CNS were labeled as MEA1 and MEA2, respectively. A steady linear downward trend on cell voltage has been observed for both the MEAs during the initial 60 h, the cathode of which was electrochemically oxidized at a potential of 1.2 V at 80°C. The fluctuation in the trend before 60 h of operation is due to the process of wetting level in the electrolyte membrane and the ionomer in the catalyst layer. After 60 h, a marked decrease in the cell potential was observed for MEA2, whereas a steep downward trend was observed for MEA1. It can be seen that almost 95% of the cell voltage was lost for MEA1 after 140 h of accelerated oxidation treatment, while only a 25% loss in cell voltage was observed for MEA2. The major drop in cell voltage for both MEAs occurred between 60 and 140 h of oxidation treatment, as shown in the figure. However, the progress of the voltage drop is lower for MEA2 even after 140 h. The drop was merely 2.36% even after continuous oxidation for an additional

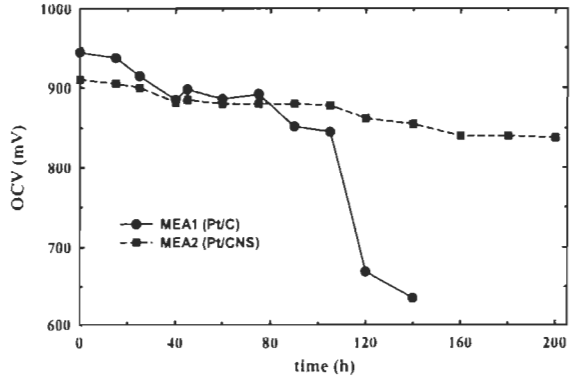

Figure 2. Measurements of OCV showing degradation of membrane in MEA1, which is accountable for poor cell performance after 75 h.

60 h. A similar trend was observed for the OCV measurements during the same time intervals of electrochemical oxidation as shown in Fig. 2. The sudden decline in OCV after electrochemical oxidation treatment can be due to the degradation of the polymer electrolyte membrane resulting in fuel crossover.[11] Further analysis of the degradation mechanism is currently in progress. These results demonstrate that CNS with high graphitic content and long-range order show a higher resistance to corrosion under oxidative conditions when compared with Vulcan XC-72. On a long run, MEAs prepared with Pt/CNS could potentially provide better durability than MEAs prepared with Pt/C.

To quantify the extent of loss in platinum surface area, cyclic voltammetry was performed on Pt/C and Pt/CNS in a N_2 purged 0.5 M H_2SO_4 electrolyte at different time intervals during their treatment at 1.2 V and 80°C. The amount of coulombic charge involved during hydrogen desorption was used to calculate the active platinum surface of the electrodes, after correcting for double-layer capacitance.[15] Figure 3 shows the drop in electrochemical active surface area for the case of Pt/C and Pt/CNS at different time intervals of potential hold. During the initial 15 h of oxidation, a nearly 35% loss in Pt surface area was observed for Pt/C, while there is a considerable 20% loss for Pt/CNS as shown in the figure. Because the Pt(0) supported on CB (2.2 nm) is twice as small as the Pt(0) supported on CNS (4.5 nm), the smaller size Pt(0) particles supported on C tend to dissolve/agglomerate faster than the larger Pt(0) particles in CNS.[16] Not just the size of the Pt(0) particles influences the drop in the active surface area of the catalyst, but also the interactions between Pt(0) and the carbon support material. An electronic structure change of the platinum catalytic layer by the presence of interaction between the platinum active phase and the carbon support phase leads to changes of catalyst durability. Although the electronic interaction effects between Pt catalyst and the carbon support can be studied by a variety of conventional physical, spectroscopic, and electrochemical methodologies, the objectives of the current work are to quantify the loss in the surface area of the supported catalysts during the course of electrochemical oxidation and to compare the durability of the catalysts despite the variations in size of Pt(0) particles and Pt–C interactions. Now, after 75 h of oxidation, a steady decline in active surface area of Pt/C at a rate of 3.2 $\times 10^{-2}$ m^2 g^{-1} h^{-1} vs 1.52 $\times 10^{-2}$ m^2 g^{-1} h^{-1} for Pt/CNS was observed resulting in active surface areas, 25.81 and 30.17 m^2 g^{-1},

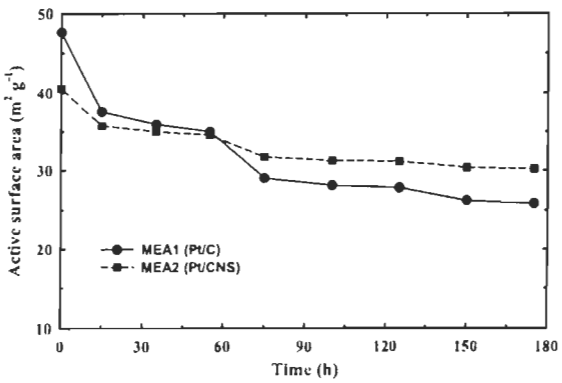

Figure 3. Comparison of Pt active surface area loss for the case of Vulcan XC-72 and CNS at different time intervals during oxidation treatment.

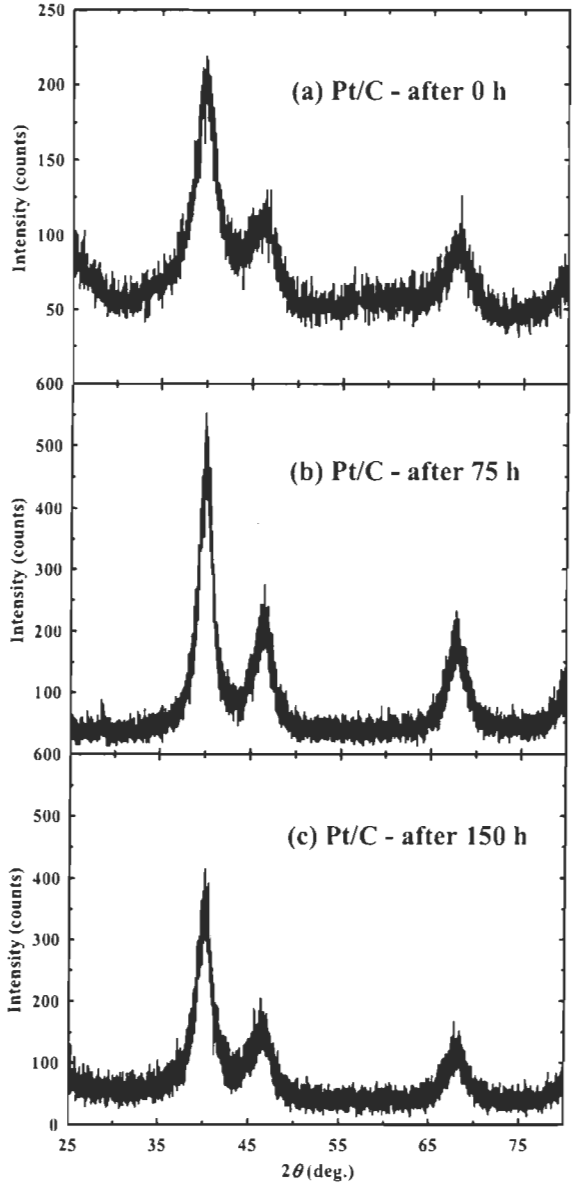

Figure 4. XRD patterns for Pt/C after electrochemical oxidation at 1.2 V for different time intervals.

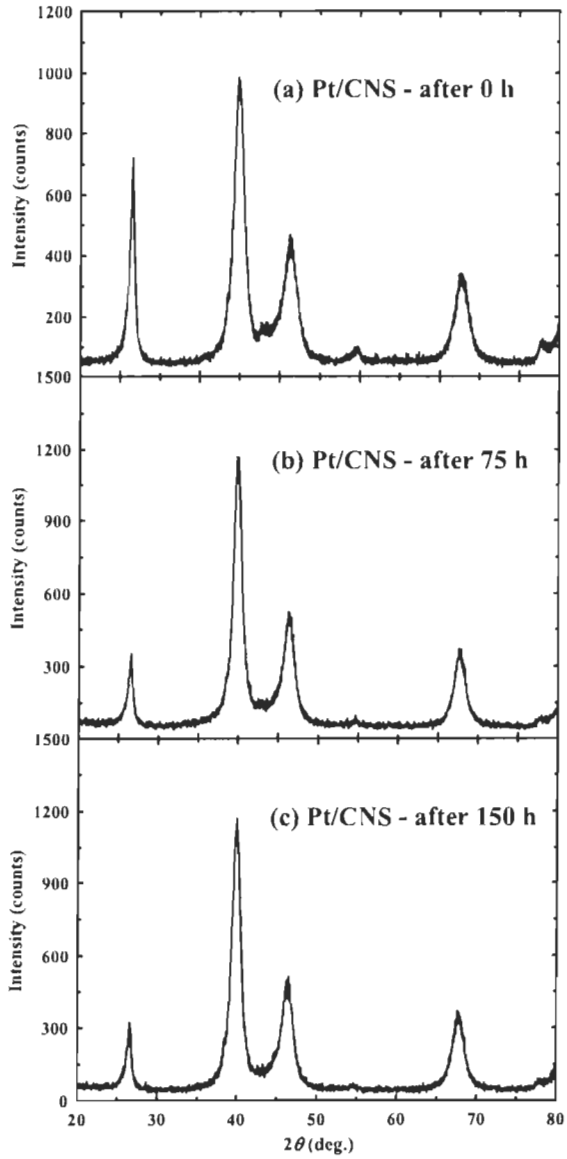

Figure 5. XRD patterns for Pt/CNS after electrochemical oxidation at 1.2 V for different time intervals.

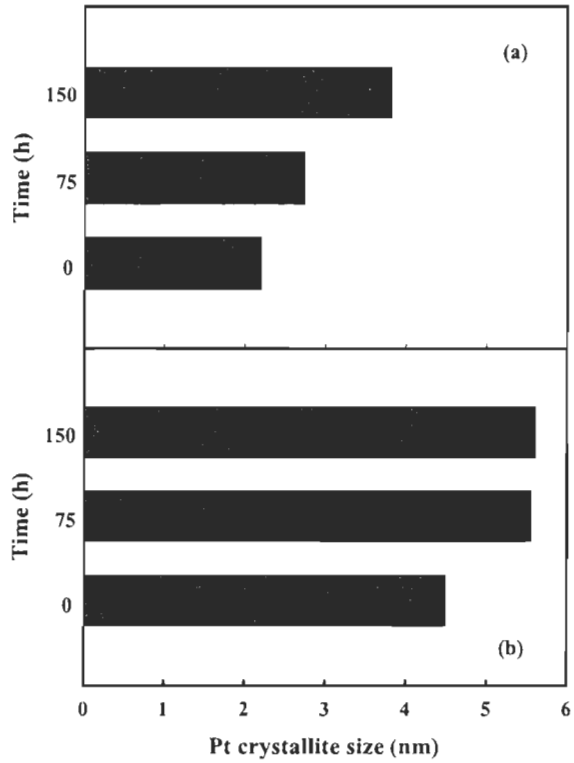

Figure 6. Growth of Pt particle size in (a) Pt/C and (b) Pt/CNS as observed by XRD during electrochemical oxidation of Pt/C and Pt/CNS.

respectively. Although the smaller Pt(0) particles in Pt/C tend to dissolve/agglomerate faster than in Pt/CNS, the excess loss in the Pt surface area after 175 h of oxidation treatment and degradation of OCV does not exclude the possibility that some of the Pt particles diffused into the polymer electrolyte membrane. However, uncertainties on this phenomenon still exist. The dissolution of Pt(0) in aqueous electrolyte solution due to the potential effect on the working electrode was studied by Rand et al.[17,18] The loss in Pt surface area supported on Vulcan or CNS in an aqueous electrolyte can be due to the dissolution of Pt(0) particles, reprecipitation of Pt ions, and diffusion of Pt ions into the membrane. Although CNS prepared in our lab has nearly 50% of C=O groups as Pt anchoring sites, we cannot exclude the possibility of Pt particle growth by migration (surface diffusion of Pt particles). Therefore, the decrease in the electrochemically active surface area of Pt supported on CNS is caused mainly by the dissolution of Pt(0) anchored on other functional groups. Improving the interaction of Pt precursor with CNS during platinization can be achieved by increasing the specificity of the surface functional groups in the support material.

Powder XRD study was used to observe the changes in particle size during the course of oxidation at different time intervals. The XRD patterns for Pt/C and Pt/CNS electrochemically oxidized at 0, 75, and 150 h are plotted in Fig. 4 and 5, respectively. XRD shown in the above figures identifies the face-centered cubic structure of the characteristic crystalline Pt peaks for Pt(111), Pt(200), Pt(220), Pt(311), and Pt(222). The crystallite size of Pt nanoparticles (d) estimated using Scherrer's equation as shown in Fig. 6 is given by

$$d = \frac{0.9\lambda}{B \cos \theta}$$

where λ is the wavelength of X-ray radiation, numerically equal to 1.54051 Å; B is the full width at half-maximum measured in radians; θ is the angle measured at the position of platinum peaks. The narrowing of characteristic Pt diffraction peaks during the course of electrochemical oxidation is a clear indication of larger Pt particles when compared with fresh Pt particles. It can be observed from Fig. 6 that smaller Pt crystallites tend to agglomerate faster than larger particles of Pt supported on CNS.[16] The results shown in Fig. 6 can be correlated with the electrochemically active surface area measurements plotted in Fig. 3. It can be observed that the estimated value of active surface area for fresh Pt particles (~4 nm) supported on CNS is 40.55 $m^2 g^{-1}$ and the surface area of Pt (~4 nm) on oxidized Pt/C catalyst is 25.81 $m^2 g^{-1}$. The morphology of supports and dispersion of Pt particles along with the MEA fabrication technique (includes the ink preparation, electrode preparation, and hot-pressing) can alter the estimated active surface area of Pt particles

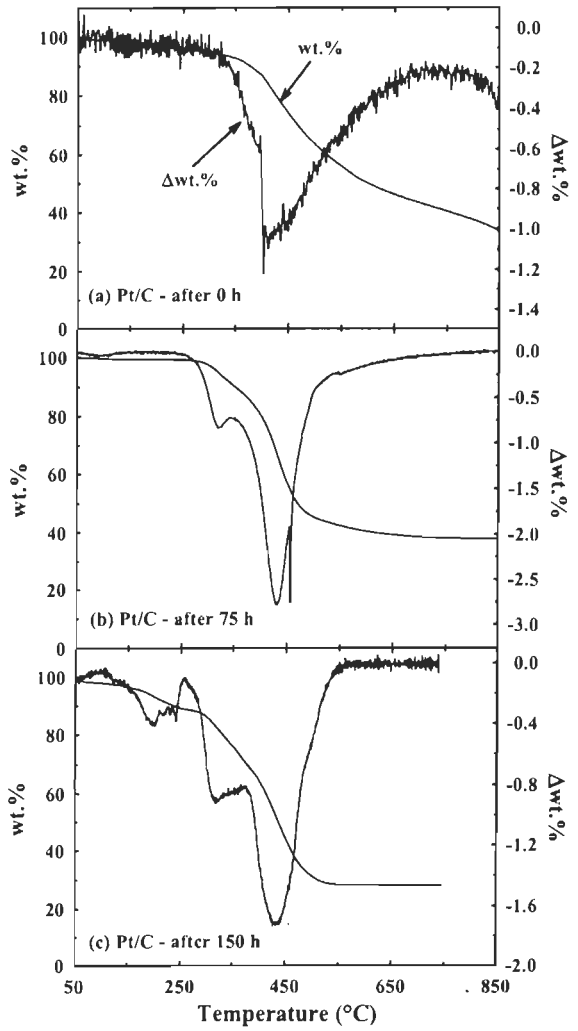

Figure 7. TGA profiles for Pt/C after electrochemical oxidation at 1.2 V for different time intervals.

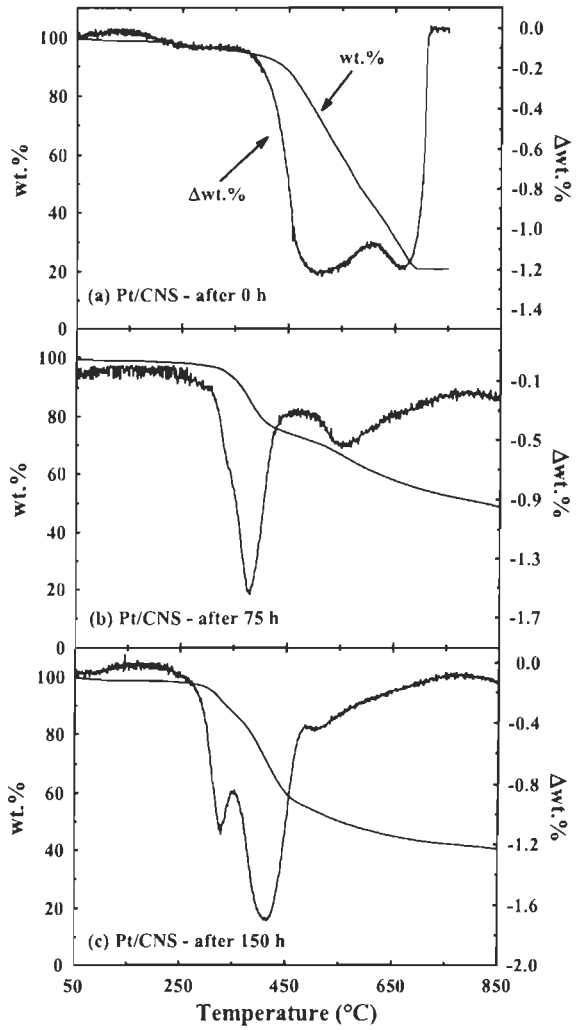

Figure 8. TGA profiles for Pt/CNS after electrochemical oxidation at 1.2 V for different time intervals.

with similar size. However, considering the fact that the particle size of Pt in Pt/C is estimated after oxidation treatment, a significant loss in surface area can also be attributed to Pt ion migration into the polymer electrolyte membrane or Pt being simply washed away with the cathode stream.

Kangasniemi et al.[5] performed thermal desorption studies on carbon to assign decomposition temperature for different functional species and their thermal decomposition products. The amount of surface oxygen on carbon was estimated using a mass spectrometer by analyzing the volatile surface oxides from the TGA instrument. In summary, evolution of CO_2 observed at low temperatures (approximately 250°C) are usually assigned to the acidic functional group, carboxylic acids and those at higher temperatures (approximately 625°C) to lactones. At higher temperatures (600–900°C), the evolution of CO observed corresponds to ethers, phenols, carbonyls, and quinines, while carboxylic anhydrides give rise to both CO and CO_2 peaks. Therefore, to characterize the surface functional groups during electrochemical oxidation of Pt/C and Pt/CNS, TGA was performed under argon on the dried samples at oxidation time periods of 0, 75, and 150 h. Figures 7 and 8 show the TGA profiles of Pt/C and Pt/CNS after electrochemical oxidation at different time intervals. It is observed that, on both catalyst surfaces, the composition of –COOH intermediate for evolution of CO_2 remains almost unchanged. However, a huge variation in the composition of lactone was observed at different oxidation periods for the evolution of CO_2 between 350 and 400°C. Figure 7 shows an increase in the density of surface oxides on carbon surface in the form of an intermediate, lactone over a period of electrochemical oxidation up to 150 h. Similarly, the CO_2 evolution from Pt/CNS was observed throughout the temperature range, confirming the presence of different functional groups generated during the electrochemical oxidation of the catalyst. In addition to the functional groups involved for the evolution of CO_2, carbonyls and quinones, as well as phenols and ethers, decompose at temperatures higher than 700°C to evolve CO. The apparent density of these functional groups responsible for the evolution of CO tends to decrease during the course of electrochemical oxidation, which is well in agreement with the generic mechanism of surface oxide formation proposed by Yue et al.[19] During the course of oxidation, an increase in surface oxygen content decreases the hydrophobic properties of the catalyst support, thus

breaking down the surface oxides to CO_2. A similar decrease in density of surface functional groups for the evolution of CO is observed for Pt/C.

Conclusions

We have reported a study on electrode material durability for the platinum catalysts supported on Vulcan XC-72 and CNS. In summary,

1. Electrochemical characterizations show that CNS prepared in our laboratory has improved corrosion resistance and better performance than Vulcan XC-72.

2. Although CNS tends to corrode under simulated conditions of cathode, it is observed that, after an initial period of time for which the oxidation is attributed to the surface defects caused during functionalization, the rate of surface corrosion becomes smaller compared with CB. However, the functional groups such as –COOH, –OH, and –CO formed during the surface modification of CNS enhanced the Pt–CNS interaction in the electrocatalyst.

3. Loss in active Pt surface area and a decline in MEA1 performance was due to the dissolution of Pt(0), aggregation of Pt ions in the catalyst layer, and diffusion/precipitation inside the membrane.

4. Loss in activity of Pt/CNS is mostly due to the dissolution of Pt(0) and aggregation of Pt ions in the catalyst layer. This may be due to the thermal treatment done on CNS prior to platinization that increases the basicity of the carbon surface. This increase in Pt-CNS interaction is attributed to the π-sites on CNS, which act as anchoring sites for Pt particles.

5. The rate of growth of Pt particle size in Pt/CNS stabilizes after 75 h of electrochemical oxidation.

From the results obtained in this paper, we can conclude that CNS with a better electrode durability can be a good candidate for PEMFC catalyst support. Currently, we are studying Pt dissolution and deposition in the polymer electrolyte membrane of PEMFCs by potential cycling and potentiostatic holds.

Acknowledgments

This work is financially supported by National Resources and Engineering Research Council of Canada (NSERC). We are grateful to Daniel Cossement, Lyubov Lafi, Robert Drolet, and Marie-Hélène Bégin for their technical expertise.

Université du Quebec à Trois-Rivières assisted in meeting the publication costs of this article.

References

1. M. S. Wilson, F. H. Garzon, K. E. Sickafus, and S. Gottesfeld, *J. Electrochem. Soc.*, **140**, 2872 (1993).
2. M. Mathias, H. Gasteiger, R. Makharia, S. Kocha, T. Fueller, and J. Pisco, *Abstr. Pap. - Am. Chem. Soc.*, **228**, U653 (2004).
3. D. A. Stevens and J. R. Dahn, *Carbon*, **43**, 179 (2005).
4. J. Willsau and J. Heitbaum, *J. Electroanal. Chem. Interfacial Electrochem.*, **161**, 93 (1984).
5. K. H. Kangasniemi, D. A. Condit, and T. D. Jarvi, *J. Electrochem. Soc.*, **151**, E125 (2004).
6. R. L. Borup, J. R. Davey, F. H. Garzon, D. L. Wood, and M. A. Inbody, *J. Power Sources*, **163**, 76 (2006).
7. J. Xie, D. L. Wood, D. M. Wayne, T. A. Zawodzinski, P. Atanassov, and R. L. Borup, *J. Electrochem. Soc.*, **152**, A104 (2005).
8. X. Wang, W. Li, Z. Chen, M. Waje, and Y. Yan, *J. Power Sources*, **158**, 154 (2006).
9. T. Yoda, H. Uchida, and M. Watanabe, *J. Power Sources*, **52**, 5997 (2007).
10. L. Li and Y. Xing, *J. Electrochem. Soc.* **153**, A1823 (2006).
11. K. Yasuda, A. Taniguchi, T. Akita, T. Ioroi, and Z. Siroma, *Phys. Chem. Chem. Phys.*, **8**, 746 (2006).
12. S. D. Knights, K. M. Colbow, J. St-Pierre, and D. P. Wilkinson, *J. Power Sources*, **127**, 127 (2000).
13. S. K. Natarajan, D. Cossement, and J. Hamelin, *J. Electrochem. Soc.*, **154**, B310 (2007).
14. S. K. Natarajan and J. Hamelin, *Electrochim. Acta*, **52**, 3751 (2007).
15. A. Pozio, M. De Francesco, A. Cemmi, F. Cardellini, and L. Giorgi, *J. Power Sources*, **105**, 13 (2002).
16. R. Makharia, S. Kocha, P. Yu, M. A. Sweikart, W. Gu, F. Wagner, and H. A. Gasteiger, *ECS Trans.*, **1**(8), 3 (2006).
17. D. A. J. Rand and R. Woods, *J. Electroanal. Chem. Interfacial Electrochem.*, **35**, 209 (1972).
18. A. Ohma, S. Suga, S. Yamamoto, and K. Shinohara, *J. Electrochem. Soc.*, **154**, B757 (2007).
19. Z. R. Yue, W. Jiang, L. Wand, S. D. Gardner, and C. U. Pittman, *Carbon*, **37**, 1985 (1999).